LPTV-Aware Bit Loading and Channel Estimation in Broadband PLC for Smart Grid

By

Muharrem Ali Tunç

Submitted to the graduate degree program in the Department of Electrical Engineering & Computer Science and the Graduate Faculty of the University of Kansas in partial fulfillment of the requirements for the degree of Doctor of Philosophy.

Dissertation Committee:

Erik S. Perrins, Chairperson

Shannon D. Blunt

James P.G. Sterbenz

Lingjia Liu

Atanas Stefanov

Date Defended

The Dissertation Committee for Muharrem Ali Tunç
certifies that this is the approved version of the following dissertation:

LPTV-Aware Bit Loading and Channel Estimation in Broadband PLC for Smart Grid

Erik S. Perrins, Chairperson

Date approved: _____

Abstract

Power line communication (PLC) has received steady interest over recent decades because of its economic use of existing power lines, and is one of the communication technologies envisaged for Smart Grid (SG) infrastructure. However, power lines are not designed for data communication, and this brings unique challenges for data communication over power lines. In particular for broadband (BB) PLC, the channel exhibits linear periodically time varying (LPTV) behavior synchronous to the AC mains cycle. This is due to the time varying impedances of electrical devices that are connected to the power grid. Another challenge is the impulsive noise in addition to power line background noise, which is due to switching events in the power line network. In this work, we focus on two major aspects of an orthogonal frequency division multiplexing (OFDM) system for BB PLC LPTV channels; bit and power allocation, and channel estimation (CE).

First, we investigate the problem of optimal bit and power allocation, in order to increase bit rates and improve energy efficiency. We present that the application of a power constraint that is averaged over many microslots can be exploited for further performance improvements through bit loading. Due to the matroid structure of the optimization problem, greedy-type algorithms are proven to be optimal for the new LPTV-aware bit and power loading. Significant gains are attained especially for poor (i.e. high attenuation) channel conditions, and at reduced transmit-power levels, where the energy per bit-transmission is also low. Next, two mechanisms are utilized to reduce the complexity of the optimal LPTV-aware bit loading and peak microslot power levels: (i) employing representative values from microslot transfer functions, and (ii) power clipping. The ideas of LPTV-aware bit loading, complexity reduction mechanism, and

power clipping are also applicable to non-optimal bit loading schemes. We apply these ideas to two additional sub-optimal bit loading algorithms that are based on even-like power distribution for a portion of the available spectrum, and demonstrate that similar gains in bit rates are achieved.

Second, we tackle the problem of CE for BB PLC LPTV channels. We first investigate pilot based CE with different pilot geometry in order to reduce interpolation error. Block-type, comb-type, and incline type pilot arrangements are considered and a performance comparison has been made. Next we develop a robust CE scheme with low overhead that addresses the drawbacks of block-type pilot arrangement and decision directed CE schemes such as large estimation overhead for block-type pilot geometry, and difficulty in channel tracking in the case of sudden changes in the channel for decision directed approaches. In order to overcome these drawbacks, we develop a transform domain (TD) analysis approach to determine the cause of changes in the channel estimates, which are due to changes in the channel response or the presence of impulsive noise. We then propose a robust CE scheme with low estimation overhead, which utilizes pilot symbols placed widely apart and exploits the information obtained from TD analysis as a basis for switching between various CE schemes. The overhead of the proposed scheme for CE is low, and sudden changes in the channel are tracked affectively. Therefore, the effects of the LPTV channel and the impulsive noise on CE are mitigated.

Our results indicate that for bit and power allocation, the proposed reduced complexity LPTV-aware bit loading with power clipping algorithm performs very close to the optimal LPTV-aware bit loading, and is an attractive solution to bit loading in a practical setting. Finally, for the CE problem, the proposed CE scheme based on TD analysis has low estimation overhead, performs well compared to block-type pilot arrangement and decision directed CE schemes, and is robust to changes in the channel and the presence of impulsive noise. Therefore, it is a good alternative for CE in BB PLC.

Acknowledgments

Praise be to *God*, the *Most Gracious* and the *Most Merciful*...

First and foremost, I would like to thank Dr. Erik Perrins for his excellent guidance and support during my studies. Without his support and guidance, this work would not have been accomplished. I would also like to thank Dr. Lutz Lampe for his guidance and collaboration. I would like to thank Dr. James Sterbenz and Dr. Shannon Blunt, from whom I took classes and learned a lot.

I also thank my family: my wife Sevde, my mother and father to whom I *dedicate this dissertation*, and my brothers Gokturk and Yavuz for their support throughout my studies. Special thanks to my friends Fatih, Zeynep, and Oguzhan who have always been much more than a friend to me. Many thanks to Mustafa, Esin, Erkan, Hale, Ferhat, Rabia, Neslihan, Kursat, Selahaddin, Abdulbaki, Ismet, Murat, Erhan, Eyyup, Akif, Mucahit, Oguz, Songul, Elmeddin, Nurullah, Senem, Pasha, Anastasia, Cal, Jolene, and Steve (and many others that I could not list here), for their invaluable friendship. Finally, thanks to my classmates Ehsan, Zaid, Daniel, Egemen, and Cenk for their valuable company and friendship...

Page left intentionally blank.

Table of Contents

Page left intentionally blank.

List of Figures

Chapter 1

Introduction and Motivation

1.1 Introduction

In this effort, two major aspects of an orthogonal frequency division multiplexing (OFDM) communication system for broadband (BB) power line communication (PLC) are addressed; (i) bit and power allocation, and (ii) channel estimation (CE). Optimal and reduced complexity bit and power allocation algorithms, and a robust CE scheme with low estimation overhead are developed.

1.2 Power Line Communication

PLC [1] has been a topic of continued interest over time because it allows for dual use of existing power line infrastructure. This economic advantage makes PLC a focus of study for notable applications that include broadband distribution over power lines (BPL), automatic metering infrastructure (AMI), and *Smart Grid* (SG) communications infrastructure, to name a few [2].

Historically, early in the twentieth century, PLC was used for switching in substations, metering and basic load control. The interest for PLC research gained momentum in 1980s and increased further in 1990s. Much research has been done since then, along with products developed in the industry during this time. Power lines are usually classified into high (>100

kV), medium (1–100 kV) and low (<1 kV) voltage networks, with increasing challange for communication respectively. LV distribution networks have been the focus of the most research in PLC, which provides easy access to the network in various buildings. The utility companies have had interest in PLC with the motovation of load management, which requires switching on and off devices at the times of peak power demand. Another incentive for electric companies has been automatic metering to reduce costs in labor, and utilization of PLC in SG infrastructure. In the case of power outages in the cellular and wireless communication networks, PLC can also play an important role in disaster recovery for communication over some critical links, where there may be no other technology available for communication [1].

One challenge for the development of PLC technology has been the widely different wiring and grounding practices in different parts of the world such as Europe and United States. International harmonization efforts have been initiated in the past 20–30 years, and many regulatory bodies (for instance, US National Electric Code (NEC)) have mandated certain set of practices for wiring. Although there is still no set of practices that is followed all around the world, these regulations helped greatly simplify the analysis of signal transmission over power lines [1].

The PLC technology can be grouped into three categories based on the bandwidth they occupy: 1) The *Ultra narrow band (UNB)* technology provides very low data rates in the order of hundred bits per second (bps) in the ultra low 0.3–3 kHz frequency band. Some applications of UNB technology are the Ripple Carrier Signaling that supports load control applications, AMR turtle system, and Two-Way Automatic Communications System (TWACS). 2) The *Narrowband (NB)* technology operates in 3–148.5 kHz CENELEC (European Committee for Electrotechnical Standardization) frequency band in Europe, and 10–490 kHz FCC frequency band in United States. Within this category, single carrier low data rate (LDR) solutions can provide data rates of a few kbps, and multicarrier high data rate (HDR) solutions can provide up to 500 kbps. 3) The *Broadband (BB)* technology operates in 1.8–250 Mhz frequency band, can provide up to a few hundred Mbps data rate, and is the focus of our work [2].

Some of the applications of BB PLC include the collection and distribution of data on energy consumption of smart appliances, demand response and management programs, dynamic pricing and flexible power control of appliances, communication between Plug-in Electric Vehicles (PEV) and their charging stations, and communications between smart appliances. These applications are envisaged for the in-home (IH) domain of SG, and often require devices with low complexity and reduced power consumption, since they will likely be deployed in large quantities in the SG [3].[1] These criteria are essential for technologies targeting the IH domain of SG [4]. The following BB PLC standards are worth mentioning in this domain: IEEE 1901 [5], ITU-T G.hn [3], and the HomePlug Green PHY (HPGP) [4] specification. Each of these standards has design features that are relevant to our work in terms of reducing the power consumption and providing low complexity solutions.

1.3 BB PLC Channel Characteristics

Two important characteristics of the BB power line channel are; (i) its transfer function exhibits a linear periodically time varying (LPTV) behavior [6], and (ii) impulsive noise is present in addition to the power line background noise. The LPTV behavior of the BB PLC channel stems from the time-varying impedances of the electrical devices that are connected to the power grid and the impulsive noise is caused by the switching events in the power line network. These channel and noise characteristics must be taken into account when designing a communication system for BB PLC.

1.4 Problem Statement

In this work, we address two aspects of an OFDM system for BB PLC LPTV channels: i) bit and power allocation, and ii) CE.

[1] There is also a valid discussion about the application of BB versus narrowband PLC technology for SG, considering that envisaged use cases often require moderate data rates and device complexity and power consumption are reduced for narrowband systems. But these considerations are outside the scope of this work focusing on BB PLC.

For bit and power allocation, conventional algorithms designed for LPTV channels in the literature adapt to the LPTV channel via so called *microslots* in time. However, these algorithms do not consider the time-varying conditions of the channel transfer function over one AC mains cycle and allocate power to each microslot regardless of its channel condition (i.e. channel attenuation). Therefore, these algorithms are not optimal in terms of maximizing the achieved data rates. In this work, we show that the optimal bit and power allocation algorithm for LPTV channels can be developed by considering the fluctuations in the transfer function over one AC mains cycle and allocating power accordingly. This results in significant improvement in achieved data rates. Next, we show that the complexity of the optimal algorithm can be reduced if the task of bit and power allocation over one AC mains cycle is divided into smaller tasks, which makes the algorithm work on a smaller data set.

For the CE aspect, the LPTV channel requires a large number of transfer functions to be estimated over one AC mains cycle. If we assume that the channel remains constant for one OFDM symbol time, and can vary from one OFDM symbol to the next, depending on the channel bandwidth this may result in hundreds of microslots for CE during one AC mains cycle (i.e. 20 ms. for 50 Hz. in Europe and 16.6 ms. for 60 Hz. in United States). When pilot symbols are utilized with high density—for instance in the case of block-type pilot geometry—to estimate the channel, the estimation overhead is large. When decision directed approaches are utilized, the overhead is minimal, but the channel tracking capabilities are limited in the case of abrupt changes in the channel transfer function and noise due to the LPTV channel and the impulsive noise. Therefore, a low overhead CE scheme that is robust to abrupt changes in the channel transfer function and considers the presence of impulsive noise is needed. In this work, we first examine pilot based CE with various pilot geometry to reduce *interpolation error* inherent in comb-type pilot arrangement. We then develop a transform domain (TD) analysis that examines the change in two consecutive channel estimates in a TD, and determines the changes in the estimate due to a change in the transfer function or the presence of impulsive noise. Next, a final CE scheme that switches between various CE schemes based on the result

of TD analysis for different cases is developed. The proposed scheme has low overhead, and is robust to changes in the transfer function and the noise.

1.5 Contributions

For the bit loading aspect of an OFDM system, we consider two essential design criteria for BB PLC devices for the IH domain of SG; (i) reducing the power consumption (ii) reducing the complexity. We address these two criteria in two steps. In the first step, we address the problem of optimal bit and power allocation for BB PLC LPTV channels, which increases the achieved data rate, and in return reduces the power consumption. In the second step, we address the issue of complexity, and provide mechanisms that reduce the complexity of the proposed bit loading scheme, while maintaining a near-optimal performance.

- **Step 1:** It was shown in the previous works that some improvement in bit loading can be achieved simply by adapting to the LPTV channel for a BB PLC OFDM system via microslots, on which bit loading is based on. Our solution to the problem of bit loading also uses microslots, except it makes the bit loading procedure *fully aware* of the LPTV behavior of the channel in order to achieve higher data rates, and consequently significant power savings. In this step, we carefully formulate the optimal integer bit loading problem for LPTV channels as a matroid structure and show that greedy-type algorithms yield the maximum data rate when combined with our LPTV fully aware bit loading scheme.

- **Step 2:** As for the second step, our solution involves reducing the complexity of the system by making use of representative values from microslot transfer functions, instead of using a long *combined transfer function*. Our approach considers the problem of bit and power allocation during one AC mains cycle as a series of two simpler tasks: i) finding out the power to allocate to microslots within one AC mains cycle using representative values, ii) finding out bit and power allocation for subchannels of a microslot using the power levels computed in the initial step. Our proposed schemes result in a fluctuation of the

microslot power levels within one AC cycle of the mains, rather than a constant power level for all microslots. In order to avoid peak power levels, the reduced complexity bit loading scheme enables a power clipping algorithm that limits the total power to allocate to a microslot. Additionally, we analyze the energy efficiency, microslot power level variations, and peak-to-average power ratio (PAPR) analysis for the proposed bit loading schemes. We observe that transmitting at reduced power levels can be more energy efficient, where we also have bigger gain due to the proposed bit loading schemes, and power clipping is not necessary.

Finally, LPTV-aware bit loading, reducing complexity, and power clipping can also be applied to non-optimal bit loading algorithms, since these ideas are independent of the underlying bit loading algorithm. In order to quantify the improvement for non-optimal algorithms, in addition to the optimal greedy-type algorithm, these ideas are implemented for two bit loading algorithms that are based on even-like power distribution. Our results indicate that similar gains in bit rates are achieved.

For the CE aspect, the existing CE schemes such as pilot-based and decision directed approaches have certain drawbacks. Pilot based schemes may result in high estimation overhead when pilot symbols are placed densely in the OFDM symbol (i.e. block-type pilot arrangement, all subchannels carry pilot symbols.), since the number of channels to estimate during one AC mains cycle in large. On the other hand, decision directed approaches have low estimation overhead but their channel tracking capabilities in the case of abrupt changes in the channel transfer function and presence of impulsive noise is low. First, we analyze least squares (LS) and linear minimum mean squared error (LMMSE) algorithms for CE from certain practical considerations. Next, we examine pilot based CE with various pilot geometry; block-type, comb-type, and incline-type. Incline-type pilot arrangement is considered to help reduce interpolation error inherent in comb-type pilot arrangement, and a comparison is made.

We then develop the TD analysis approach. By comparing the estimates for two consecutive OFDM symbols in a TD, the analysis determines if the channel has changed or if the impulsive

noise is present. High and low frequency metrics in TD are defined to quantify the effect of changes in the channel response and noise. TD analysis provides useful information for CE even when pilots are spaced widely apart, which results in low estimation overhead. Next, we develop a robust CE scheme that is based on TD analysis, has low overhead, and is robust to changes in the LPTV channel and noise. The proposed scheme has the ability to switch between various CE schemes based on the result of TD analysis, unlike conventioanal schemes that are based on a single scheme in all cases.

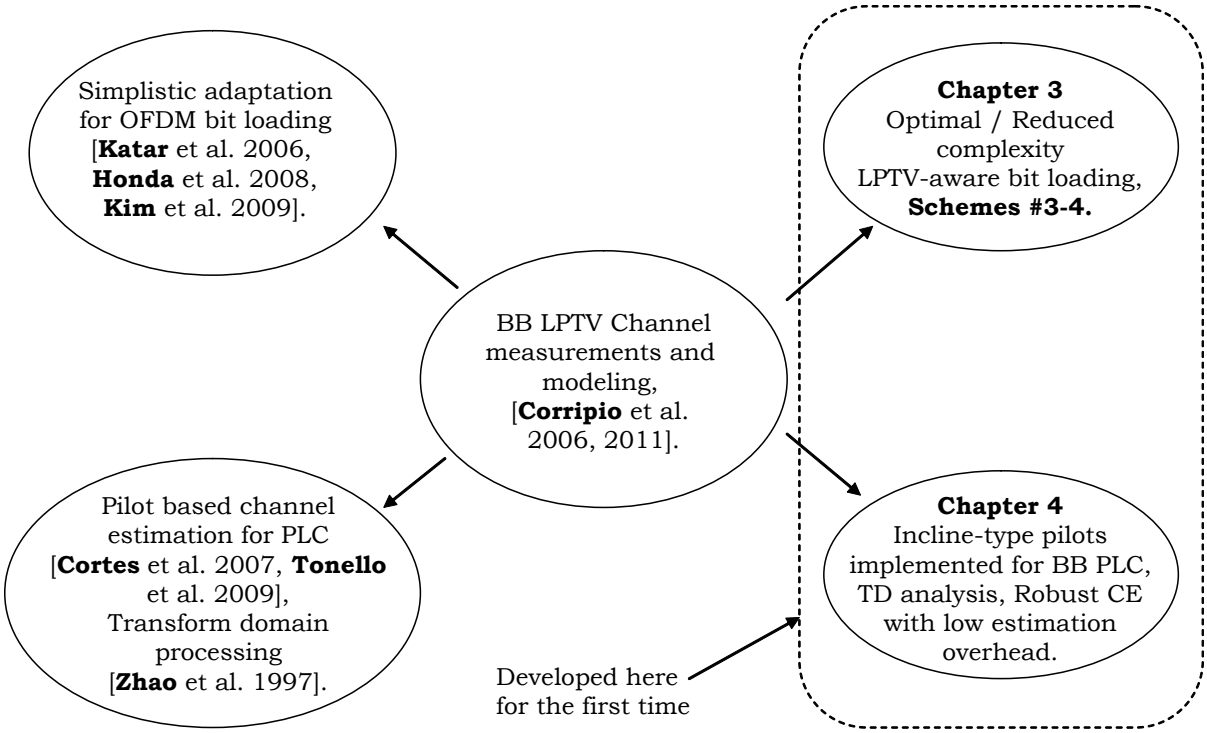

Figure 1.1. Development of optimal and reduced complexity LPTV-aware bit loading schemes.

In summary, our contributions in this work are depicted in Figure 1.1. As for the bit loading in our work, we refer to four bit loading schemes that are of interest: #1 the non-adaptation scheme, where the lowest transfer function is utilized for all microslots [7]; #2 the simplistic adaptation scheme that is not fully LPTV-aware, where distinct transfer functions are exploited for each microslot but the microslots allocations are independent of each other [8, 9, 7]; #3 the optimal LPTV-aware scheme (as pointed out above), and #4 the sub-optimal (practical) LPTV-

aware scheme, which has notably lower complexity and incorporates power clipping. Schemes #3 and #4 are central contributions of this work for the bit loading aspect.

As for the CE aspect, our contribution for pilot-based CE is the application of incline-type pilot arrangement for BB PLC channels to help reduce interpolation error. Additionally, TD analysis approach and the robust CE scheme with low overhead based on TD analysis are our main contributions for CE.

1.6 Outline of the Chapters that Follow

In Chapter 2, the channel model used to generate LPTV channels throughout this work and OFDM system are explained. The channel capacity computation for non-adaptation and adaptation cases and the formulation of the optimal bit loading algorithm based on a greedy-type algorithm is developed in Chapter 3. Next, the mechanisms that reduce the complexity of the optimal bit loading algorithm and peak power levels are explained. The performance evaluation for even-like power distribution algorithms is in Section 3.7.

In Chapter 4, various pilot arrangement for pilot-based CE are examined, and TD analysis based on pilots placed widely apart is developed. Then, a robust CE scheme with low estimation overhead is designed for LPTV channels that exploits the result of TD analysis, and is compared to pilot-based and decision-directed CE schemes. Finally, we offer conclusions in Chapter 5.

Chapter 2

System Model

In this chapter, we explain the channel model used to generate LPTV channels for analysis and OFDM system utilized in this dissertation.

2.1 Channel Model

The LPTV behavior of the BB PLC channel stems from the time-varying impedances of the electrical devices that are plugged into the power grid and it manifests itself in two distinct forms. Some devices (such as low power lamps and light dimmers) have two separate impedances during one AC mains cycle and these induce a *commuted LPTV channel*, which alternates sharply between high and low values. Other devices (such as monitors and microwave ovens) have smooth time variations in their impedances and these lead to a *harmonic LPTV channel*, which is a combination of several transfer functions that have a progressive variation within one cycle of the mains [6, 10]. Examples of commuted and harmonic channels are illustrated in Fig. 2.1.

In this work, we adopt the channel model in [11] to generate BB LPTV channels. The model generates realistic LPTV channel realizations based on a simplified parametric representation of a PLC network as shown in Fig. 2.2 from [11, Fig. 1]. The transmitter and the receiver are connected via four line segments $L_1 \dots L_4$, and three loads are connected to the power grid with

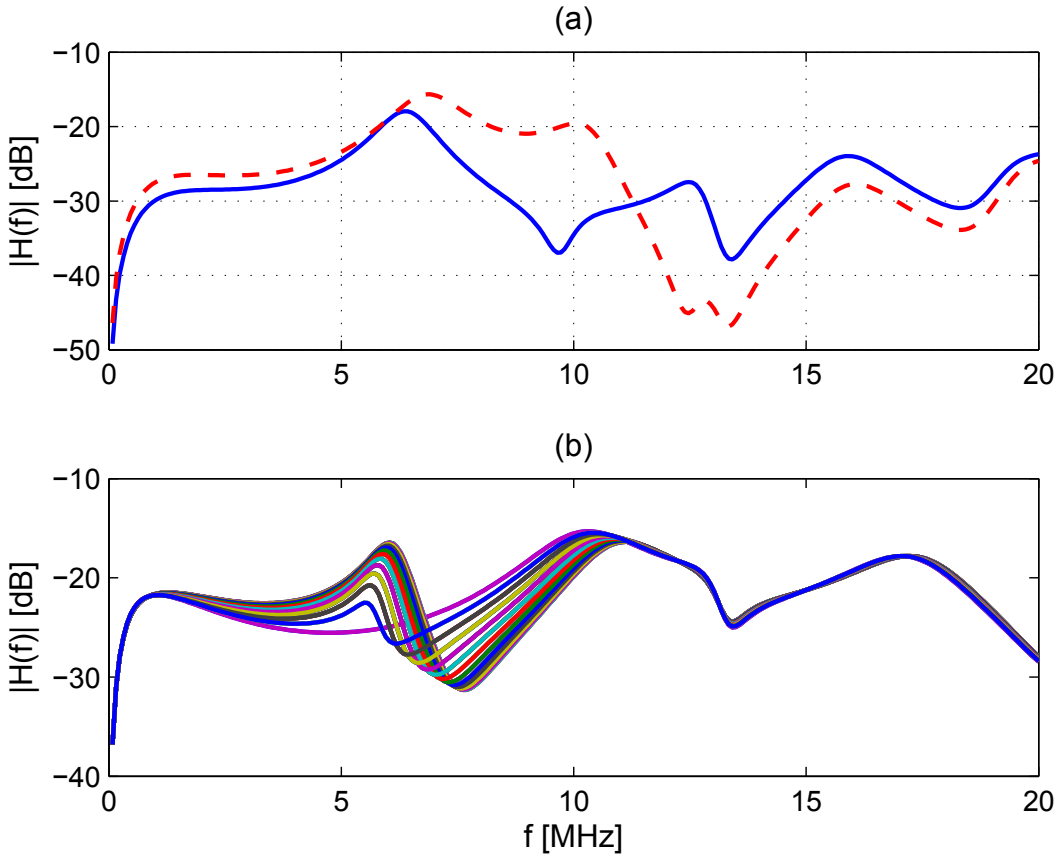

Figure 2.1. LPTV channels: (a) commuted; (b) harmonic.

distances $S_1 \ldots S_3$. The lengths of the line segments and the distances of the loads are adjusted in the model to generate channels that correspond to different topologies.

The loads are modeled to be selective in frequency and time. Three types of impedances are considered:

1. Approximately constant impedances
2. Time-invariant, but frequency-selective
3. Time-varying and frequency selective.

The constant impedances can be $\{5, 50, 150, 1000, \infty\}$, which stand for low, RF standard, similar to transmission line Z_0, high, and open circuit impedances, respectively. Time-invariant and

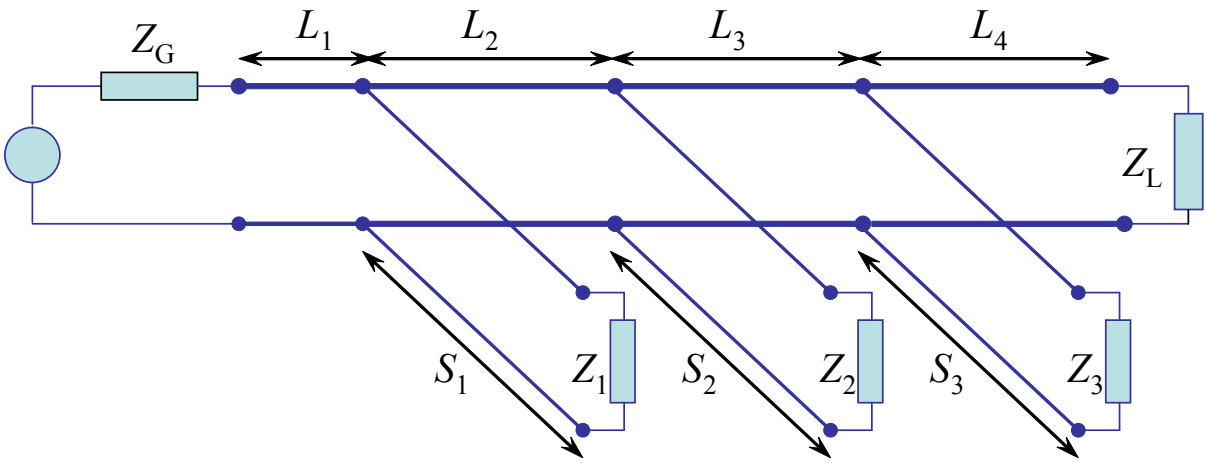

Figure 2.2. Network topology used for the channel model [11, Fig. 1]

frequency-selective impedances can be described by

$$Z(w) = \frac{R}{1 + jQ\left(\frac{w}{w_0} - \frac{w_0}{w}\right)}, \tag{2.1}$$

where R is the resistance at resonance, w_0 is the resonance angular frequency, and Q is the quality factor to determine selectivity. Finally, time varying impedances can have either commuted behavior between two values Z_A and Z_B synchronous to the AC mains cycle, or a harmonic behavior

$$Z(w,t) = Z_A(w) + Z_B(w)|\sin(\frac{2\pi}{T_0}t + \phi)|,\ 0 \le t \le T_0, \tag{2.2}$$

where Z_A is the offset impedance, Z_B reflects the amplitude of variation, T_0 is the duration of one AC mains cycle, and ϕ is the variation with respect to the mains voltage zero-crossing point.

In both commuted and harmonic channels, the AC mains cycle is divided into M microslots in time, where each microslot has a distinct transfer function, $H_j(f)$, $j \in \{0, \ldots, M-1\}$. The model in [11] uses $M = 50$, and in each microslot the spectrum is divided into N subchannels, for example, later we choose $N = 256$. $H_{j,i}$ is then the value of the channel transfer function $H_j(f)$ in the i-th subchannel, $i \in \{0, \ldots, N-1\}$.

2.1.1 Channel Parameters

In order to have some measure of the strength of the LPTV behavior for an LPTV channel, we define the *excursion parameter* for the i-th subchannel in the j-th microslot as

$$\gamma_{j,i} = \frac{|H_{j,i}|}{|H_{\text{low},i}|}, \tag{2.3}$$

where $H_{\text{low},i}$ is the lowest of all transfer functions in the i-th subchannel and is defined as

$$H_{\text{low},i} = H_{j_{\text{low}},i} : j_{\text{low}} = \underset{0 \le j \le M-1}{\text{argmin}} |H_{j,i}|. \tag{2.4}$$

A related quantity, $H_{\text{high},i}$, is defined implementing argmax instead of argmin in (2.4). We then define $[\gamma]_{\text{avg}}$ as the average of $\gamma_{j,i}$ values—in dB—over all subchannels and microslots:

$$[\gamma]_{\text{avg}} = \frac{1}{MN} \sum_{j=0}^{M-1} \sum_{i=0}^{N-1} 20 \log_{10}(\gamma_{j,i}), \tag{2.5}$$

which is an overall indicator of how far apart the microslot transfer functions $H_j(f)$ are from $H_{\text{low},i}$. The rationale behind averaging $\gamma_{j,i}$ values in dB, rather than averaging in linear scale and then converting to dB, will be justified in Section 3.4 along with our channel capacity calculations. As for the channel attenuation, we define the average attenuation for an LPTV channel as

$$[H_{\text{avg}}] = 10 \log_{10} \left(\frac{1}{MN} \sum_{j=0}^{M-1} \sum_{i=0}^{N-1} |H_{j,i}|^2 \right). \tag{2.6}$$

These parameters defined in this section help characterize LPTV channels in the following chapters based on the channel conditions (i.e. low, medium, high channel attenuation) and LPTV channel strength.

2.2 OFDM System

OFDM [12] is a multicarrier modulation that divides the available bandwidth W into many subchannels with relatively narrower width $\Delta f = W/N$ as illustrated in Fig. 2.3, where N is the number of subchannels. The signal in each subcarrier can be independently coded and modulated with the rate $1/\Delta f$, via the *bit loading* process. A small enough Δf results in a constant channel response at each subchannel. The carrier sinusoid for the subchannel i is

$$s_i(t) = \cos(2\pi f_i t), \ i = 0, 1, 2, \ldots, N-1, \tag{2.7}$$

where f_i is the mid frequency in the i-th subchannel. The symbol rate $1/T$ is chosen to be

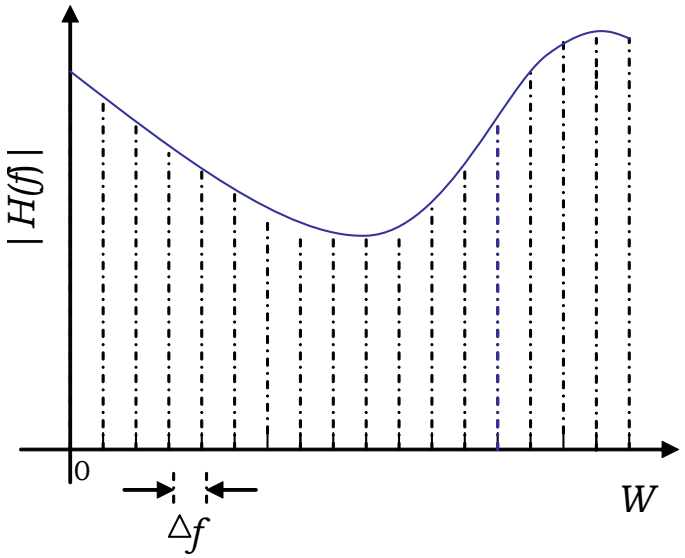

Figure 2.3. Illustration of division of available bandwidth in an OFDM system.

equal to Δf, such that the integral

$$\int_0^T \cos(2\pi f_i t + \phi_i)\cos(2\pi f_l t + \phi_l)dt = 0, \tag{2.8}$$

is zero for one symbol time, where $f_i - f_l = n\Delta f, \ n = 1, 2, \ldots, N-1$. Therefore, the subchannels are mutually orthogonal.

For an OFDM system, the symbol rate is N times less than a single carrier system that occupies the whole bandwidth W. Thus, the arrival time between two symbols is $T = NT_s$, where $T_s = 1/W$ is the symbols time for the single carrier system. When N is large, symbol arrival time can become much larger than the channel-time dispersion, which helps reduce intersymbol interference. The M-ary quadrature amplitude modulation (QAM) time domain signal on the i-th subchannel is

$$\begin{aligned} u_i(t) &= \sqrt{\frac{2}{T}} A_{ic} \cos(2\pi f_i t) - \sqrt{\frac{2}{T}} A_{is} \sin(2\pi f_i t) \\ &= \mathrm{Re}\left[\sqrt{\frac{2}{T}} A_i e^{j\theta_i} e^{j2\pi f_i t} \right] \\ &= \mathrm{Re}\left[\sqrt{\frac{2}{T}} X_i e^{j2\pi f_i t} \right], \end{aligned} \tag{2.9}$$

where

$$X_i = A_i e^{j\theta_i} \tag{2.10}$$

is the complex signal from available M-ary QAM constellation on the i-th subcarrier, and

$$A_i = \sqrt{A_{ic}^2 + A_{is}^2} \tag{2.11}$$

$$\theta_i = \tan^{-1}\left(\frac{A_{is}}{A_{ic}} \right). \tag{2.12}$$

For large N, the channel frequency response can be approximated to a constant

$$H_i(f_i) = H_i = |H_i| e^{j\phi_i}, \tag{2.13}$$

where the received symbol at subchannel i in time domain is

$$\begin{aligned} r_i(t) &= \sqrt{\frac{2}{T}} |H_i| A_{ic} \cos(2\pi f_i t + \phi_i) + \sqrt{\frac{2}{T}} |H_i| A_{is} \sin(2\pi f_i t + \phi_i) + n_i(t) \\ &= \mathrm{Re}\left[\sqrt{\frac{2}{T}} H_i X_i e^{j2\pi f_i t} + n_i(t) \right], \end{aligned} \tag{2.14}$$

where $n_i(t)$ is the additive noise in the i-th subchannel. At the receiver, assuming CE is done a priori, the received signal can be demodulated by cross-correlating the received symbol at i-th subchannel with two basis functions

$$\psi_1(t) = \sqrt{\frac{2}{T}}\cos(2\pi f_i t + \phi_i), \quad 0 \le t \le T$$
$$\psi_2(t) = -\sqrt{\frac{2}{T}}\sin(2\pi f_i t + \phi_i), \quad 0 \le t \le T, \tag{2.15}$$

and sampling at T. The received signal vector is then

$$y_i = (|H_i|A_{ic} + \eta_{ir},\ |H_i|A_{is} + \eta_{ii}), \tag{2.16}$$

where

$$\eta_i = \eta_{ir} + j\eta_{ii} \tag{2.17}$$

is the noise expressed as a complex number. y_i can also be expressed as a complex number

$$Y_i = H_i X_i + \eta_i. \tag{2.18}$$

The channel effect can be undone by

$$Y_i' = \frac{Y_i}{H_i} = X_i + \eta_i', \tag{2.19}$$

where

$$\eta_i' = \frac{\eta_i}{H_i}. \tag{2.20}$$

The detector then can compute the distance between Y_i and possible QAM constellation points, and selects the signal with the shortest distance. The resultant OFDM system with the implementation of two cross-correlators for each subchannel requires $2N$ cross-correlators, or 2N matched filters at the demodulator, and $2N$ parallel filters at the modulator. The system can rather be implemented by the equivalent discrete Fourier transform (DFT) and its inverse, or

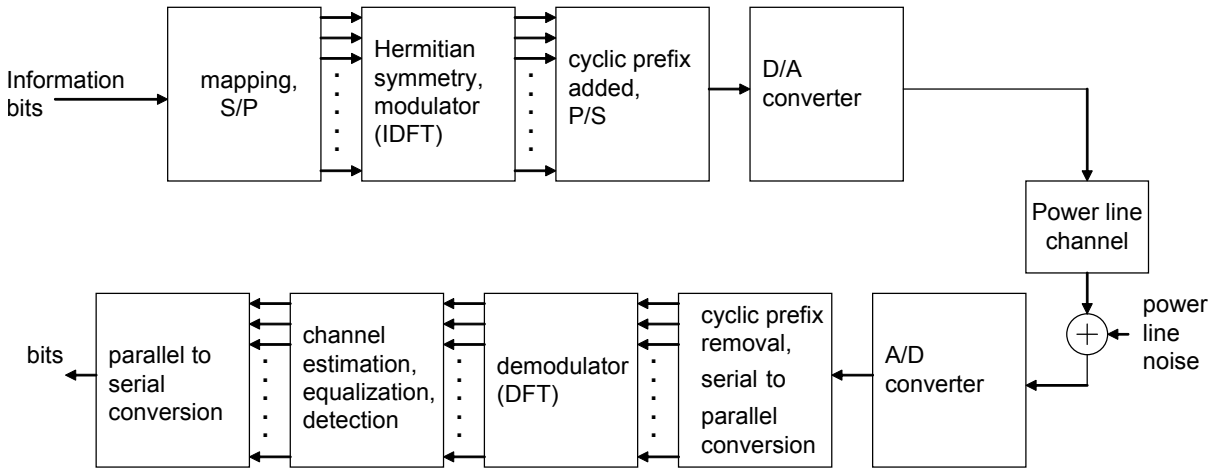

Figure 2.4. Illustration of an OFDM system for PLC.

its efficient implementation fast Fourier transform (FFT) and the inverse [12].

2.2.1 DFT Implementation of an OFDM System

The multicarrier OFDM system implemented in this work is illustrated in Fig. 2.4. Since, the available bandwidth for communication is divided into many subchannels, the equalization is a simple task at the receiver. At the transmitter, the information bits are grouped and mapped into symbols from available complex constellations at each subcarrier i, X_i. Then, the OFDM signal can be obtained by an IDFT. If N is the number of subcarriers, N complex frequency domain symbols X_i can be arranged into $2N$ Hermitian symmetric symbols. The output of the $2N$-point IDFT is then $2N$ real samples of the time domain signal. A cyclic prefix (CP) is added to the OFDM symbol in order to eliminate inter-symbol interference (ISI) due to the multipath channel. The CP must be longer than the channel delay, and is copied from samples at the end of the OFDM symbol. The OFDM signal then goes through the power line channel and power line noise is added to the signal. At the receiver, the operation at the transmitter is reversed. First, the CP is removed, then a $2N$-point DFT is performed on the received symbol. Due to the Hermitian symmetry of the DFT operation on a real sequence, only N complex symbols out of $2N$ are passed on to the next stage for CE. The received demodulated noisy

OFDM symbol $\mathbf{y}$ can be described in the frequency domain as:

$$\mathbf{y} = \mathbf{X}\mathbf{h} + \mathbf{n}, \tag{2.21}$$

where $\mathbf{X}$ is an $N \times N$ matrix with all zeros except the diagonal terms being transmitted symbols X_i, $i = 0 \ldots N-1$, $\mathbf{h}$ is the $N \times 1$ channel frequency response, and $\mathbf{n}$ is the $N \times 1$ complex additive noise.

In this work, we use $N = 256$, and QAM is implemented in each subcarrier. The channel $h[n]$ is implemented by $N_{\mathrm{B}} = 50$ real samples of a finite impulse response (FIR) filter, and the CP is the last N_{B} samples of the OFDM symbol. The transmitted signal's power spectral density is -55 dBm/Hz, and we assume that the channel transfer function remains the same for the duration of one OFDM symbol. The power line background noise is additive white Gaussian noise (AWGN), with $\mathcal{N}(0, \sigma^2)$ -110 dBm/Hz PSD, and the impulsive noise is modeled as $\mathcal{N}(0, K\sigma^2)$, where $K = 100$ [13].

Page left intentionally blank.

Chapter 3

Bit and Power Allocation

3.1 Key Points of the Chapter

- Previous work has demonstrated that improvements in bit loading can be achieved with LPTV channel adaptation via microslots in time for an OFDM system.
- The application of a power constraint that is averaged over many microslots can be exploited for further performance improvements through loading.
- Due to the matroid structure of the optimization problem, greedy-type algorithms are proven to be optimal for the new LPTV-aware bit and power loading.
- Significant gains are attained especially at reduced transmit-power levels, where the energy per bit-transmission is also low, and for poor (i.e. high attenuation) channel conditions.
- Two mechanisms are utilized to reduce the complexity of the optimal LPTV-aware bit loading and peak microslot power levels: (i) employing representative values from microslot transfer functions, and (ii) power clipping.
- The reduced complexity LPTV-aware bit loading with power clipping performs very close to the optimal LPTV-aware bit loading, which makes it an attractive option in a practical setting.

- The idea of LPTV-aware bit loading, complexity reduction via representative values, and power clipping are also applicable to non-optimal bit loading algorithms, for which similar increase in bit rates are observed.

3.2 Introduction

Two crucial characteristics of the BB power line channel are that its transfer function exhibits a linear periodically time varying (LPTV) behavior [6], and impulsive noise is present in addition to the power line background noise due to switching events; the former of these two is our focus in this chapter.

The BB power line channel characteristics have been the subject of recent study. The authors in [14] derive an algorithm to detect the transition between transfer functions of the LPTV channel to overcome the effects of periodic switching events. In [7], an adaptation scheme is presented that allows for the BB PLC cyclo-stationary noise and results in higher data rates. In [15], the effect of the LPTV channel on the performance of several commercial PLC adapters is studied. In [8], a fast bit loading algorithm for orthogonal frequency division multiplexing (OFDM) is proposed that adapts to the BB LPTV channel; similarly, in [9] a scheme is developed that adapts to the LPTV channel and the noise synchronized with the AC mains cycle. In [16], the optimal time slot design for various medium access control (MAC) procedures for a multiuser scenario is examined for BB LPTV channels.

In this chapter, we demonstrate that much higher data rates, and consequently appreciable power savings can be achieved when the bit loading algorithm is *fully aware* of the LPTV behavior of the channel. The AC mains cycle is divided into *microslots*, on which bit loading is handled. It is aware of and exploits the fact that some time microslots have better channel conditions than others; in practical terms, this suggests that the algorithm views the entire AC mains cycle when allocating bits and power, instead of allocating for individual time microslots independently of each other. We address the issue of optimal bit loading by carefully formulating the integer bit loading problem for LPTV channels and show that greedy-type algorithms yield

the maximum data rate. We also develop reduced complexity bit loading schemes that also handle possible practical considerations such as avoiding peak power levels. Finally, we include energy efficiency, microslot power level variations, and peak-to-average power ratio (PAPR) analysis.

In order to motivate our bit loading schemes listed in Section 1.5, we begin in Section 3.4 by computing the improvement in channel capacity from non-adaptive (case #1) to adaptive schemes (cases #2–4) for various LPTV channels. In Section 3.4.1, we explain and compute bit allocation for non-adaptation and simplistic adaptation schemes (cases #1–2) using a greedy-type algorithm. In Section 3.5, we elaborate the optimal LPTV-aware bit loading scheme of case #3 and we illustrate its improved performance over the simplistic adaptation scheme of case #2; we also explore the energy efficiency of the proposed bit loading algorithm and the variation of the microslot power levels over one AC mains cycle. The optimal algorithm is a critical reference, but it has a certain amount of complexity and it is oblivious to possible constraints on peak power levels. Because of these issues, in Section 3.6 we develop the sub-optimal reduced complexity LPTV-aware bit loading with power clipping of case #4 and demonstrate that its performance is very close to that of case #3. Next, we demonstrate that LPTV-aware bit loading, complexity reduction and power clipping are also suitable for non-optimal bit loading algorithms and significant gains in bit rates can be achieved. Two non-optimal bit loading algorithms that are based on the idea of even distribution of power for a limited number of good (i.e. low attenuation) subchannels are considered in Section 3.7. Finally, Section 4.6 summarizes our findings.

3.3 Channel Parameters

In this chapter, we employ three commuted channels and three harmonic channels for which the type, frequency range, $[\gamma]_{\text{avg}}$, and $[H_{\text{avg}}]$ values are shown in Table 3.2. We consider 1 MHz transmission bands for which, utilizing the model from [11], the periodic time variance is significant and matching to those observed in measurements in [14, 15, 8], where channels vary

significantly over 2–30 MHz band. The generated channels are comparable to each other in terms of $[\gamma]_{\text{avg}}$, and $[H_{\text{avg}}]$, and results similar to the ones obtained in the following sections would be observed for channels in the typical BB PLC 2–30 MHz range with comparable $[\gamma]_{\text{avg}}$, and $[H_{\text{avg}}]$. We note that the extent of the LPTV behavior is a function of the loads and topologies of the power line network. In situations where the LPTV behavior is weak, the improvements in capacity and bit loading that we present below may not be attainable.

Table 3.1. Channel Parameters

Channel #	Type	$[\gamma]_{\text{avg}}$	$[H_{\text{avg}}]$	Frequency Range (MHz)
1	Commuted	3.62	-42.3	16.5 - 17.5
2	Commuted	3.69	-53.3	16.5 - 17.5
3	Commuted	3.68	-70.2	16.5 - 17.5
4	Harmonic	3.67	-50.6	7.95 - 8.95
5	Harmonic	3.67	-60.6	7.95 - 8.95
6	Harmonic	3.67	-77.6	7.95 - 8.95

3.4 Channel Capacity

For the channel capacity computation, we recognize two cases for LPTV channels: non-adaptation (case #1) and adaptation (cases #2–4). That is, we compute the data rate achievable taking the communication-system constraints into account and refer to this value as capacity, which is also known as constrained channel capacity. For the non-adaptation case, $H_{\text{low},i}$, $i \in \{0, \ldots, N-1\}$ is utilized as the transfer function for each microslot when computing the channel capacity, because designing for the poorest channel is required to guarantee reliable communication in each microslot. For the adaptation case, on the other hand, distinct microslot transfer functions $H_j(f)$ are put into use for the capacity calculation in each microslot. More specifically, considering OFDM with N subcarriers, $H_{j,i}$, $i \in \{0, \ldots, N-1\}$, are employed. We assume the noise is additive white Gaussian noise (AWGN) with N_0[1] power spectral density

[1]Generalizations to include colored and cyclo-stationary noise, as often experienced in PLC, are straightforward in that their presence can be accounted for by the transfer factors $H_{j,i}$. More specifically, if the colored

(PSD) of -110 dBm/Hz, where the transmitted signal's PSD is -55 dBm/Hz. The capacity of the j-th microslot then can be calculated via

$$C_j = W \sum_{i=0}^{N-1} \log_2 \left(1 + \mathrm{SNR}_{j,i}\right), \tag{3.1}$$

where W is the subchannel bandwidth and $\mathrm{SNR}_{j,i}$ is the signal-to-noise ratio (SNR) in the i-th subchannel of the j-th microslot and is defined as

$$\mathrm{SNR}_{j,i} = P_{j,i} \frac{|H_{j,i}|^2}{N_0 W}, \tag{3.2}$$

and $P_{j,i}$ is the power allocated for the i-th subchannel of the j-th microslot. For simplicity, for the capacity considerations in this section, the available power is distributed evenly across all microslots and subchannels in order to probe the effect of the LPTV behavior.[2] Hence, in (3.2), $P_{j,i}$ is the same for all subchannels and the only variation is with $H_{j,i}$. The average system capacity for one cycle is then

$$C_{\mathrm{avg}} = \frac{1}{M} \sum_{j=0}^{M-1} C_j. \tag{3.3}$$

For the commuted channel case, C_j takes only two distinct values in (3.1) when calculating C_{avg} in (3.3). We denote these two capacities as C_{high} and C_{low}, and δ as the fraction of microslots with C_{high}. By use of these terms, the average system capacity of (3.3) for the commuted channel case can be expressed simply as

$$C_{\mathrm{avg}} = \delta C_{\mathrm{high}} + (1 - \delta) C_{\mathrm{low}}. \tag{3.4}$$

and cyclo-stationary noise statistics (variances) are estimated along with the channel gain, they can be incorporated into the bit loading schemes by scaling the channel gain $|H_{j,i}|$ accordingly. Their presence may change the amount of improvement in bit loading, but if they are considered, the proposed schemes will still be effective. Hence, the following discussion also applies to this generalized case.

[2]The even distribution of power is not optimal when the actual bit loading is done because of the integer constraint on bits; however, our capacity results here give strong motivation for the bit loading schemes that follow.

The above formula assumes a fast transition between the transfer functions of microslots with C_{high} and C_{low}. In reality with slower transitions, a conservative treatment for reliable communication is to count the microslots in which the high/low transition is taking place as belonging to C_{low}.

Because channel capacity is computed as the average of logarithms [as in (3.1) and (3.3)], we are also motivated to average the excursion parameter over logarithms, i.e. $[\gamma]_{\text{avg}}$ in (2.5). In fact, because $\gamma_{j,i}$ is the ratio of $|H_{j,i}|$ and $|H_{\text{low},i}|$, which are employed in the adaptation and non-adaptation cases, respectively, $[\gamma]_{\text{avg}}$ is a very meaningful parameter related to the improvement in channel capacity and bit loading due to adaptation [17].

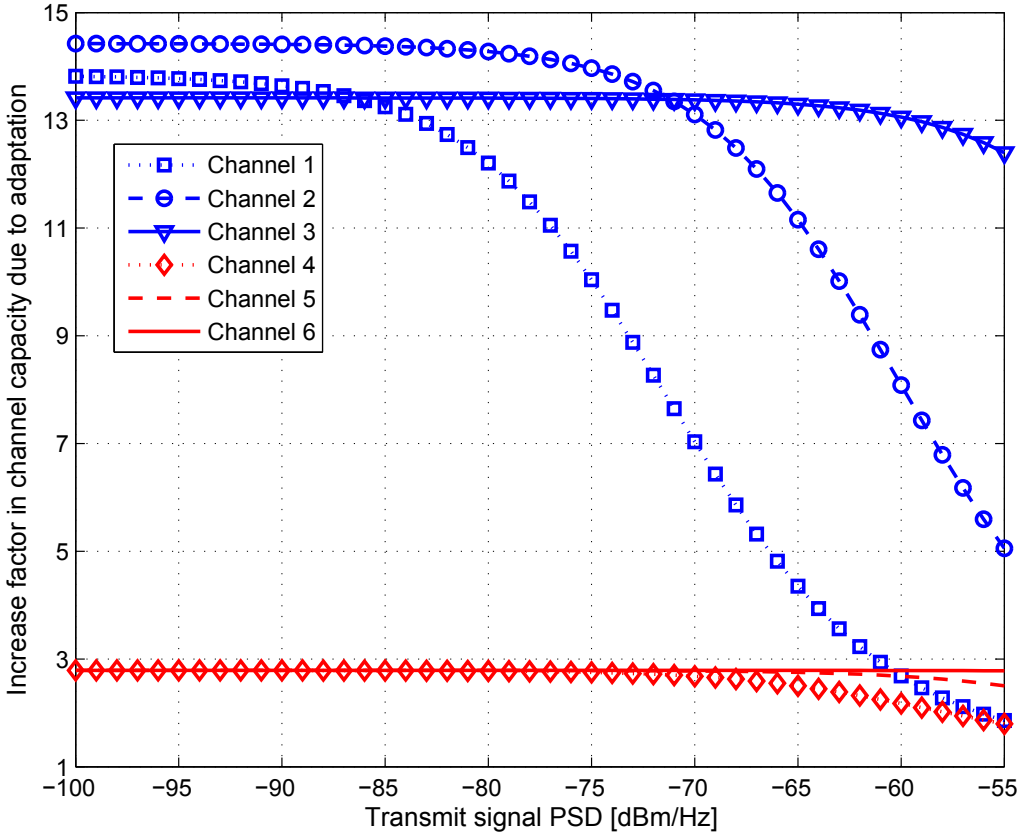

Figure 3.1. Increase in channel capacity due to channel adaptation for commuted and harmonic channels.

The increase in capacity of the six LPTV channels in Table 3.2 due to channel adaptation is illustrated in Fig. 3.1. We define the *increase factor* as the ratio of the channel capacity for the adaptation case to the channel capacity for the non-adaptation case. For a similar $[\gamma]_{\text{avg}}$ value, the capacity increase is mostly higher for channels with poor channel conditions (i.e. high attenuation). The increase in capacity for a channel is also non-decreasing for decreasing transmit signal PSD. This suggests that greater improvement in bit loading can be achieved for poor channels conditions and reduced transmit signal power levels. We also notice a greater increase for commuted channels compared to harmonic channels for most cases. The reason for this behavior is the compactness of the harmonic channels compared to commuted channels for a given $[\gamma]_{\text{avg}}$. In other words, the divergence between $H_{\text{high},i}$ and $H_{\text{low},i}$ for harmonic channels is smaller than that for commuted channels.

3.4.1 Greedy Algorithm for Optimal Bit Allocation

The well known water filling algorithm for bit loading maximizes the channel capacity for band-limited AWGN channels. However, the water filling method is not optimal in the sense that it does not guarantee integer bit loading. It allows the resultant number of bits to take non-integer values, which is not practical for a real OFDM system. The necessary and sufficient conditions for optimal bit allocation in multicarrier modulation systems, and the optimality of greedy algorithms for bit loading was introduced in [18]. In this work, we follow the approach in reference [19] to prove the optimality of greedy algorithms for bit loading in LPTV channels. Consider the following maximization:

$$\max_{\{b_i, i=0,\ldots,N-1\}} B_{\text{tot}} = \sum_{i=0}^{N-1} b_i, \tag{3.5}$$

subject to three constraints:

$$\sum_{i=0}^{N-1} \epsilon_i \leq \epsilon_{\text{tot}}, \tag{3.6a}$$

$$\{b_i, i = 0, \ldots, N-1\} \text{ are nonnegative integers,} \tag{3.6b}$$

$$0 \leq \epsilon_i \leq \epsilon_i^{\max}, i = 0, \ldots, N-1, \tag{3.6c}$$

where b_i is the number of bits transmitted in the i-th subchannel, B_{tot} is the total number of bits transmitted in all subchannels, ϵ_{tot} is the total energy available for the OFDM symbol, and $\epsilon_i^{\max}$ is the maximum energy allowed for the i-th subchannel. Water filling solves (3.5) subject to constraint (3.6a) only, and lets b_i take non-integer values. Since all the subchannels have the same bandwidth, constraints (3.6a) and (3.6c) can also be written using the corresponding power levels for the total power available for the OFDM symbol, and the maximum allowed power level for each subchannel accordingly. The optimality of the greedy-type algorithms in solving (3.5) was shown in [19] to be due to the matroid structure of the considered optimization problem (See Appendix A and reference [19] for detailed proof). In summary, a greedy approach is optimal for searching the maximal minimum-weight member of a matroid, and the bit loading problem in question represents a matroid structure as follows. Let S be the set of all possible (k, i) pairs, where the (k, i) stands for the k-th bit conveyed in i-th subchannel, and k does not exceed a certain maximum $b_i^{\max}$ in each subchannel by translating (3.6c) on $\epsilon_i^{\max}$ into an equivalent constraint on $b_i^{\max}$. Similarly, let $\mathfrak{I}$ be the collection of all subsets of S, for which the number of elements in each subset is less than or equal to a certain maximum c, the cardinality of the subset. Each member of $\mathfrak{I}$ represents a particular bit allocation pattern for the OFDM system with total bit transmission not more than c. When the weight for each element (k, i) in S is defined as the excess energy required to transmit k-th bit in the i-th subchannel, the greedy algorithm ends up with the bit loading pattern with minimum energy for a given cardinality c. Since B_{tot} is not known initially for given constraints (3.6a) and (3.6c), the greedy algorithm starts with $B_{\text{tot}} = 0$, and increments B_{tot} at each step as long as the constraint (3.6a) or (3.6c) is not violated.

In the context of the LPTV channels, analogous to the above defined problem, we define the optimization problem for the j-th microslot transfer function $H_j(f)$ as the maximization:

$$\max_{\{b_{j,i}, i=0,\ldots,N-1\}} B_{j,\text{tot}} = \sum_{i=0}^{N-1} b_{j,i}, \tag{3.7}$$

where $b_{j,i}$ is the number of bits allocated to i-th subchannel of the j-th microslot, subject to the following constraints:

$$\sum_{i=0}^{N-1} P_{j,i} \leq P, \tag{3.8a}$$

$$\{b_{j,i}, i = 0, \ldots, N-1\} \text{ are nonnegative integers,} \tag{3.8b}$$

where $P_{j,i}$ is the power allocated for the i-th subchannel of the j-th microslot, and P is the total power available for each microslot. Here, we have a total power constraint for a microslot, and the integer bit loading constraint for the maximization problem. Similar to (3.5), for the (k, i) pair, we formulate the weight function as the excess power required to convey the k-th bit in the i-th subchannel as

$$w_j(k, i) = P_{j,i}(k) - P_{j,i}(k-1),\ 1 \leq k \leq b_{j,i}^{\max},\ P_{j,i}(0) = 0, \tag{3.9}$$

where $P_{j,i}(k)$ is the power required to convey k bits in the i-th subchannel of the j-th microslot, and $b_{j,i}^{\max}$ is the maximum number of bits conveyable by i-th subchannel of the j-th microslot. For the sake of simplicity, by assuming $b_{j,i}^{\max}$ to be sufficiently large, we allow $b_{j,i}$ to be as large as it can be for a subchannel, while maintaining the matroid structure of the problem and the greedy-type nature of the solution to the maximization in (3.7). In practice, BB PLC standards allow transmission of up to 10–12 bits per sub-channel [5, 3, 4]. For the generated LPTV channels, $b_{j,i}^{\max}$ turns out to be less than 12 bits for most cases including high transmit power levels (i.e. -55 dBm/Hz). Since $b_{j,i}^{\max}$ gets smaller for lower data rate tone maps with reduced power levels, it is less than 12 bits per subchannel at reduced power levels. This leads to a modified algorithm that can be used for reduced power levels, and is slightly simpler (see Algorithm 1), which does not put a limit on $b_{j,i}^{\max}$. For both (3.5) and (3.7), the greedy-type algorithm works in an iterative fashion, and at each step, it looks for the (k, i) pair that has the minimal weight $w_j(k, i)$. In other words, it looks for the subchannel that requires the least amount of power to add one more bit.

This optimization can also be identified as a knapsack problem, where, for a given set of

Algorithm 1 Greedy algorithm

Set $b_{j,i} = P_{j,i} = 0$, $i = 0, \ldots, N-1$;
Set $P_{j,\text{sum}} = B_{j,\text{tot}} = 0$;
Set $\Delta P_{j,i} = w_j(1, i)$, $i = 0, \ldots, N-1$;
while $(P_{j,\text{sum}} < P)$ **do**
    Find index l such that $l = \text{argmin}_{0 \le i \le N-1} \Delta P_{j,i}$;
    Update $P_{j,\text{sum}} = P_{j,\text{sum}} + \Delta P_{j,l}$;
    if $(P - P_{j,\text{sum}}) \ge 0$ **then**,
        Set $b_{j,l} = b_{j,l} + 1$;
        Set $B_{j,\text{tot}} = B_{j,\text{tot}} + 1$;
        Update $P_{j,l} = P_{j,l} + \Delta P_{j,l}$;
        Update $\Delta P_{j,l} = w_j(b_{j,l} + 1, l)$;
    end if;
end while
exit.

items with a weight and a value, the goal is to fill the knapsack in such a way that the total value of the knapsack is maximized while the total weight of the knapsack does not exceed a certain maximum. In this case, the weight of each item is the power required to transmit that item, the value is the number of bits allocated, and the maximum allowed weight of the knapsack is the total power available. If the items are designed as (k, i) pairs with a weight of $w_j(k, i)$, then each item has a value of one, and maximizing the value of the knapsack is equivalent to maximizing the number of items in the knapsack. Intuitively, this can be done by prioritizing items with less weight, which brings about more items to be placed in the knapsack. This solution is analogous to the greedy approach, an example of which is the fractional knapsack algorithm in [8].

The solution to (3.5) is provided in Table 2 of [19], where the algorithm terminates when the maximum number of bits that can be transmitted due to (3.6c), are conveyed in each subchannel. This is unnecessary for the solution of (3.7) since (3.7) allows $b_{j,i}^{\max}$ be as large as it can be. For the optimization problem in (3.7), we adapted the greedy-like algorithm in Table 2 of [19] in our implementation of the greedy-like algorithm, for which the pseudocode is presented in Algorithm 1. In this algorithm, $\Delta P_{j,i}$ represents the power required to transmit one more bit in the i-th subchannel of the j-th microslot. At each iteration, the algorithm

locates the subchannel that requires the least amount of power to add one more bit, adds one bit to that subchannel, updates power allocated to that subchannel, total power allocated to all subchannels, and updates $\Delta P_{j,i}$ for that subchannel. For a given minimum symbol error rate constraint, $P_{j,i}(k)$ is calculated using the relation for quadrature amplitude modulation (QAM) symbols [12] as

$$P_e \approx 4Q\left(\sqrt{\frac{3P_{j,i}(k)|H_{j,i}|^2}{N_0(k-1)}}\right), \tag{3.10}$$

where P_e is the symbol error probability. The relation in (3.15) assumes the ideal case of no SNR margin, which accounts for the reduction in SNR due to non-ideal issues in the implementation such as imperfect synchronization. However, this does not affect the comparison of the schemes in the sections that follow.

3.4.2 Simplistic Adaptation Scheme

We now compare bit loading for LPTV channels for non-adaptation (case #1) and simplistic adaptation (case #2) schemes using the optimal greedy-type power allocation algorithm of Section 3.4.1. Parallel to the capacity comparison in Section 3.4, when computing B_{tot} for a microslot, $H_{\text{low},i}$ and $H_j(f)$ are employed as the transfer functions for the non-adaptation and simplistic adaptation cases, respectively. Also, the *increase factor* is the ratio of total number of bits conveyed B_{tot} for the simplistic adaptation case, to B_{tot} for the non-adaptation case. The increase in raw bit rate due to simplistic adaptation for commuted and harmonic channels is demonstrated in Fig. 3.2. This agrees with the increase in capacity in Fig. 3.1. More improvement in bit loading is observed in commuted channels compared to harmonic channels, and also in channels with higher attenuation compared to channels with lower attenuation. The improvement also increases with lower transmit signal PSD levels. For Channels 2, 3, 5, and 6, no transmission is taking place for the non-adaptation case below some transmit signal PSD. For instance, for Channel 6, the increase factor is infinite for a wide range of low transmit signal PSDs, where bits are only transmitted for the simplistic adaptation case. In addition, the actual raw bit rate for the non-adaptation and simplistic adaptation cases in commuted channels are

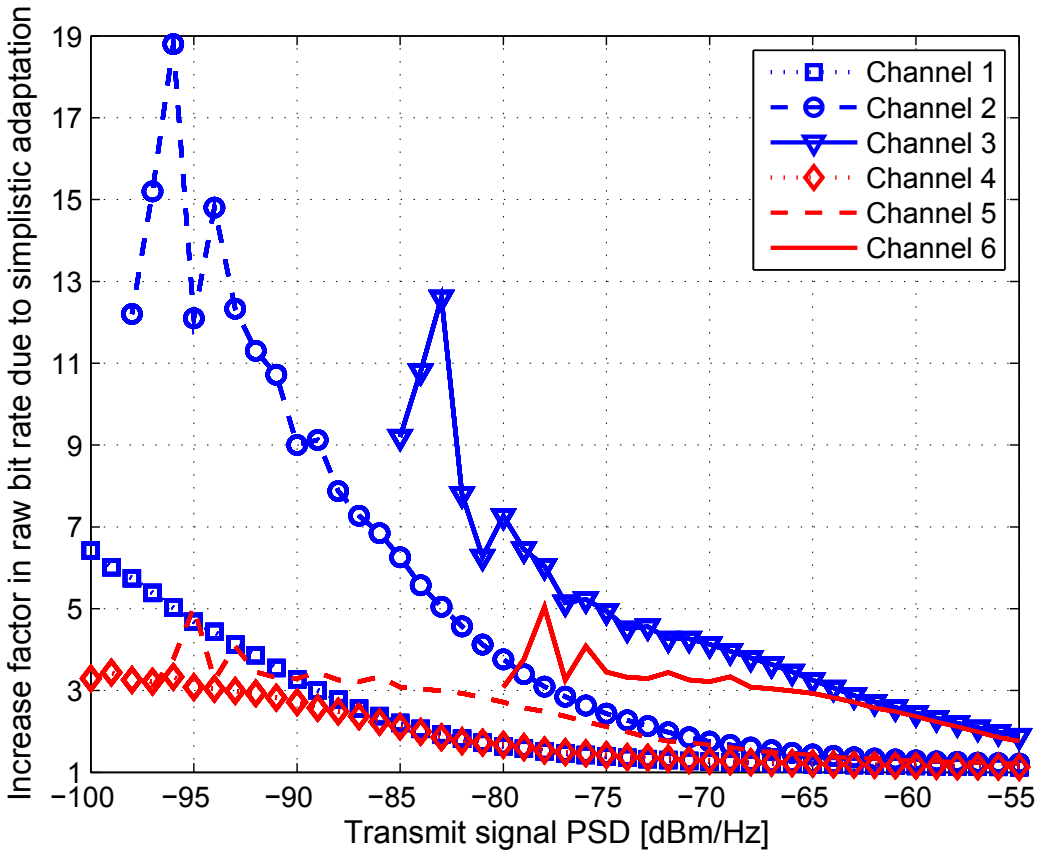

Figure 3.2. Increase in raw bit rate due to the simplistic adaptation scheme compared to the non-adaptation scheme for commuted and harmonic channels.

depicted in Fig. 3.3. The figure indicates that there is a 4–8 dB gain and significant increase in raw bit rate due to simplistic adaptation in commuted channels. The raw bit rate for non-adaptation and simplistic adaptation cases in harmonic channels are comparable to the case of commuted channels, where there is a 4–5 dB gain, and notable increase in raw bit rate due to simplistic adaptation.

3.5 Optimal LPTV-aware Bit Loading Scheme

In this section, we now formulate the proposed optimal LPTV-aware bit loading scheme for BB LPTV channels (case #3), and evaluate its performance in comparison with that of the

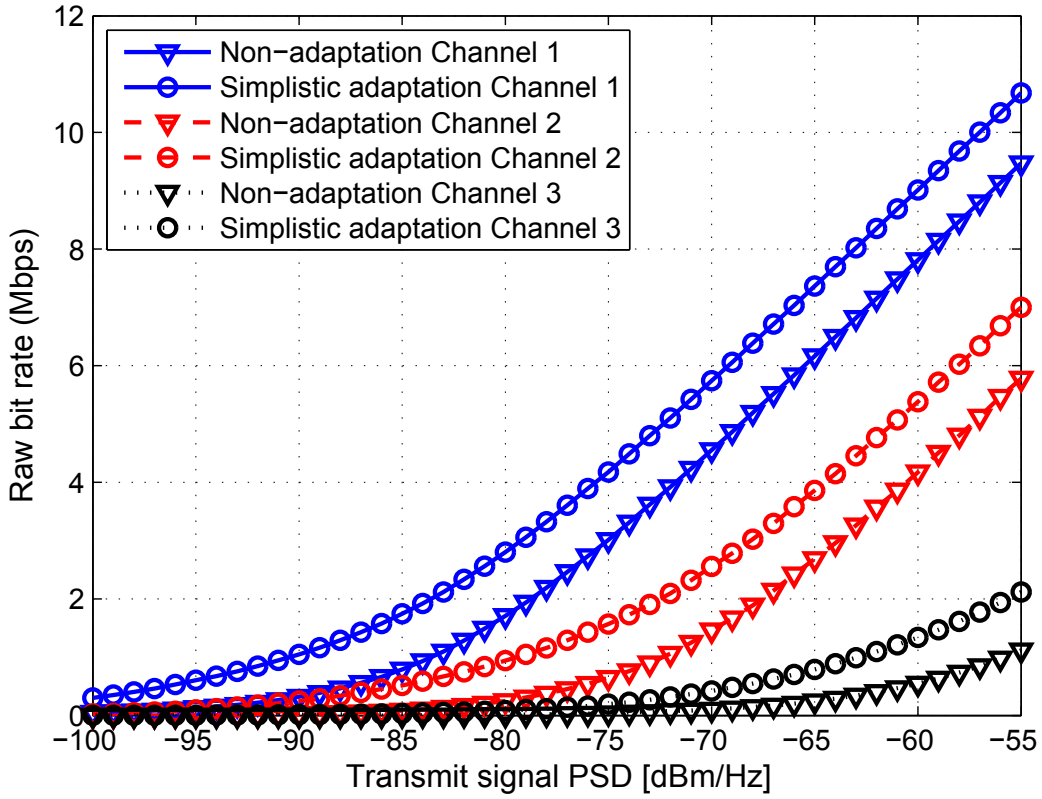

Figure 3.3. Raw bit rate for the non-adaptation and simplistic adaptation schemes for commuted channels.

simplistic adaptation scheme (case #2). We then explore the resultant microslot power levels and the energy efficiency of the proposed scheme.

3.5.1 Problem Definition

The success of water filling and greedy approaches for bit loading lies in their ability to favor the subchannels with less channel attenuation in power allocation for an OFDM system, rather than distributing the power evenly. In the simplistic adaptation case of Section 3.4.2, this property is exploited via the greedy approach only within each microslot transfer function $H_j(f)$. Hence, the simplistic adaptation case does not recognize the relative variation of the transfer function $H_j(f)$ over the AC mains cycle and regards every microslot equal in total

power allocation. That is to say, same total power P is allocated for each microslot no matter how good or bad the channel attenuation is in that microslot. To attain further improvement in bit loading, we suggest allowing different power levels for each microslot, while maintaining the average power over the AC mains cycle to be the same as for the simplistic adaptation case.

To accomplish LPTV-awareness and optimal bit loading for LPTV channels, we aggregate the two-dimensional transfer function, $H_{j,i}$, into a large one-dimensional transfer function, which we call the *combined transfer function*. The combined transfer function is of size MN, and includes all the subchannels of all microslots within the AC mains cycle. For the combined transfer function, we formulate the bit loading problem as maximizing the total bit transmission over one AC mains cycle as:

$$\max_{\{b_{j,i}, i=0,\ldots,N-1, j=0,\ldots,M-1\}} B_{\text{tot}} = \sum_{j=0}^{M-1} \sum_{i=0}^{N-1} b_{j,i}, \tag{3.11}$$

subject to the following constraints:

$$\sum_{j=0}^{M-1} \sum_{i=0}^{N-1} P_{j,i} \leq MP, \tag{3.12a}$$

$$\{b_{j,i}, i = 0, \ldots, N-1, j = 0, \ldots, M-1\} \text{ are nonnegative integers,} \tag{3.12b}$$

where constraint (3.12a) is the total power constraint[3] over the AC mains cycle, and constraint (3.12b) guarantees the integer bit loading. The constraint (3.12a) can also be regarded as the average power constraint when M is on the left hand side of the inequality. By utilizing the combined transfer function along with the total power constraint over the AC mains cycle, the system acquires the ability to favor subchannels with less attenuation not just within a microslot, but across microslots. Moreover, (3.11) has a structure that is similar to (3.7), with a longer transfer function of size MN, and a total power constraint over the AC mains

[3]In fact, it is the energy budgets that are added over time, not the power budgets. If the energy budget during one microslot is E, then it is ME for M microslots. However, since the microslots are of equal duration, and the term "power" is typically used in the context of loading, we refer to it as a power budget for the AC mains cycle instead of an energy budget.

cycle as MP from (3.12a). Hence, the proof of the optimality of the greedy-type algorithm of Section 3.4.1 in solving (3.7), is also valid for solving (3.11), with the combined transfer function and total power MP as its inputs. In other words, the matroid structure of (3.11) can be proven by the same arguments of Section 3.4.1 and Appendix A, due to the similarity of the two maximizations (3.7) and (3.11). Thus, the optimality and LPTV-awareness are both realized for bit loading within one AC mains cycle.

3.5.2 Performance Evaluation

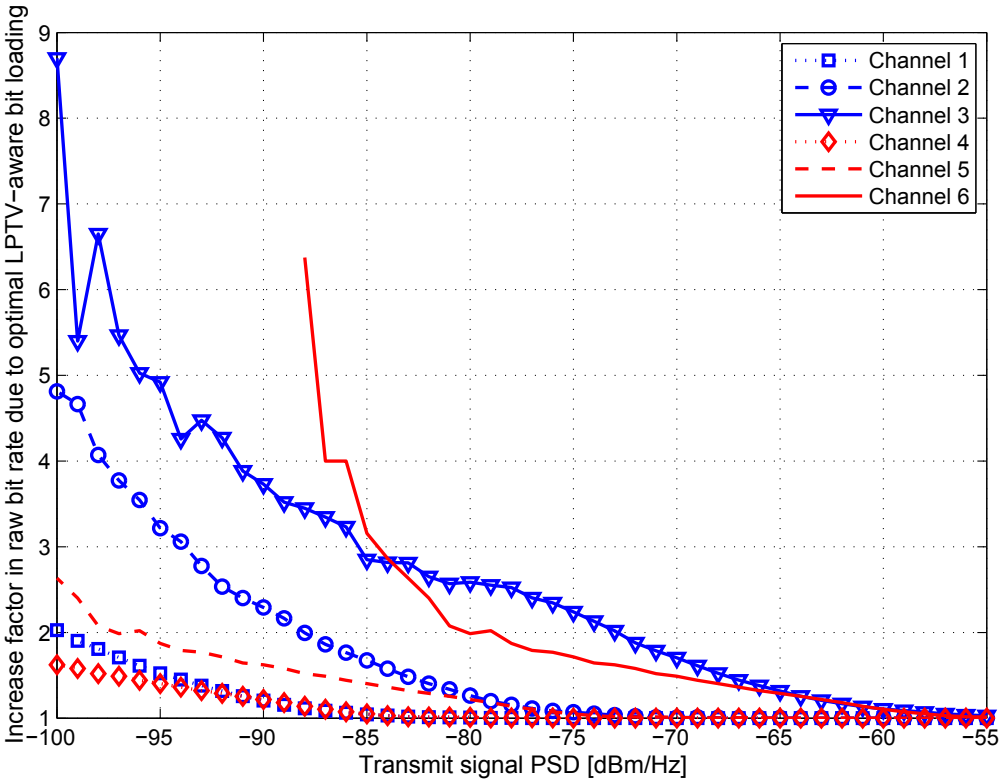

Figure 3.4. Increase in raw bit rate due to the optimal LPTV-aware bit loading compared to the simplistic adaptation scheme for commuted and harmonic channels.

In this section, we assess the performance of the optimal LPTV-aware bit loading scheme compared to the simplistic adaptation scheme. The increase in raw bit rate due to LPTV-aware bit loading for commuted and harmonic channels is depicted in Fig. 3.4. The *increase factor*

is now the ratio of total number of bits conveyed for the optimal LPTV-aware bit loading case to the simplistic adaptation case. For all transmit signal PSD values and for all channels, the increase factor in raw bit rate is greater than one. In other words, the optimal LPTV-aware bit loading is always slightly or significantly better than the simplistic adaptation scheme, depending on the transmit signal PSD. This is an anticipated result due to the optimality of the LPTV-aware bit loading of Section 3.5.1 over one AC mains cycle. In general, there is more increase in raw bit rate for lower transmit signal PSD values, and for channels with higher attenuation, which is in line with the results of improvements in channel capacity due to adaptation, and improvements in bit loading due to simplistic adaptation. Moreover, for Channel 6, below a certain transmit signal PSD level, no transmission takes place for the simplistic adaptation case. In this interval, there still is some bit transmission for the optimal LPTV-aware bit loading case. For this reason, the increase factor is infinite and there is no data point for this PSD range in Fig. 3.4. Additionally, the actual raw bit rate for the simplistic adaptation and optimal LPTV-aware bit loading schemes in commuted channels are depicted in Fig. 3.5. The figure presents that there is up to 6 dB gain due to LPTV-awareness in commuted channels depending on the channel attenuation and the transmit signal PSD. The raw bit rate for simplistic adaptation and optimal LPTV-aware bit loading schemes in harmonic channels are analogous to the case of the commuted channels, where there is up to 2 dB gain due to LPTV-awareness. The simplistic adaptation is quasi-optimal in these cases for the sample channels considered.

3.5.3 Resultant Power Levels

The key idea of the optimal LPTV-aware bit loading is to implement an average microslot power constraint over one AC mains cycle rather than a fixed power level for each microslot, and to favor microslots with better channel conditions in power allocation in order to improve bit loading. This causes fluctuation of microslot power levels over one AC mains cycle. This behavior is illustrated in Fig. 3.6 for Channel 5, where up to 2 dB more power than the average

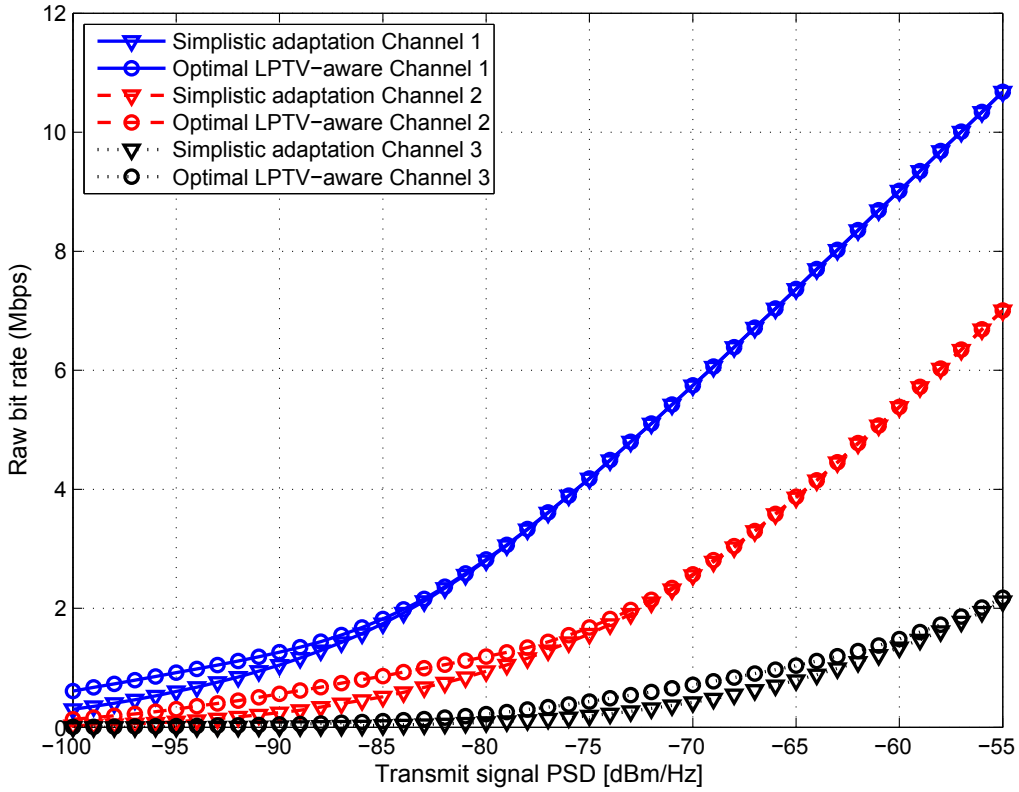

Figure 3.5. Raw bit rate for simplistic adaptation and optimal LPTV-aware bit loading schemes for commuted channels.

is allocated to some of the microslots. In this case, the resultant microslot power levels are at most -73.0 dBm/Hz, which is 2 dB higher than the average -75 dBm/Hz. As for the resultant subchannel power levels, the maximum power level is -71.1 dBm/Hz, which is 3.9 dB more than the average, due to both the greedy algorithm for bit allocation among subchannels and LPTV-awareness. Furthermore, with an increase factor of 1.05, 5% improvement in bit loading is achieved compared to the simplistic adaptation case via a small variation in the microslot power levels, essentially with the same total power consumption over the AC mains cycle. The microslot power level variation becomes less for higher transmit signal PSD values, where the distribution is more flat and little gains are achieved in the data rate. For instance, the variation is less than 0.5 dB for the same channel at -55 dBm/Hz transmit signal PSD, where the raw

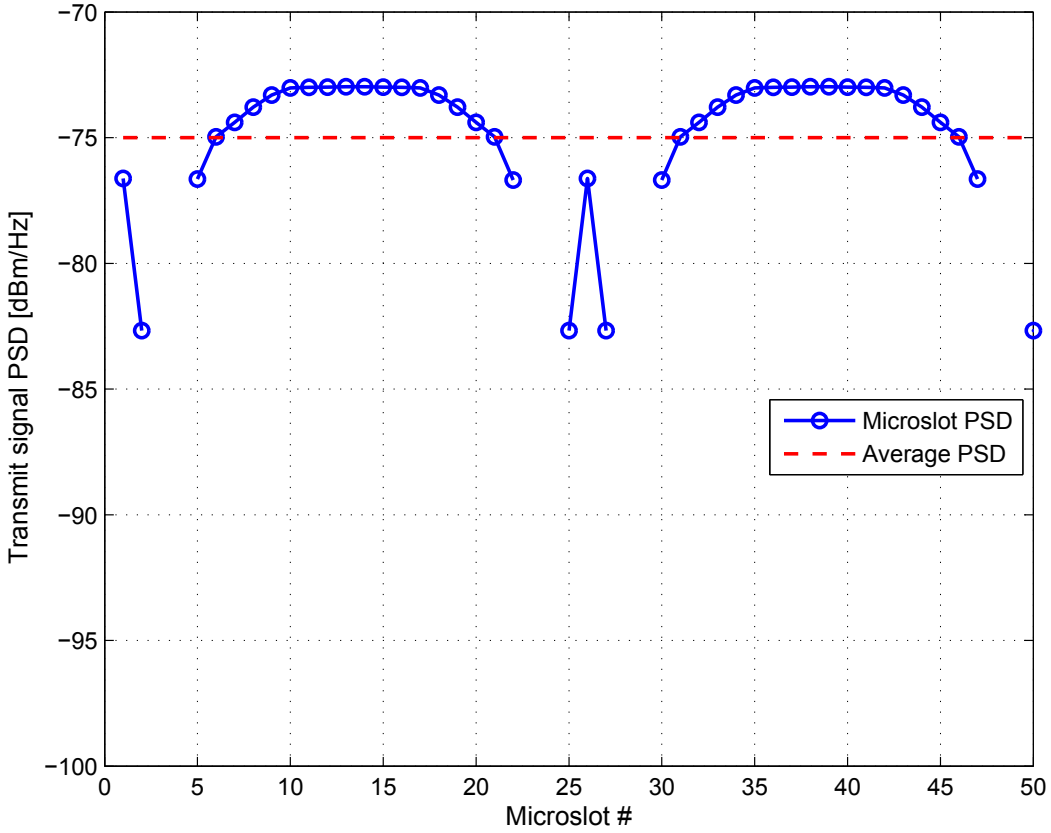

Figure 3.6. Resultant microslot transmit signal PSD levels for Channel 5, with -75 dBm/Hz average transmit signal PSD over one AC mains cycle, for the optimal LPTV-aware bit loading.

bit rate increase is little, too. On the other hand, the microslot power level variation and the improvement in the data rate is more for smaller transmit signal PSD values, where some microslots are not even assigned any power in some cases as a result of the optimal LPTV-aware bit loading.

3.5.4 Energy Efficiency

In the previous sections, we have demonstrated that significant improvement in bit loading can be accomplished due to simplistic adaptation and optimal LPTV-aware bit loading. Improvement in bit loading also implies energy saving, since energy per bit transmission is

smaller. Additionally, energy saving is a principal design criterion for lower data-rate BB PLC applications, for which the energy efficiency over a long period is more important than providing peak data rates. For such cases, transmitting at reduced power levels can be preferable for two reasons. First, when the transmission power is increased, the channel capacity is also increased, but only logarithmically. Hence, transmitting at lower power levels and data rates can be more energy efficient. Second, we can realize more improvement in bit loading due to simplistic adaptation and optimal LPTV-aware bit loading at reduced power levels as brought out in the previous sections. To illustrate this, energy per one bit transmission in commuted and harmonic channels for the case of optimal LPTV-aware bit loading is depicted in Fig. 3.7. The figure suggests that it is more energy efficient to transmit at lower transmit signal levels, along with more improvement in bit loading due to LPTV-awareness. However, this comes with a cost of reduced data rate at reduced power levels as was displayed in Fig. 3.5, which can be tolerated for lower data-rate BB PLC applications since they usually do not require high data rates. Reducing power levels also helps reduce interference to other devices, the size of the tone maps and the encoding complexity at the transmitter; it also reduces the heat dissipation that could increase the design complexity, and the range for eavesdropping [20].

3.5.5 Power Saving in BB PLC Standards

BB PLC standards IEEE 1901, ITU-T G.hn, and HPGP have mechanisms to reduce power consumption for devices in the in-home (IH) domain. For instance, IEEE 1901 standard employs reduced power states, and power management capabilities of stations in order to reduce the power consumption and electromagnetic emissions [5]. ITU-T G.hn enables *low complexity profile* nodes with reduced power consumption levels and reduced data rates. It allows dynamic and flexible PSD control, where PSD ceiling can be minimized per connection. Furthermore, devices may have scheduled inactivity inside the AC mains cycle, to reduce the power consumption [3]. Likewise, HPGP specification allows low power modes via *reduced duty cycle*, in other words *awake times* in the power save mode. It utilizes automatic reduction of the transmit

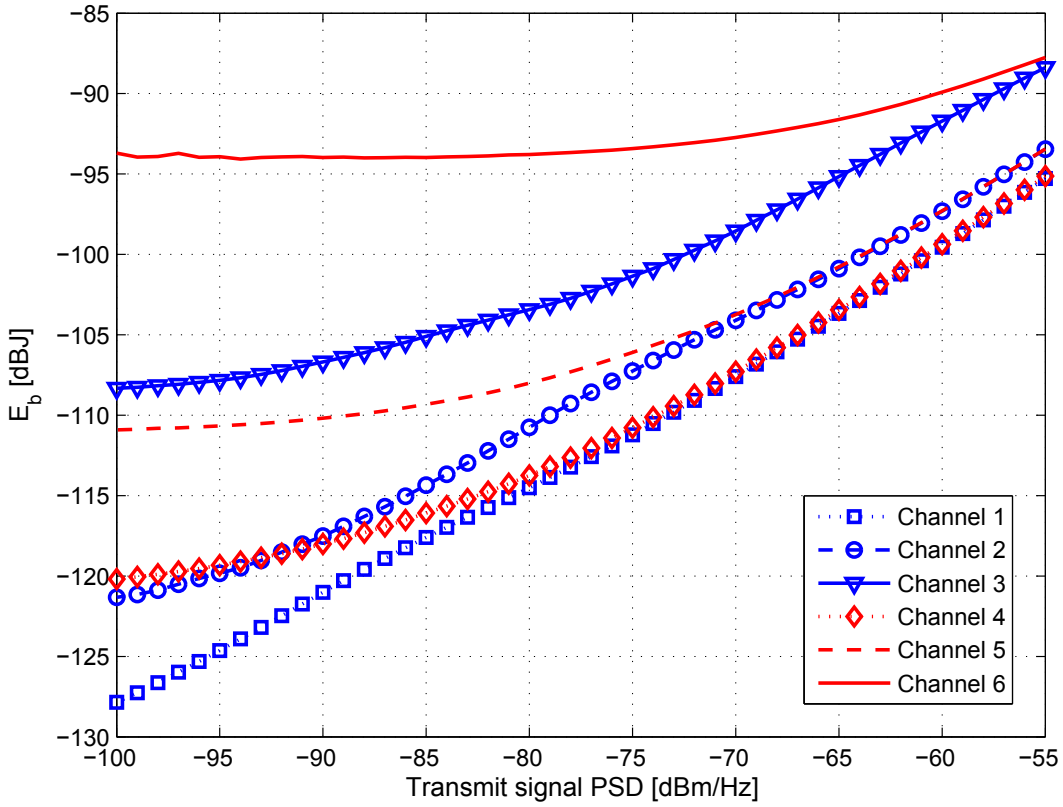

Figure 3.7. Energy per one bit transmission for the optimal LPTV-aware bit loading scheme in commuted and harmonic channels.

power as long as reliable communication is achieved, and no hidden nodes are created in the network. It employs a channel estimation procedure that allows the transmitter to obtain *tone maps* for bit loading in various intervals of the AC mains cycle, which can then be used for channel adaptation [4].

These mechanisms can be combined with the optimal LPTV-aware bit loading to reduce power consumption of BB PLC devices. The low data rate requirement for lower data-rate BB PLC allows devices to operate at reduced power levels, where the improvement in bit loading due to LPTV-awareness is high, and energy per bit transmission is low. Additionally, power save modes allow some microslots to be idle for transmission. As discussed earlier in Section 3.5.3, for reduced power levels, some microslots may not be allocated any power for transmission as

a result of the bit loading algorithm. This behavior is illustrated in Fig. 3.6, which can be used when scheduling sleep and awake times for the lower data-rate BB PLC devices for minimizing power consumption and maximizing the raw bit rate in the power save modes.

3.6 Sub-optimal Reduced Complexity LPTV-aware Bit Loading

In this section, we apply two modifications to the optimal LPTV-aware bit loading with the purpose of reducing complexity and microslot peak power, respectively. The optimal LPTV-aware bit loading maximizes the raw bit rate over the AC mains cycle, but it also increases the system complexity since the algorithm has to work on a long combined transfer function of size MN. Because of this drawback, the sub-optimal reduced complexity LPTV-aware bit loading with power clipping scheme (case #4) initially limits the problem to only allocating M microslot power levels, P_j. This requires the algorithm to work on a much smaller data set of size M initially, compared to MN, and only store M microslot power levels in the end, compared to MN subchannel bit and power values. Once the algorithm finds M microslot power values, the computational complexity of the system is the same compared to the simplistic adaptation case during the AC mains cycle.

3.6.1 Reduced Complexity LPTV-aware Bit Loading

In order to determine P_j, the transfer function for the j-th microslot, $H_{j,i}$, $0 \leq i \leq N-1$, is represented by (i.e. reduced to) a single value denoted as $\tilde{H}_j$. By doing so, the algorithm computes $\{P_j\}$ to maximize the transmission rate. Then $\{P_j\}$ is stored for use during the AC mains cycle. The other important step is to properly normalize the input power level seen by the algorithm, so that (3.15) works properly, and thus $\tilde{P} = PM/N$ is used in the algorithm. The proposed reduced complexity LPTV-aware bit loading works as follows:

1. Represent each microslot by a single value $\tilde{H}_j$.

2. Compute $\tilde{P}_j$, an N-normalized microslot power allocation, using the algorithm in Section 3.4.1 with $\tilde{H}_j$ and $\tilde{P}$ as inputs.

3. Compute the final distribution P_j as

$$P_j = \frac{\tilde{P}_j}{\sum_{j=0}^{M-1} \tilde{P}_j} PM. \tag{3.13}$$

where the normalization by N is undone and possible rounding errors are eliminated.

4. During the j-th microslot of the AC mains cycle, use the algorithm in Section 3.4.1 to allocate P_j for the subchannels in that microslot, $H_{j,i}$.

Because the algorithm works on $\tilde{H}_j$ first, instead of $H_{j,i}$ in its entirety, it reduces the complexity by a factor of N.

We propose two ways of determining $\tilde{H}_j$. The first method is to use the mean magnitude value, the maximum magnitude value, or a weighted sum of the two, which works well for mildly frequency-selective channels such as the ones in Table 3.2. However, for channels in the 2–30 MHz frequency band, a more elaborate approach is needed due to the highly frequency selective channels. For these channels, we propose to select a representative channel gain for a microslot such that its associated capacity is equal to the average subchannel capacity of that microslot, for a given transmit signal PSD. That is, we choose $|\tilde{H}_j|$ according to:

$$\frac{C_j}{N} = W \log_2 \left(1 + P_{j,i} \frac{|\tilde{H}_j|^2}{N_0 W} \right). \tag{3.14}$$

3.6.2 Power Clipping

Since the optimal LPTV-aware bit loading permits the variation of microslot power levels, when operated at close vicinity of maximum power levels, the resultant microslot power levels may exceed a certain maximum allowed power level, which is not a concern when operated at the reduced power levels for energy efficiency. In the following we describe a simple power clipping procedure for reduced complexity LPTV-aware bit loading such that maximum microslot power levels are not exceeded. Given the final power distribution for microslots P_j, and denoting the maximum power level by $P_{\max}$, proceed as follows:

1. Limit the power assigned to microslots exceeding $P_{\max}$ to $P_{\max}$.

2. Look for the highest power value that is less than $P_{\max}$ among the remaining power levels.

3. Add the excess power remaining due to clipping to this microslot, and check if the power for this microslot is less then $P_{\max}$:

   (a) If Yes, terminate the algorithm.

   (b) If No, clip the power for this microslot at $P_{\max}$, and go back to Step 2.

Here, because the bit loading algorithm favors the microslots with relatively better conditions, they are once more given preference at Step 2.

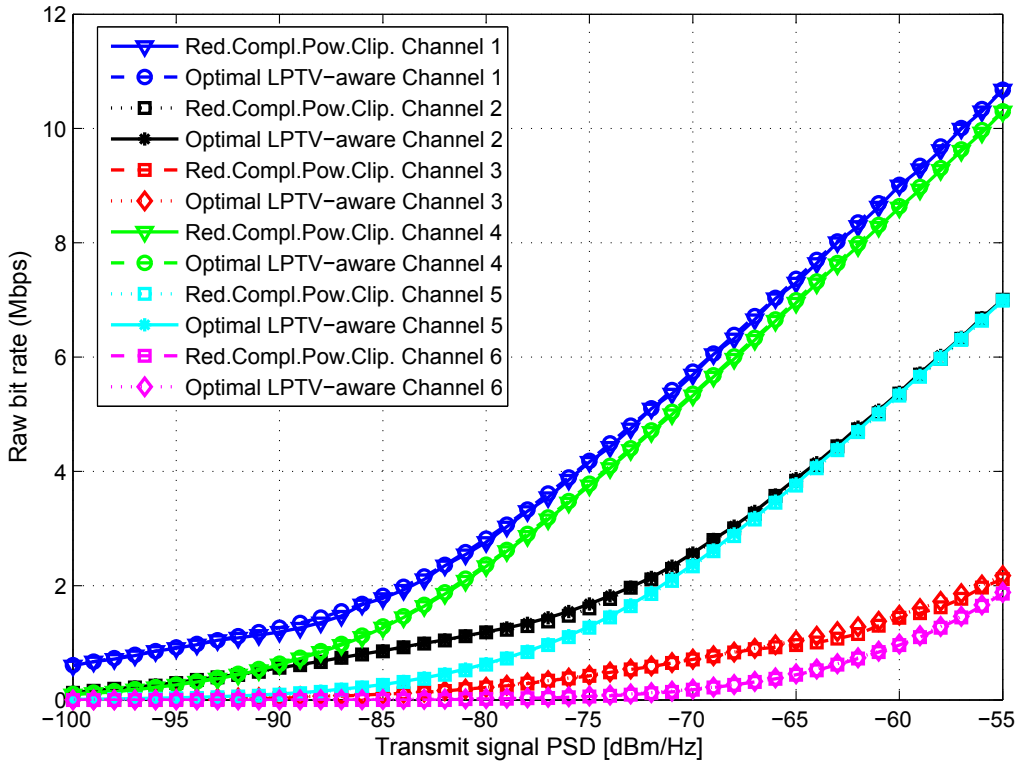

Figure 3.8. Raw bit rate for the sub-optimal reduced complexity LPTV-aware bit loading with power clipping, and the optimal LPTV-aware bit loading schemes in commuted and harmonic channels.

3.6.3 Performance Results

In this section, we compare the performance of the sub-optimal reduced complexity LPTV-aware bit loading with power clipping (case #4) with the optimal LPTV-aware bit loading of Section 3.5.1 (case #3). The raw bit rate results for commuted and harmonic channels are depicted in Fig. 3.8. For all channels and transmit signal PSD levels, the sub-optimal reduced complexity LPTV-aware bit loading with power clipping performs very close to the optimal LPTV-aware bit loading, which makes it an attractive solution for the problem of bit loading in LPTV channels. For these results, we have picked the maximum magnitude values for determining $\tilde{H}_j$, which is a good choice for especially low input transmit signal PSD levels for mildly frequency-selective channels. For the low transmit signal power levels, only the subchannels with high $|H_{j,i}|$ qualify to transmit, and in this case the maximum magnitude values for $\tilde{H}_j$ are good representatives of these channels. For highly-frequency selective channels in 2–30 MHz range, when $\tilde{H}_j$ are chosen according to (3.14), the reduced complexity Scheme 4 achieves raw bit rates close to the optimal Scheme 3, and outperforms Scheme 2 for the most transmit signal PSD levels, similar to the results illustrated in this chapter.

As for the power clipping, the resultant microslot power levels of the reduced complexity LPTV-aware bit loading are assured not to exceed a certain power level $P_{\max}$. For the results in Fig. 3.8, we choose $P_{\max}$ such that the PSD of -55 dBm/Hz is not exceeded (e.g. the transmit spectrum mask, Figs. 13–20, IEEE 1901 [5]). In general, when the average and the maximum transmit signal PSDs are equal, no improvement can be achieved exploiting the LPTV behavior if the power clipping is in place. This is the case where the transmit signal PSD is in the close vicinity of -55 dBm/Hz. However, when the average transmit signal PSD is several dB lower than the maximum allowed transmit signal PSD, as is the case for the reduced transmit signal power levels, the power clipping is not needed and the resultant microslot power allocation P_j is not adjusted by power clipping.

Additionally, the gains in raw bit rates due to the proposed schemes in previous sections would also be observed when error-correcting codes are utilized, since coding can similarly be

applied regardless of the specifics of the bit loading scheme employed.

3.6.4 Peak-to-average Power Ratio

We also examined the peak-to-average power ratio (PAPR) of the transmitted time domain OFDM signal, which is a concern for OFDM systems. OFDM systems may suffer from high PAPR, which affects the performance of the power amplifier at the transmitter. We compared the PAPR for Schemes 2 and 4. The results indicate that the PAPR is about the same for the two schemes, which also results in a similar quantizing noise. We considered PAPR for each microslot, as well as the PAPR over the whole AC cycle. For both cases, the difference between the PAPRs for Schemes 2 and 4 is less than 0.5 dB for all ranges of transmit signal PSDs. For some cases, the PAPR for Scheme 4 is smaller than Scheme 2, and for some cases, it is larger. For very low transmit signal PSDs, the PAPR for Scheme 4 can be up to 9 dB more than Scheme 2. This is due to the idle microslots, which results in a much lower average power. However, when the average power is computed considering only non-idle microslots, the PAPR is again about the same as Scheme 2. In general, the PAPR over the whole AC cycle is between 9–11 dB, which is about 2 dB larger than the PAPR computed by averaging the PAPR of individual microslots for both schemes.

3.7 LPTV-aware Bit Loading for Non-optimal Algorithms

The ideas presented in this chapter such as LPTV-aware bit loading, complexity reduction via representative values, and power clipping can be applied to not only the optimal greedy-type bit loading algorithms, but also to other non-optimal bit loading algorithms. In this section, we implement LPTV-aware bit loading and its reduced-complexity version with power clipping on two other algorithms that utilize even-like power distribution [17, 21]. The algorithms presented here are not optimal in terms of bit loading, but similar improvements in bit rate can be achieved by utilizing LPTV-aware bit loading approach.

3.7.1 Algorithm A

Algorithm A simply allocates power evenly for subchannels that can support a signal constellation of size $K_i = 4$ according to a given error-rate criterion (cf. [12]). Hence, for a given total power and a minimum symbol error rate constraint, Algorithm A is as follows:

1. Allocate power evenly to all subchannels.
2. For subchannels that cannot support $K_i = 4$, and a target error rate according to (3.15), set power to 0.
3. Allocate the total power evenly to remaining subchannels.
4. Compute unquantized K_i for the best channel using (3.15)

$$P_e \approx 4Q\left(\sqrt{\frac{3P_i|H_{j,i}|^2}{N_0(K_i-1)}}\right). \tag{3.15}$$

5. Quantize K_i for that subchannel.
6. Compute power required for that subchannel and update the remaining unallocated power.
7. Return to Step 3 and continue until all subchannels are assigned a bit and power value.

In this algorithm, K_i is allowed to be as large as it can be to support the desired P_e.

3.7.2 Algorithm B

In this section, we describe Algorithm B, which we obtained by modifying Algorithm A with some enhancements. Steps 1 and 2 of Algorithm A disqualify many subchannels of the transfer function based on the average transmit signal PSD. Since the algorithm does not take into account the possibility that excess power might be available for subchannels with moderate channel conditions, it forces the algorithm to allocate as many bits as possible to a limited portion of the spectrum. Algorithm B avoids this shortcoming in that disqualifies only one subchannel at a time. After a subchannel is disqualified, it updates the average power level

available for the remaining subchannels and discards the next subchannel based on this new increased power level. Algorithm B works as follows:

1. Allocate power evenly to all subchannels. Assume all subchannels are in the list of qualifying subchannels.
2. Find the worst subchannel among qualifying subchannels, check if it supports transmission with $K_i = 4$:
   (a) If Yes, go to Step 3.
   (b) If No:
      i. Delete that subchannel from qualifying subchannels list.
      ii. Allocate power evenly to remaining qualifying subchannels. Go back to Step 2.
3. Allocate the total power evenly to qualifying subchannels.
4. Follow Steps 4–7 of original LPTV-aware bit loading.

3.7.3 Performance Analysis

Table 3.2. Channel Parameters

Channel #	Type	$[H_{\text{avg}}]$	$[\gamma_{\text{avg}}]$
1	Commuted	-42.3	3.62
2	Commuted	-53.3	3.69
3	Commuted	-70.2	3.68
4	Harmonic	-50.6	3.67
5	Harmonic	-60.6	3.67
6	Harmonic	-77.6	3.67

In this section, we analyze the performace of the non-optimal Algorithms A and B. For both algorithms, we choose 10^{-5} as the bit-error-rate (BER) requirement, -55 dBm/Hz as the average power spectral density (PSD) of the transmit signal, and -110 dBm as the noise PSD

as practical values for Equation (3.15). Also for all cases, there are $N = 256$ subchannels and $M = 50$ microslots in the OFDM system. The parameters for the channel generated for analysis are listed in Table 3.2.

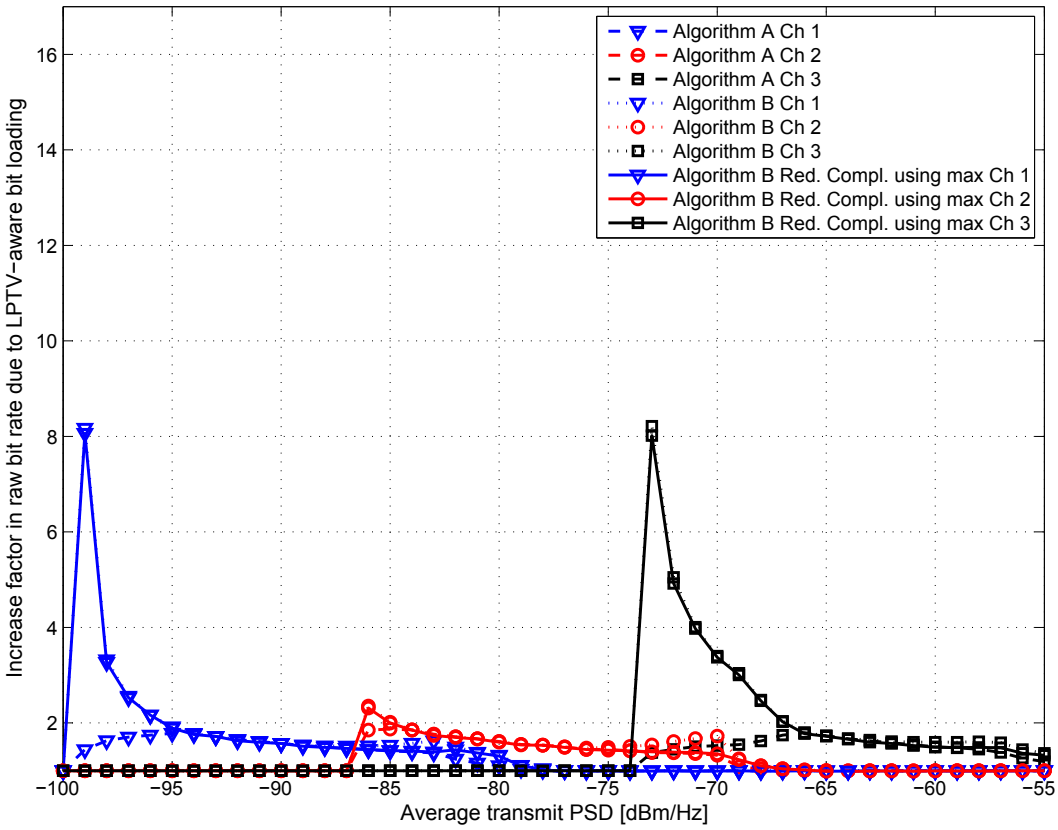

Figure 3.9. Algorithm A LPTV-aware, Algorithm B LPTV-aware, and Algorithm B reduced complexity LPTV-aware bit loading with power clipping using the maximum magnitude values for $\tilde{H}_j$ for commuted channels.

The results for the comparison of: (i) Algorithm A LPTV-aware, (ii) Algorithm B LPTV-aware, and (iii) Algorithm B reduced complexity LPTV-aware bit loading with power clipping, for commuted and harmonic channels are depicted in Figs. 3.9 and 3.10, respectively. For both commuted and harmonic channels, Algorithm B LPTV-aware bit loading outperforms the Algorithm A LPTV-aware bit loading in all cases. Also, Algorithm B reduced complexity

LPTV-aware bit loading with power clipping performs very close to Algorithm B LPTV-aware bit loading in all cases, and outperforms the Algorithm A LPTV-aware bit loading in most cases. For only a few input transmit signal PSD levels, Algorithm B reduced complexity LPTV-aware bit loading with power clipping performs 2–3% worse than Algorithm B LPTV-aware bit loading. Our results show that using the maximum magnitude values for $\tilde{H}_j$ is a good choice compared to the mean value. When the input transmit signal PSD is low, only the subchannels with high $|H_{j,i}|$ qualify to transmit, and in this case the maximum magnitude values in $\tilde{H}_j$ are good representatives of these channels. Also, when a weighted sum of the mean and the maximum value is chosen for $\tilde{H}_j$, the improvement is in between the two improvements when the maximum is used alone and the mean is used alone.

For all channels, we also observe peaks in the increase factor curves, beyond which no transmission is taking place because the SNR is too low. These are the power levels that only a limited spectrum of a portion of the microslots can support transmission with channel adaptation or Algorithm A LPTV-aware bit loading algorithm. For instance, for Channel 4 with -86 dBm/Hz input transmit signal PSD, for the channel adaptation case, Algorithm A disqualifies 42 of the microslots for transmission based on the given power level. With $P_j = P$, 5–6 bits in only 14–24 subchannels are transmitted in the eight remaining microslots. With Algorithm A LPTV-aware bit loading, the same spectrum is initially disqualified, but the excess power from 42 microslots is transferred to these eight microslots and eight bits are now transmitted in these same subchannels, which results in 1.50 increase factor. However, with Algorithm B LPTV-aware bit loading algorithm, since each time it disqualifies subchannels based on an updated power level, 24 microslots can support transmission. In each of these 24 microslots, 2–3 bits are transmitted in 157–256 subchannels. This better utilization of the available spectrum results in the peak improvements in all of the six LPTV channels.

When power clipping is in place, the algorithm forces the Algorithm B reduced complexity LPTV-aware bit loading not to exceed a certain power level $P_{\max}$. For the results, we choose $P_{\max}$ such that the PSD of -55 dBm/Hz is not exceeded. For instance at -55 dBm/Hz transmit

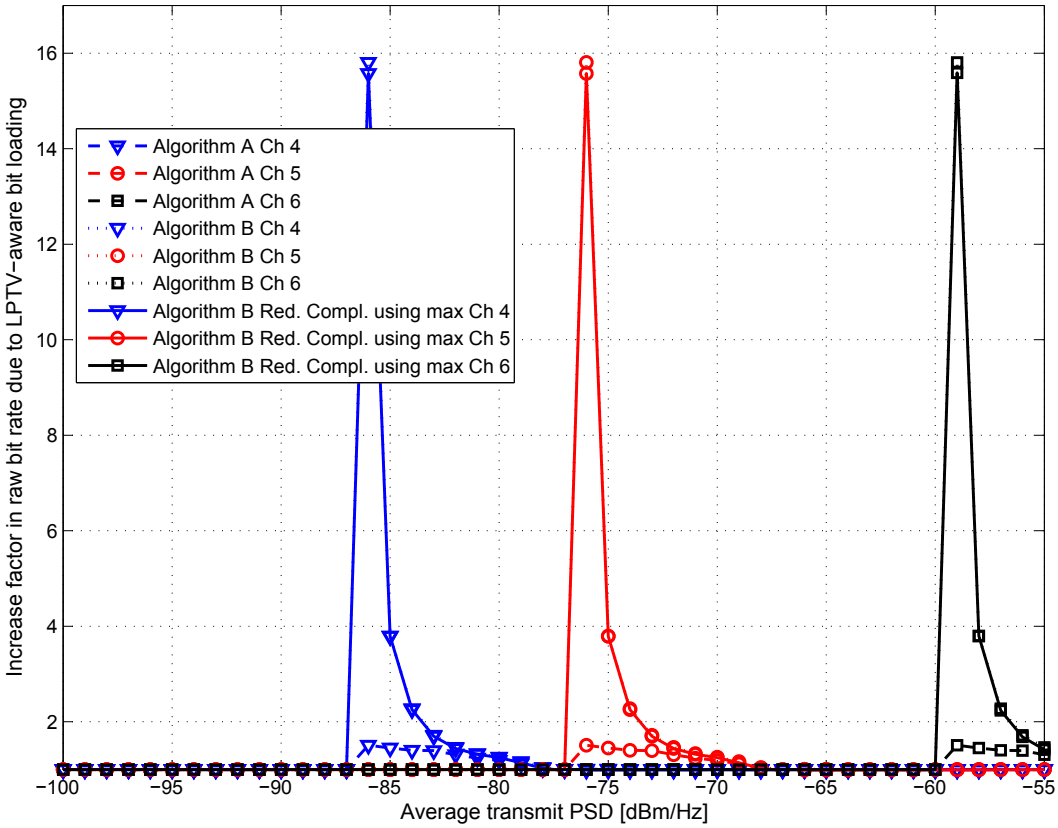

Figure 3.10. Algorithm A LPTV-aware, Algorithm B LPTV-aware, and Algorithm B reduced complexity LPTV-aware bit loading with power clipping using the maximum magnitude values for $\tilde{H}_j$ for harmonic channels.

PSD for Channel 3 and 6, P_j is forced to be the same for all microslots, and an increase factor of 1.32 and 1.42 is only due to the deployment of the enhanced algorithm as shown in Figs. 3.11 and 3.12, respectively. Still at this power level, Algorithm B reduced complexity LPTV-aware bit loading with power clipping performs better than Algorithm A LPTV-aware bit loading due to the enhanced algorithm. When the average and the maximum transmit signal PSDs are equal, no improvement can be achieved exploiting the LPTV behavior. However, when the average transmit signal PSD is lower than the maximum transmit signal PSD, as is the case for the rest of the improvement range for Channel 3 and 6, and for the remaining channels, the

power clipping does not change P_j because P_j does not exceed $P_{\max}$.

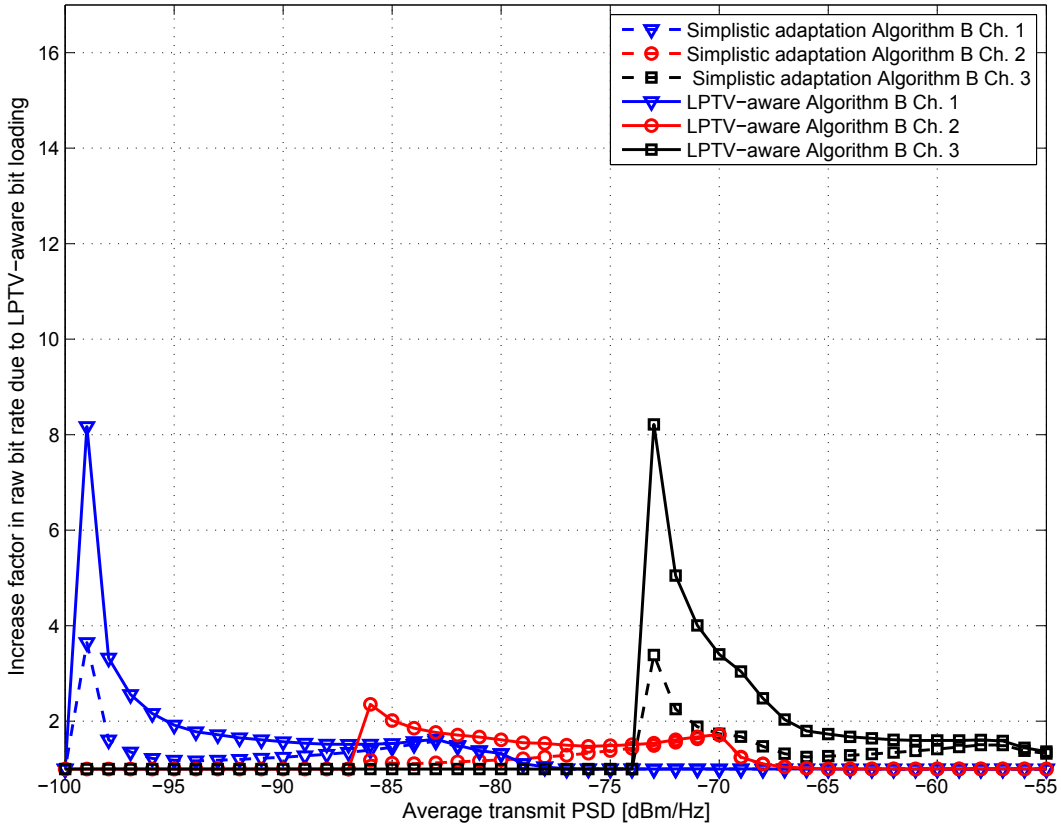

Figure 3.11. Simplistic channel adaptation with Algorithm B, and Algorithm B LPTV-aware bit loading for commuted channels.

Additionally, because Algorithm B LPTV-aware bit loading uses a modified algorithm and applies it to the combined transfer function, large increase factors we observe are due to both the enhanced algorithm, and the LPTV awareness of the algorithm. To see the effect of LPTV-awareness only, we also examined the simplistic channel adaptation case using Algorithm B. In this case, $P_j = P$, and Algorithm B is employed for all microslots. Hence, the improvement is due to the utilization of Algorithm B only. As shown in Figs. 3.11 and 3.12, significant increase factors are achieved due to LPTV-awareness in commuted and harmonic channels, respectively. However, for harmonic channels, the improvement due to LPTV-awareness is smaller than that

of the commuted channels, which is a similar result to the case for the Algorithm A LPTV-aware bit loading.

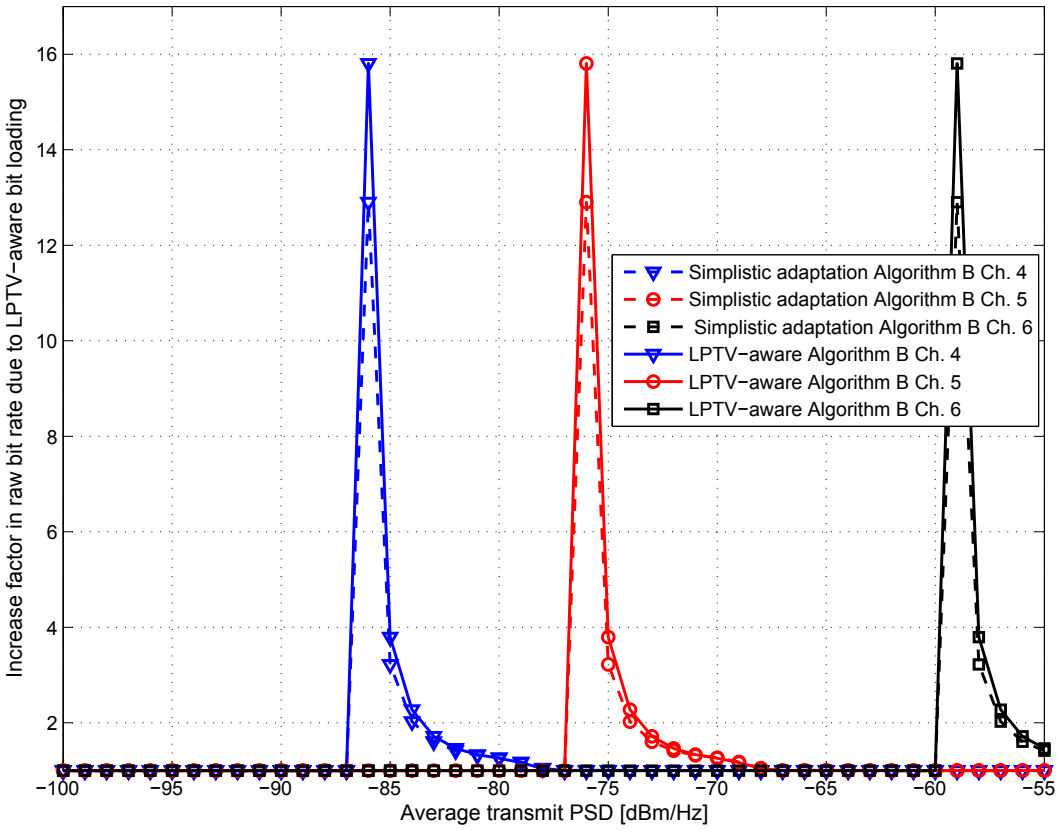

Figure 3.12. Simplistic channel adaptation with Algorithm B, and Algorithm B LPTV-aware bit loading for harmonic channels.

3.8 Summary and Conclusions

In this chapter, we examined the problem of optimal bit loading in LPTV channels for BB PLC. We demonstrated that a significant increase in channel capacity can be attained by adaptation to the LPTV channel, and the greedy-type algorithms are optimal for bit loading, when the combined transfer function and an average power constraint over one AC mains cycle is utilized. In addition, it can be more energy efficient to transmit at reduced power levels,

which is also the regime where the most significant gains in raw bit rate are achieved due to the proposed LPTV-aware bit loading. Next, we presented that when representative values from the microslot transfer functions are employed, the computational complexity of the system is greatly reduced, while at the same time preserving nearly all of the gains in bit loading. Finally, power clipping algorithms can be practical in avoiding peak power levels for the case of LPTV-aware bit loading schemes, since they allow for variation of microslot power levels. The ideas presented in this chapter are also applicable to non-optimal bit loading algorithms, for which similar increase in bit rates are observed. All of our contributions have the aim of saving power and improving bit loading appreciably for BB PLC systems with little additional complexity. The proposed schemes are suitable for both multimedia and SG-type applications, and also applicable to BB PLC standards such as IEEE 1901, ITU-T G.hn, and HPGP.

Page left intentionally blank.

Chapter 4

Channel Estimation

4.1 Key Points of the Chapter

- Incline-type pilot arrangement can be utilized for BB PLC channels to help reduce the interpolation error inherent in comb-type pilot arrangement.
- Block-type pilot arrangement can be utilized for CE, for which the overhead due to pilot symbols is high. On the other hand, decision directed approaches require less overhead, but their ability to track sudden changes in the channel is limited.
- The difference between the channel estimates of two consecutive OFDM symbols—when analyzed in a transform domain (TD)—are different in their frequency content. A change in the transfer function appears as an increase in the low frequencies, and the presence of impulsive noise appears as an increase in all frequencies in TD.
- The proposed final scheme utilizes pilot symbols placed widely apart in order to extract information about the changes in the transfer function and the power line noise via TD analysis, and exploits this information for switching between various CE schemes.
- The overhead of the proposed scheme for CE is low, and sudden changes in the channel are tracked effectively. Therefore, the effects of the LPTV channel and the impulsive noise on CE are mitigated.

4.2 Introduction

In Chapter 3, we developed optimal and reduced complexity LPTV-aware bit loading schemes for BB PLC orthogonal frequency division multiplexing (OFDM) systems to improve data rates for LPTV channels. In a practical setting, channel estimation (CE) must be done prior to bit loading for these algorithms to work properly. In this chapter, we study pilot-based and decision directed CE schemes and develop a robust CE method based on TD analysis approach.

One way to estimate the channel is to transmit a sequence known by the receiver. This is called *pilot based* (data-aided, supervised, or trained) CE, which is one of the widely used OFDM CE techniques. In this approach, pilot symbols are inserted into the OFDM symbol at certain subcarrier locations for CE. When all subcarriers carry pilot symbols (i.e. block-type pilot geometry), no interpolation is needed, but *estimation overhead* due to pilots is high. Instead, the density of the pilots can be decreased, with the cost of increase in *interpolation error* [22].

In [13], non-adaptive least squares (LS) and TD algorithms are used initially to estimate the channel at pilot locations for an LPTV channel in the presence of power line *impulsive noise*. Different interpolation techniques are used to estimate the channel for the remaining subchannels, and their performances are evaluated. The tradeoff between channel estimation accuracy and system throughput is studied in [23] for a Multi-Input Multi-Output (MIMO) OFDM system for in-home PLC. In [24], a comparison has been made for three pilot based channel estimation schemes for the indoor power line: LS, LMS, and linear minimum mean squared error (LMMSE), and in [22], different interpolation techniques (linear, cubic, B-spline, second order Gaussian, DFT [zero padding], and nearest-neighbor) for the pilot based approach are compared for the power line channel.

In this work, we first focus on various pilot arrangement schemes with the goal of reducing interpolation error, and providing better CE with low overhead and better channel tracking capability. Different from the previous work in the literature, we study incline-type pilot ar-

rangements and show that these compare favorably against block-type and comb-type (these pilot arrangement schemes are illustrated later in Fig. 4.2). LS and LMMSE estimators with linear and cubic interpolation are implemented for pilot-based CE.

Another method for CE is the *decision directed* approach, where the channel estimate from the previous symbol is used to decode the symbols, and these decisions are then utilized to update the channel estimate. In this approach, pilot symbols can be used to obtain an initial estimate, but then the changes in the channel are tracked by the decisions with no pilot symbol assistance. Hence, the estimation overhead is lower compared to the pilot based approach. However, if the channel changes abruptly, the noise level is high, or the channel is poor (high signal attenuation), the decisions can become highly inaccurate. This may result in errors in decoding the symbol, which also results in high estimation error.

Lastly, in addition to the LPTV channel, one other challenge for CE in BB PLC is the impulsive noise caused by the switching events in the power line network. Impulsive noise typically has large amplitudes compared to the background noise and it has a short duration [1].

In this chapter, after analyzing various pilot geometry for CE, we develop a transform domain (TD) analysis approach for BB PLC channels to mitigate the effects of the LPTV channel and the impulsive noise via pilot symbols placed widely apart. TD analysis examines the difference between channel estimates of two consecutive OFDM symbols in a transform domain, and detects changes in the estimate due to a change in the transfer function or noise characteristics. We then exploit the information captured by TD analysis and develop a robust CE scheme for BB PLC channels that utilizes various CE schemes based on the outcome of TD analysis. Our method is different than conventional schemes in the literature, which are based on a single approach (e.g. pilot-based with certain pilot geometry or decision directed CE) and lack the ability to take advantage of employing different schemes for different scenarios that involves abrupt changes in the channel and the noise. The proposed final scheme has small overhead and high estimation accuracy, and is able to track changes in the channel transfer function and the noise via TD analysis.

The remainder of this chapter is as follows. In the next section, we analyze pilot-based CE with different pilot geometry for an OFDM system, explain and compare LS and LMMSE schemes for CE from different perspectives, and in Section 4.4 we develop the TD analysis for CE. In Section 4.5, we investigate various cases for CE, evaluate the performance of various schemes, and explain the proposed final CE method based on this analysis. Finally, Section 4.6 summarizes our findings.

4.3 Channel Estimation

4.3.1 LS and LMMSE Estimators

For the OFDM system described in Section 2.2.1, the LS solution for CE is simply:

$$\mathbf{h}_{\mathrm{LS}} = \mathbf{X}^{-1}\mathbf{y}. \tag{4.1}$$

For the comb-type and incline-type pilot geometries, interpolation is performed for estimating the channel for non-pilot subcarriers. The LS algorithm is simple to implement, since it requires only a division operation at the receiver, and it does not require any statistical information about the channel and the noise. Another estimator is based on LMMSE, which is attained by application of the Wiener-Hopf equation [25]:

$$\mathbf{h}_{\mathrm{LMMSE}} = \mathbf{R}_{\mathbf{hy}}{\mathbf{R}_{\mathbf{yy}}}^{-1}\mathbf{y}, \tag{4.2}$$

where $\mathbf{R}_{\mathbf{hy}}$ is the cross correlation matrix:

$$\begin{aligned}\mathbf{R}_{\mathbf{hy}} &= E[\mathbf{h}\mathbf{y}^H] = E[\mathbf{h}(\mathbf{X}\mathbf{h}+\mathbf{n})^H] \\ &= E[\mathbf{h}\mathbf{h}^H\mathbf{X}^H + \mathbf{h}\mathbf{n}^H] \\ &= \mathbf{R}_{\mathbf{hh}}\mathbf{X}^H,\end{aligned} \tag{4.3}$$

and $(\cdots)^H$ is the Hermitian operator, and $E[\mathbf{h}\mathbf{n}^H]$ is zero when the channel and the noise are assumed to be uncorrelated. Similarly, the autocorrelation of the received symbol $\mathbf{y}$ can be formulated by:

$$\begin{aligned}\mathbf{R_{yy}} &= E[\mathbf{y}\mathbf{y}^H] = E[(\mathbf{X}\mathbf{h}+\mathbf{n})(\mathbf{X}\mathbf{h}+\mathbf{n})^H] \\ &= E[\mathbf{X}\mathbf{h}\mathbf{h}^H\mathbf{X}^H + \mathbf{X}\mathbf{h}\mathbf{n}^H + \mathbf{n}\mathbf{h}^H\mathbf{X}^H + \mathbf{n}\mathbf{n}^H] \\ &= \mathbf{X}\mathbf{R_{hh}}\mathbf{X}^H + E[\mathbf{n}\mathbf{n}^H] = \mathbf{X}\mathbf{R_{hh}}\mathbf{X}^H + \sigma_n^2 I, \end{aligned} \tag{4.4}$$

where I is the $N \times N$ identity matrix, and σ_n^2 is the variance of AWGN noise. By substituting equations (4.3) and (4.4) into (4.2), we obtain

$$\mathbf{h}_{\text{LMMSE}} = \mathbf{R_{hh}}\mathbf{X}^H(\mathbf{X}\mathbf{R_{hh}}\mathbf{X}^H + \sigma_n^2 I)^{-1}\mathbf{y}. \tag{4.5}$$

As seen in equation (4.5), in order to compute $\mathbf{h}_{\text{LMMSE}}$, the channel autocorrelation function and the variance of the power line noise must be known. It also requires a matrix inverse operation that increases the complexity of the scheme. There have been several studies in the literature that focus on reducing the complexity of the LMMSE algorithm, which is out of the scope of this work. LMMSE outperforms LS provided that, the $\mathbf{R_{hh}}$ and σ_n^2 are accurate. In the case where there is a mismatch between the actual values and the estimated values for these parameters, LMMSE can result in worse performance than LS depending on how big the error is for these parameters. In practice for the receiver, computing σ_n^2 is relatively easy, since it would be sufficient to compute the noise variance simply when the channel is idle. However, computing $\mathbf{R_{hh}}$ may introduce some problems. First, $\mathbf{R_{hh}}$ is usually different for different frequency bands, so if the frequency band of communication changes, $\mathbf{R_{hh}}$ must be recomputed. Second, in practice, if it is computed by averaging $\mathbf{h}\mathbf{h}^H$ over time to replace the expectation operation, a sufficient number of distinct channel transfer functions must be used for estimating $\mathbf{R_{hh}}$, such that the error is small.

In order to find the number of distinct transfer functions needed to accurately estimate

$\mathbf{R_{hh}}$, we first computed $\mathbf{R_{hh}}$ by averaging 1000 distinct transfer functions using the model described in Section 2.1. This being the actual value for $\mathbf{R_{hh}}$, we computed the estimate $\hat{\mathbf{R}}_{\mathbf{hh}}$ for different number of distinct transfer functions, and compared it to the actual $\mathbf{R_{hh}}$. The channels generated here correspond to random topologies, where the length of the line segments are from a random uniform distribution from 1–40 m. The results for the average of 50 trials are illustrated in Fig. 4.1. Our results indicate that using more transfer functions reduces the mismatch as anticipated, and for less than 50 distinct transfer functions, the error can be large, and does affect the performance of the LMMSE estimator.

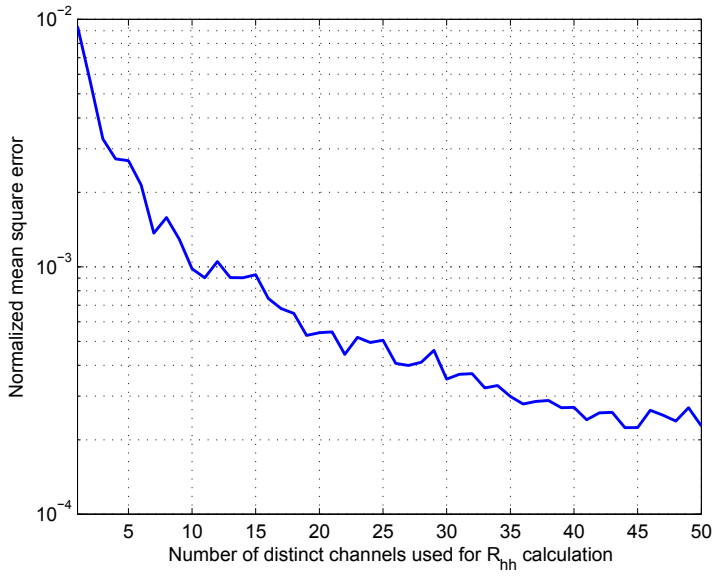

Figure 4.1. Normalized mean square error for $\mathbf{R_{hh}}$ computation using different number of distinct transfer functions.

4.3.2 Pilot-based Channel Estimation

4.3.2.1 Pilot Arrangement

For pilot-based CE, various schemes can be utilized. For the pilot-based schemes, the transmitted symbols at certain subcarriers are known by the receiver. Different pilot geometry can be utilized for CE as illustrated in Fig. 4.2. For the block-type pilot geometry, all subchannels

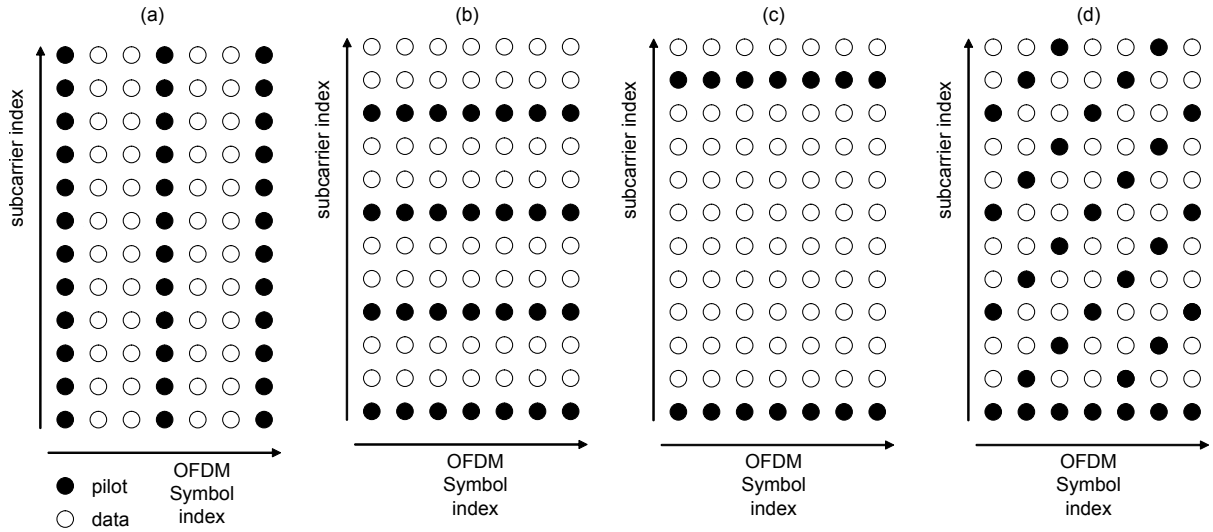

Figure 4.2. Different types of pilot arrangement: (a) block-type pilots; (b) comb-type pilots; (c) comb-type pilots where pilots are placed widely apart; (d) incline-type pilots

carry pilots. In Fig. 4.2a, one out of three OFDM symbols carry pilots[1], but more or less frequent pilot symbols can be utilized based on how fast the channel changes and how much estimation overhead can be tolerated. For the comb-type pilot arrangement, pilots are inserted at some subcarriers with certain density, and data is transmitted for the non-pilot subcarriers. In Fig. 4.2b, one out of $L = 3$ subchannels carry pilots and the remaining subchannels carry data. In Fig. 4.2c, one out of $L = 10$ subchannels carry pilots, where the pilots are placed widely apart to reduce the estimation overhead. We utilize this idea of low density pilots later in this chapter in order to be able to perform TD analysis for CE and in the meantime keep the estimation overhead low. Using the same number of pilots, the comb-type arrangement has the advantage of tracking changes in the channel over time. For BB PLC LPTV channels, there can be many channel realizations within one AC cycle of the mains [11], for which the pattern would repeat itself for some period of time. In order to estimate the LPTV channel, if

[1]For the block type arrangement, it is assumed that the channel is constant for the non-pilot OFDM symbols and there is a tradeoff between estimation accuracy and the amount of overhead required. For LPTV channels, we assume that the channel is constant for one OFDM symbol time and the channel can change from one OFDM symbol to another. For this reason, in order to track changes in the channel, when block-type arrangement is mentioned in this paper, we mean that all of the OFDM symbols carry only pilots for at least the duration of one AC mains cycle [16].

OFDM symbols carrying only pilots are transmitted for one full AC cycle, the overhead will be high compared to the comb-type arrangement [16]. Therefore, a comb-type arrangement can be preferable to reduce the overhead with some increase in complexity.

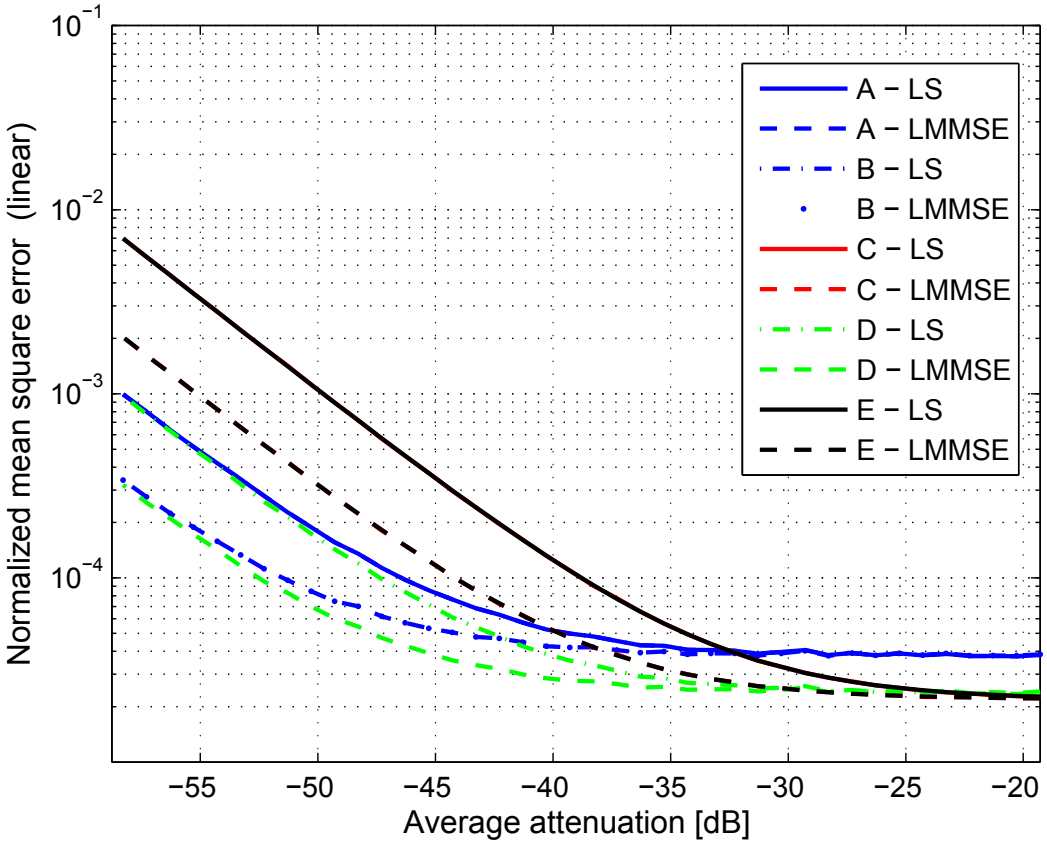

Figure 4.3. Normalized mean square error using linear interpolation, $L = 5$.

When the comb-type arrangement is deployed, CE is done at pilot symbol locations first. Then, CE for the remaining subchannels is achieved by interpolation. For these subchannels, the difference between the actual channel response and the value obtained by interpolation is the *estimation error*, part of which is caused by interpolation (See Appendix B and reference [22]). This is due to the fact that the estimates in these subchannels rely on the estimates at pilot locations and interpolation. For the comb-type arrangement with a slow fading channel, the estimates for the pilot locations can become more accurate by averaging over many OFDM

symbols. However, the interpolation error would still remain. The interpolation error can also be reduced by increasing the density of pilots, which then increases the estimation overhead. In this section, we investigate the case when the pilot locations are shifted each time a new OFDM symbol is transmitted (*incline-type* [26]) for the BB PLC channel, in comparison with block-type and comb-type arrangement. Incline-type pilot arrangement is illustrated in Fig. 4.2d. To the best of our knowledge, this is the first study that exercises incline-type pilot arrangement for the BB PLC channel.

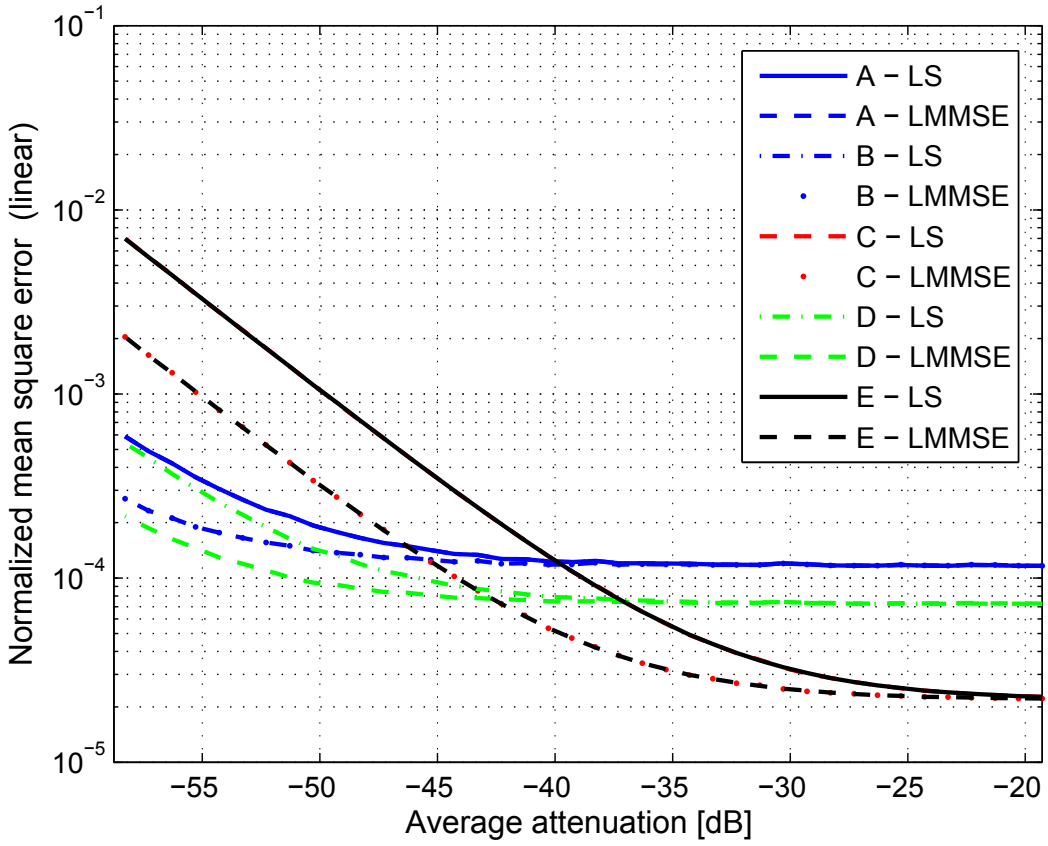

Figure 4.4. Normalized mean square error using linear interpolation, $L = 10$.

For the incline-type arrangement, unlike the comb-type, the channel estimates for non-pilot subcarriers do not rely solely on the interpolated values. Since each subcarrier carries both pilot and data symbols, the estimate is based on both pilot based estimation and interpolation. For

comparison, we assume that the channel does not change for L OFDM symbols, and consider the following schemes:

- **Scheme A:** Comb-type arrangement is utilized, and L channel estimates at pilot locations are averaged. Then, one time interpolation is performed to obtain channel estimates for the non-pilot subcarriers.
- **Scheme B:** Comb-type arrangement is utilized, and for each OFDM symbol, interpolation is performed. Then, the average is computed for all subchannels.
- **Scheme C:** Incline-type arrangement is utilized, and no interpolation is performed. The one time pilot estimates are put together to form the estimate for the whole OFDM symbol.
- **Scheme D:** Incline-type arrangement is utilized, and for each OFDM symbol, interpolation is performed. Then, the average is computed for all subchannels.
- **Scheme E:** Block-type arrangement is utilized for one out of L OFDM symbols, and no interpolation is performed.

Table 4.1. Channel Parameters

Channel #	$[h_{\text{avg}}]$
1	-19.1
2	-22.3
3	-28.3
4	-34.4
5	-41.2
6	-46.3

We also note that the first and the last suchannels are always assigned pilots in all schemes, and the number of pilots utilized for L OFDM symbols are nearly the same for all schemes. Therefore, the overhead for each scheme is approximately the same. We examined LS and

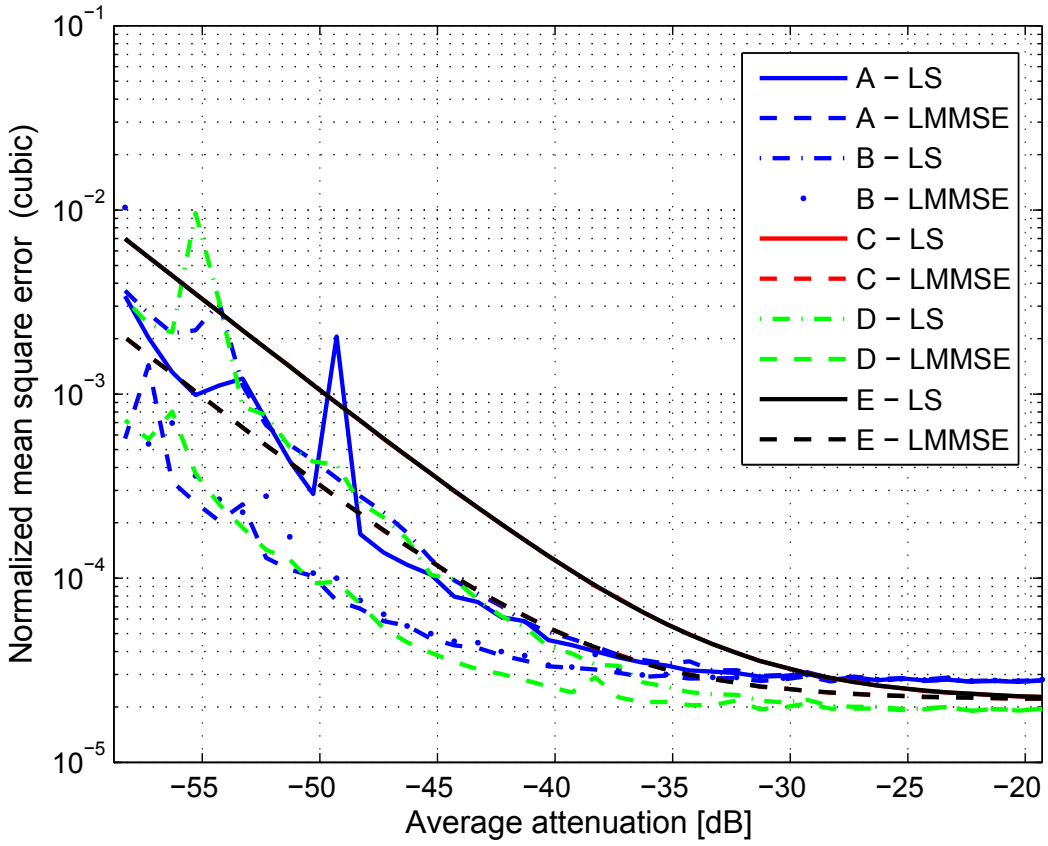

Figure 4.5. Normalized mean square error using cubic interpolation, $L = 5$.

LMMSE estimators with linear and cubic interpolation options for $L = 5$, and $L = 10$. For performance evaluation, we modified six channels for which the attenuations are given in Table 4.1, in order to generate channels from low to high attenuation range. 50 trials are computed for each channel at each attenuation level, and the average of the six is computed. To compute the normalized mean square error, the actual channels are normalized, and the estimates are scaled accordingly. The results are shown in Figs. 4.3–4.6, where the LMMSE estimator outperforms LS, and cubic interpolation outperforms linear interpolation in most cases. Schemes C and E perform the same and they are not affected by the density of pilots. This is because Scheme C is equivalent to Scheme E when the channel and noise characteristics are assumed to be the same for L OFDM symbols. We also observe that Scheme D (incline-type with interpolation)

outperforms Schemes A and B for the most part, or performs very close for the remaining part. It also outperforms Scheme E for almost all cases except for linear interpolation with $L = 5$ in the low attenuation (high signal-to-noise ratio (SNR)) region. All schemes perform close to one another and do well in the high SNR region. We notice that the benefit due to incline-type pilot arrangement with interpolation (Scheme D) decreases as the pilot density decreases for the linear interpolation case, since linear interpolation suffers when the pilots are too distant from one another. On the contrary, cubic interpolation is more immune to sparsely located pilots, and is not affected as much as the linear interpolation case. Overall, the results indicate that Scheme D is a good candidate for LPTV channels especially in the low SNR scenarios, where estimation error is large due to high attenuation and interpolation error. We note that the improvement in CE due to the incline type pilot arrangement depends on the interpolation kernel being used, and can vary based on the choice of the interpolation kernel.

4.3.3 Decision-directed Approach

In addition to pilot-based CE explained in the this section, another method for CE is the decision directed approach. This minimizes the overhead for CE by depending on the decisions made at the receiver without the knowledge of the transmitted symbol. An initial estimate can be achieved using pilots, but then no pilots are utilized. The channel estimate from the previous OFDM symbol is used to decode the current OFDM symbol, then with those decisions, the channel estimate is updated for the current OFDM symbol and used to decode the next OFDM symbol. This method has smaller overhead compared to pilot-based approaches, but for the LPTV channel, when the channel changes abruptly, the decisions based on the previous estimate are highly erroneous. This results in large estimation error and additional decoding errors. When the channel remains constant, the signal attenuation is low, and the impulsive noise is not present, the decisions are more dependable and this method can be preferred to the pilot-based approaches due to the lower overhead. However, for the BB PLC channel, the channel and the noise may change abruptly and the signal attenuation can be high. Therefore,

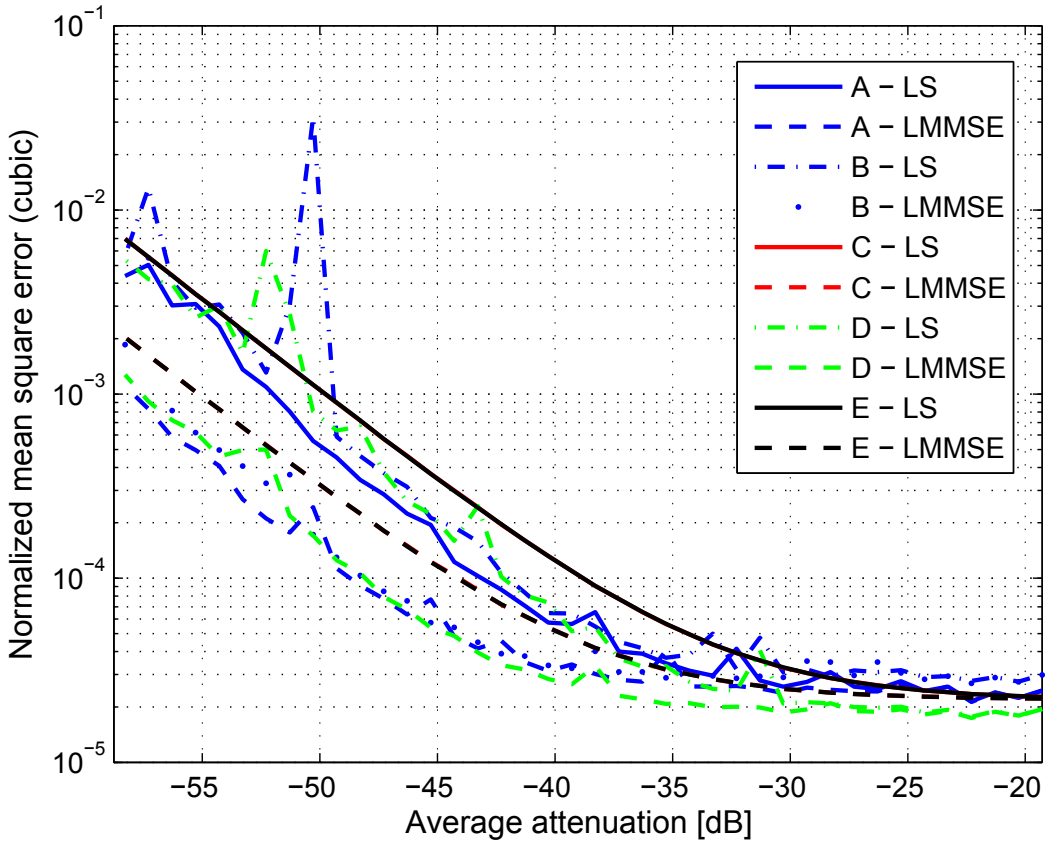

Figure 4.6. Normalized mean square error using cubic interpolation, $L = 10$.

both the pilot-based and decision directed CE approaches have some drawbacks for the BB PLC channel due to the LPTV channel characteristics and the impulsive noise.

4.4 Transform Domain Analysis

Inspired by the work in [27, 13], in this section, we explain TD analysis that we propose for CE in BB PLC channels in the presence of power line impulsive noise [28]. The goal of the TD[2] analysis is to identify the cause of a change in our channel estimates. If the receiver has the knowledge of whether a change in the estimate is due to a change in the transfer function, the presence of impulsive noise, or both, the CE algorithm can exploit this information to improve

[2]The transform domain is the Fourier transform of data that has already been Fourier transformed.

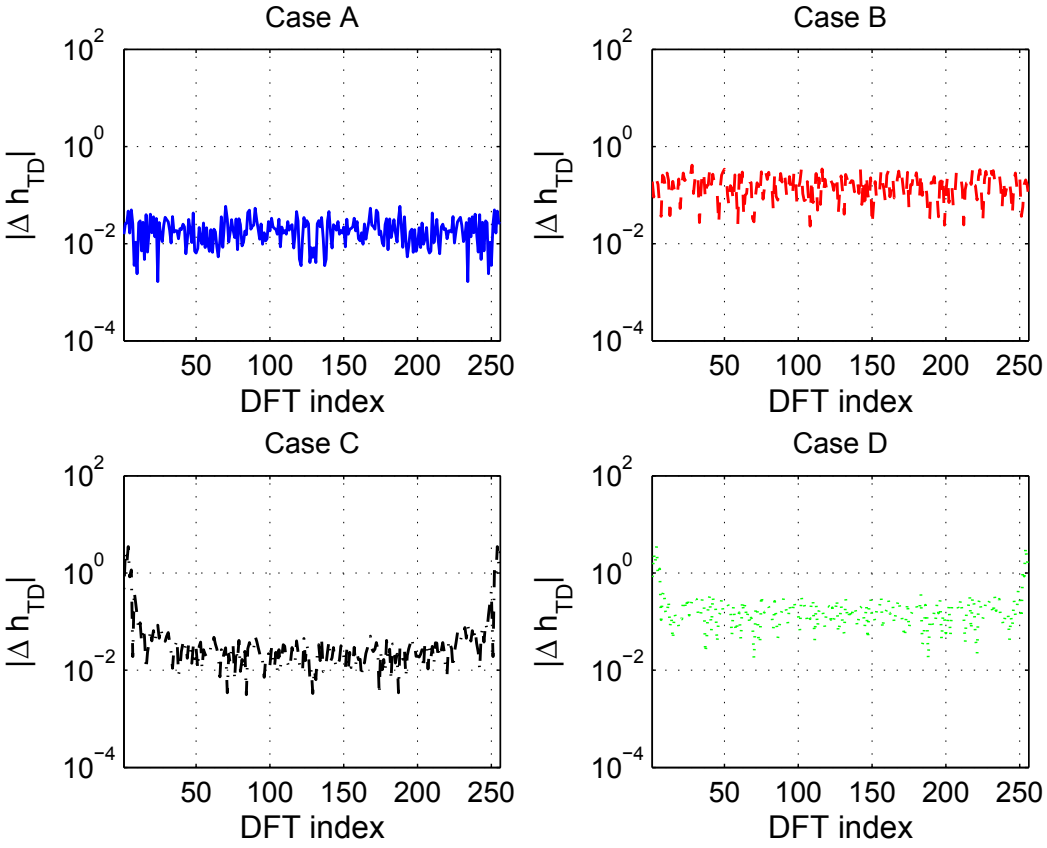

Figure 4.7. TD analysis for a single realization of four cases for LS estimates

its estimate. TD analysis proposes that the changes in the estimates will be different in their frequency content (TD), when they are caused by a change in the channel transfer function, or a change in the noise level. Let us assume that the receiver has a current estimate for the channel $\hat{\mathbf{h}}_\mathbf{1}$, and is receiving a new OFDM symbol to compute a new estimate $\hat{\mathbf{h}}_\mathbf{2}$ for the channel. Four cases can be classified for the power line:

- **Case A:** The channel remains the same ($\mathbf{h_2} = \mathbf{h_1}$). Background AWGN is present in the received OFDM symbol.

- **Case B:** The channel remains the same ($\mathbf{h_2} = \mathbf{h_1}$). Background AWGN and impulsive noise are present in the received OFDM symbol.

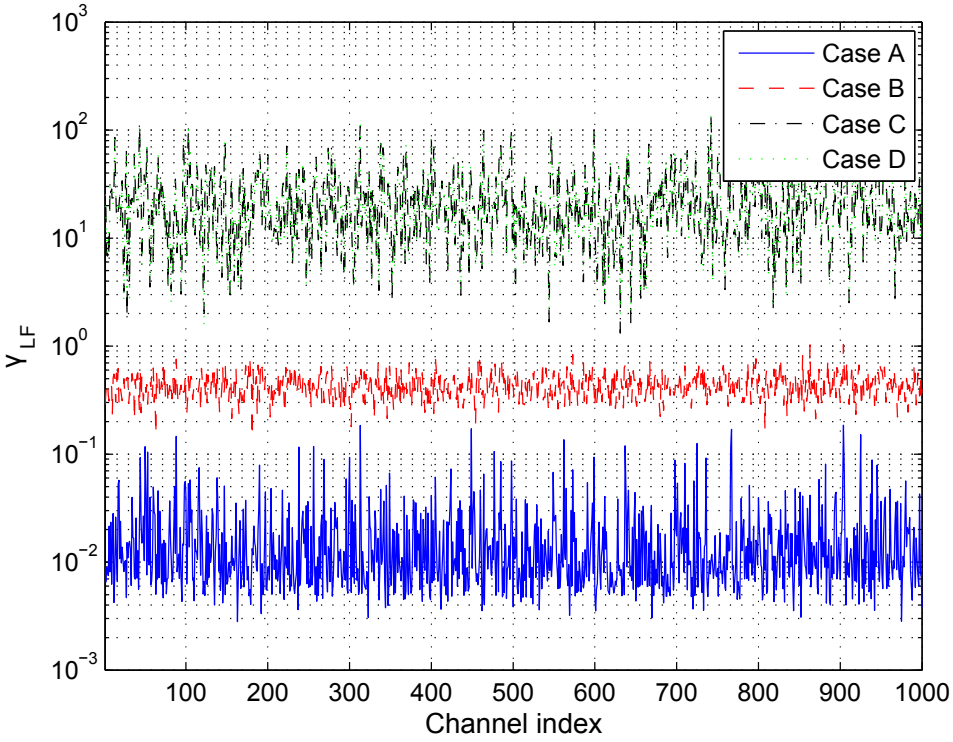

Figure 4.8. Low frequency metric for Cases A–D.

- **Case C:** The channel has changed ($\mathbf{h_2} \neq \mathbf{h_1}$). Background AWGN is present in the received OFDM symbol.
- **Case D:** The channel has changed ($\mathbf{h_2} \neq \mathbf{h_1}$). Background AWGN and impulsive noise are present in the received OFDM symbol.

In order to find out which of the above cases has occurred, TD analysis can be utilized: examining the frequency content of the change in the channel estimate via the following N point DFT:

$$\Delta h_{\mathrm{TD}} = \mathcal{DFT}(|\hat{\mathbf{h}}_\mathbf{2}| - |\hat{\mathbf{h}}_\mathbf{1}|). \tag{4.6}$$

We illustrate $|\Delta h_{\mathrm{TD}}|$ of one channel realization of $\mathbf{h_1}$ and $\mathbf{h_2}$ for Cases A–D in Fig. 4.7. Four apparent patterns are observed. For instance, for Case B compared to Case A, we notice an increase in all frequencies. For Case C compared to Case A, an increase in the edges of the

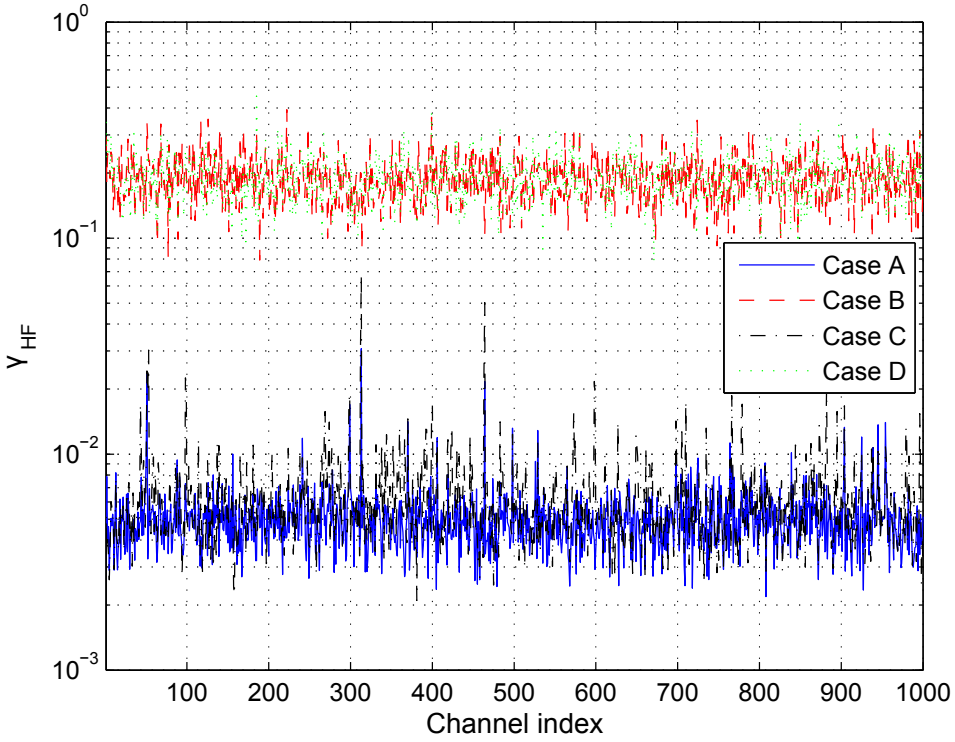

Figure 4.9. High frequency metric for Cases A–D.

spectrum is observed, which corresponds to low frequencies. And for Case D compared to Case A, a further increase in the edges for low frequencies, and an increase similar to Case B for the middle of the graph for high frequencies is recognized. The general trend is as follows: a change in the transfer function appears as an increase in the low frequencies, and the presence of impulsive noise appears as an increase in all frequencies. TD analysis motivates the following metrics to quantify these changes: the low frequency metric γ_{LF} and the high frequency metric γ_{HF}:

$$\gamma_{\mathrm{LF}} = \sum_{i=1}^{f_c} |\Delta h_{\mathrm{TD}}(i)|^2, \quad \gamma_{\mathrm{HF}} = \sum_{i=N/2}^{N/2+f_c-1} |\Delta h_{\mathrm{TD}}(i)|^2, \tag{4.7}$$

where f_c is the cut-off index in the TD, which may be chosen based on the resulting pattern of TD analysis and may depend on various factors such as the channel and noise model. f_c must be chosen properly, such that high and low frequency metric values for different cases are within

exclusive range of values. For analysis, we computed γ_{LF} and γ_{HF} for 1000 random channel pairs that correspond to different topologies for LS and LMMSE estimators with $f_c = 20$. The current channel estimate $\hat{\mathbf{h}}_\mathbf{1}$ is computed by an OFDM symbol going through the first channel, and the OFDM symbol that will be used to compute $\hat{\mathbf{h}}_\mathbf{2}$ goes through the first or the second channel of the pair depending on the four cases. The resultant metrics are presented in Figs. 4.8 and 4.9. Fig. 4.8 suggests that γ_{LF} is clearly distinct for Cases C and D compared to Cases A and B. The γ_{LF} is big, when the channel changes. Moreover, Fig. 4.8 suggests that, γ_{LF} is also bigger for Case B compared to Case A, but not as much as Cases C and D. This is due to the low frequency components of the impulsive noise. Similarly, Fig. 4.9 suggests that γ_{HF} is big for Cases B and D compared to Cases A and C. For Cases B and D, impulsive noise is present, and γ_{HF} turns out to be bigger compared to Cases A and C. The results for the LS estimator are similar to LMMSE, where it is also possible to distinguish four cases via γ_{LF} and γ_{HF}. In summary, TD analysis suggests that γ_{LF} can be considered to find out whether the channel has changed or not, and γ_{HF} can be considered to find out whether impulsive noise is present or not in addition to the background AWGN.

4.5 Performance Analysis and Proposed Final Scheme

We now propose to exploit the information captured by TD analysis for CE. This is achieved via pilots spaced widely apart (e.g. Fig. 4.2c) in order to keep the estimation overhead low and still be able to perform TD analysis. One out of L subcarriers are placed as pilots, and we choose $L = 10$. Based on the information from TD analysis, the proposed final scheme switches between various schemes, unlike the conventional CE schemes that are based on a single scheme. Different design criteria can be considered, such as minimizing the overhead while keeping the estimation error below a certain value, or just minimizing the estimation error regardless of the estimation overhead. In this work, we consider keeping the estimation overhead low and mitigating the effects of the LPTV channel and the impulsive noise as our design criteria for

the proposed algorithm. The estimation schemes we considered in this section[3] are listed in Table 4.2.

Table 4.2. CE Schemes

SCHEME #	**Description**
Scheme A	Block-type pilots.
Scheme B	Decision directed.
Scheme C	Comb-type pilots, and interpolation.
Scheme D	Discarding the current estimate based on TD analysis.
Scheme E	Comb-type pilots, decisions based on current estimate, recompute estimate based on decisions.

Scheme A is the block-type pilot arrangement, where no data transmission takes place and all of the subcarriers in the OFDM symbol carry pilots for at least the duration of one AC cycle of the mains. Therefore, the CE overhead is high. Scheme B is the decision directed CE approach, where the channel estimate from the previous OFDM symbol is utilized to decode the current symbol. Then, these decisions are used to update the estimate for the current symbol and to decode the next symbol. Other than pilot symbols that are used for initialization, this scheme does not utilize pilots. Hence, the estimation overhead is minimal. Schemes A and B are studied as a reference for comparison with the remaining schemes that have pilots placed distantly from each other and TD analysis is performed. Scheme C is the comb-type pilot arrangement, where one out of L subchannels carry pilot symbols, and the channel estimate for the whole spectrum is found by interpolation for the non-pilot subcarriers. Scheme D is the case where the current estimate is discarded and the previous estimate is kept. This scheme is examined only for Case B, where the channel remains the same and impulsive noise is present. Scheme E initially computes the channel estimate via comb-type pilots and interpolation. Next, the current OFDM symbol is detected based on this channel estimate, and decisions are obtained for non-pilot subcarriers. Then, the initial channel estimate that was obtained by interpolation

[3]Note that Schemes A–E listed in this section and schemes A–E listed in Section 4.3.2.1 refer to two different set of schemes.

for data-carrying subchannels is replaced by LS estimates as in Equation (4.1), $\mathbf{X}$ consisting of pilot values and the decisions made in non-pilot subcarriers. Scheme E is different from Scheme B in that it makes use of the current estimate to decode the symbol initially rather than the estimate from the previous symbol, and it is different from Scheme C in that it updates the interpolation-based estimate with the decision-based estimate.

We now examine the four cases listed in Section 4.4 along with the five schemes listed in Table 4.2 in more detail. In order to evaluate the performance of the CE schemes, we computed the normalized minimum mean square error (NMMSE), and the number of subchannels with decoding errors E_{d} out of the number of subchannels carrying data N_{d}. The averages of NMMSE–in dB–and the decoding errors for 1000 realizations of $\mathbf{h_1}$ and $\mathbf{h_2}$ are shown in Table 4.3. For all schemes, LS estimates are employed, and the cut-off frequency is $f_c = 20$ for TD analysis.

Table 4.3. Performance Analysis

CASE #	**Scheme A**	**Scheme B**	**Scheme C**	**Scheme D**	**Scheme E**
Case A - [$\mathrm{NMMSE_{avg}}$]	-47.32	-47.12	-42.04	N/A	-42.70
Case A - $E_{\mathrm{d,avg}}/N_{\mathrm{d}}$	N/A	0.61 / 256	1.51 / 229	N/A	1.51 / 229
Case B - [$\mathrm{NMMSE_{avg}}$]	-30.96	-31.78	-26.68	-42.04	-29.93
Case B - $E_{\mathrm{d,avg}}/N_{\mathrm{d}}$	N/A	27.97 / 256	43.15 / 229	25.77 / 229	43.15 / 229
Case C - [$\mathrm{NMMSE_{avg}}$]	-47.35	-21.03	-42.02	N/A	-42.74
Case C - $E_{\mathrm{d,avg}}/N_{\mathrm{d}}$	N/A	192.92 / 256	1.54 / 229	N/A	1.54 / 229
Case D - [$\mathrm{NMMSE_{avg}}$]	-30.99	-20.63	-30.10	N/A	-29.89
Case D - $E_{\mathrm{d,avg}}/N_{\mathrm{d}}$	N/A	192.53 / 256	43.28 / 229	N/A	43.28 / 229

4.5.1 Case A

Case A is when the channel remains the same ($\mathbf{h_2} = \mathbf{h_1}$) and the noise is background AWGN. The amplitude and phase of the channel estimates for a single realization of the channel and noise are depicted in Fig. 4.10. We note that the magnitude of the channel estimates for Schemes

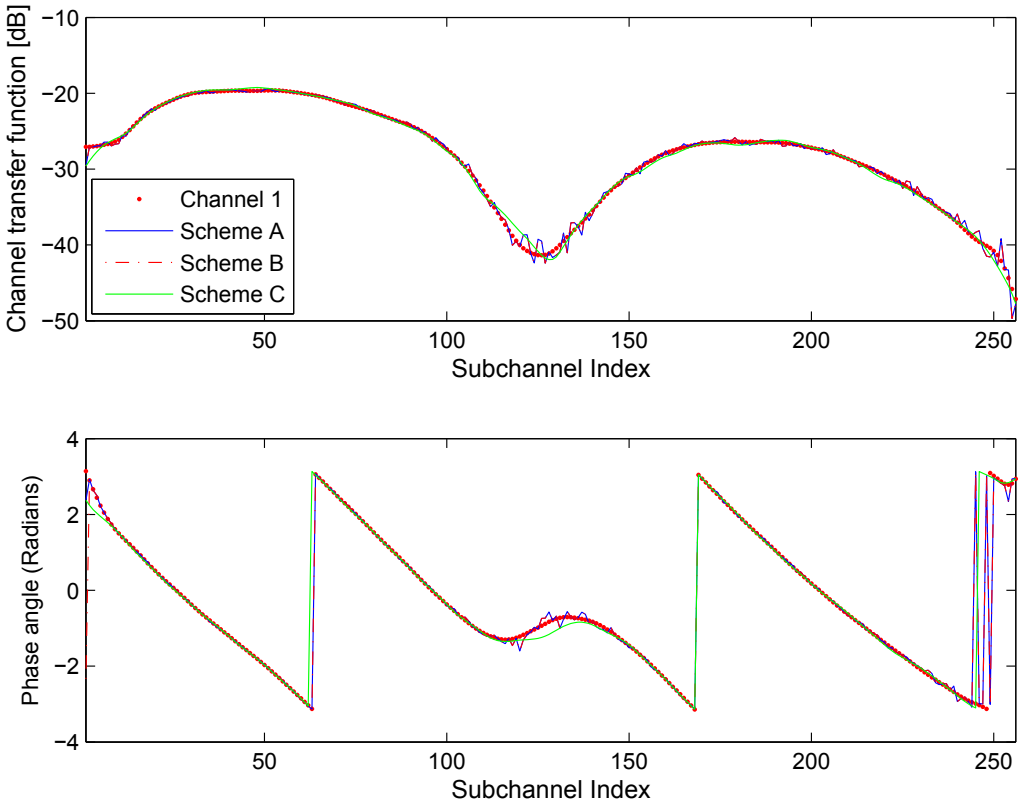

Figure 4.10. Case A channel estimates for the various schemes. The amplitude and phase of the channel transfer function are illustrated.

A and B are the same for all cases due to the constant envelope QAM symbols, but the phase is different when the symbol is detected in error for a subchannel for Scheme B. Among all schemes, Scheme A has the minimum NMMSE of -47.32 dB, and Scheme B performs very close to Scheme A with -47.12 dB NMMSE. Scheme B, the decision directed approach, has a valid estimate from the previous OFDM symbol to decode the symbol since the channel remained the same for Case A. Hence the estimate is a good one, and the average number of decoding errors is as low as 0.61 out of 256 subchannels. On the other hand, Scheme C has about 10% overhead[4] due to the scarcely placed pilots for TD processing: 27 subchannels carry pilots, and

[4]The overhead for Schemes C, D and E is the same for all cases, since they are based on TD processing made available by comb-type pilot arrangement with $L = 10$. Since the first and the last subchannels are also assigned pilots in the comb-type arrangement, there are a total of 27 subchannels out of 256, which corresponds to the

229 subchannels carry data. The NMMSE is -42.04 dB, and the average number of decoding errors is 1.51 out of 229 data-carrying subchannels. The NMMSE is about 5 dB more than Schemes A and B, but this does not affect the decoding of the data carrying subchannels, since the decoding error is small. As seen in Fig. 4.10, the estimates are very close to each other even for subchannels with high signal attenuation. Hence, when these decisions for data carrying subchannels and the pilot subchannels are used to recompute the LS estimate in the case of Scheme E, the NMMSE is improved about 0.7 dB compared to Scheme C. For Scheme E, the estimation overhead is reduced to about 10% from the 100% overhead of Scheme A, and a comparable CE with low NMSSE is achieved. Compared to Scheme B, Scheme E provides a comparable CE performance with a comparable raw data rate. Data can be carried in 229 subchannels as opposed to 256 subchannels. However, Scheme B lacks TD analysis, which results in performance degradation for the remaining Cases B, C, and D. Therefore, for Case A, we propose to employ Scheme E due to its low overhead and TD analysis.

4.5.2 Case B

In Case B, the channel remains the same ($\mathbf{h_2} = \mathbf{h_1}$) and impulsive noise is present in the channel along with background AWGN. The amplitude and phase of the channel estimates for a single realization of the channel and noise are depicted in Fig. 4.11. In this case, the channel estimates for Schemes A, B, C, and E are affected badly by the presence of impulsive noise in the channel. The NMMSE values for these schemes are -30.96, -31.78, -26.68, and -29.93 dB, respectively. This is a result of the received noisy symbol with impulsive noise. Hence, for this case, we propose to exploit the information from TD analysis that the channel has not changed and employ Scheme D. Scheme D is simply aware of the presence of impulsive noise via TD processing, and discards the channel estimate that is computed using the current noisy symbol. It instead utilizes the previous estimate. The NMMSE for Scheme D is -42.04 dB, which is much smaller than all other schemes. In terms of raw data rates, Scheme A has no data-carrying subchannels, so the raw data rate is zero. Scheme B has an average of 27.97 decoding errors

actual 10.54% overhead.

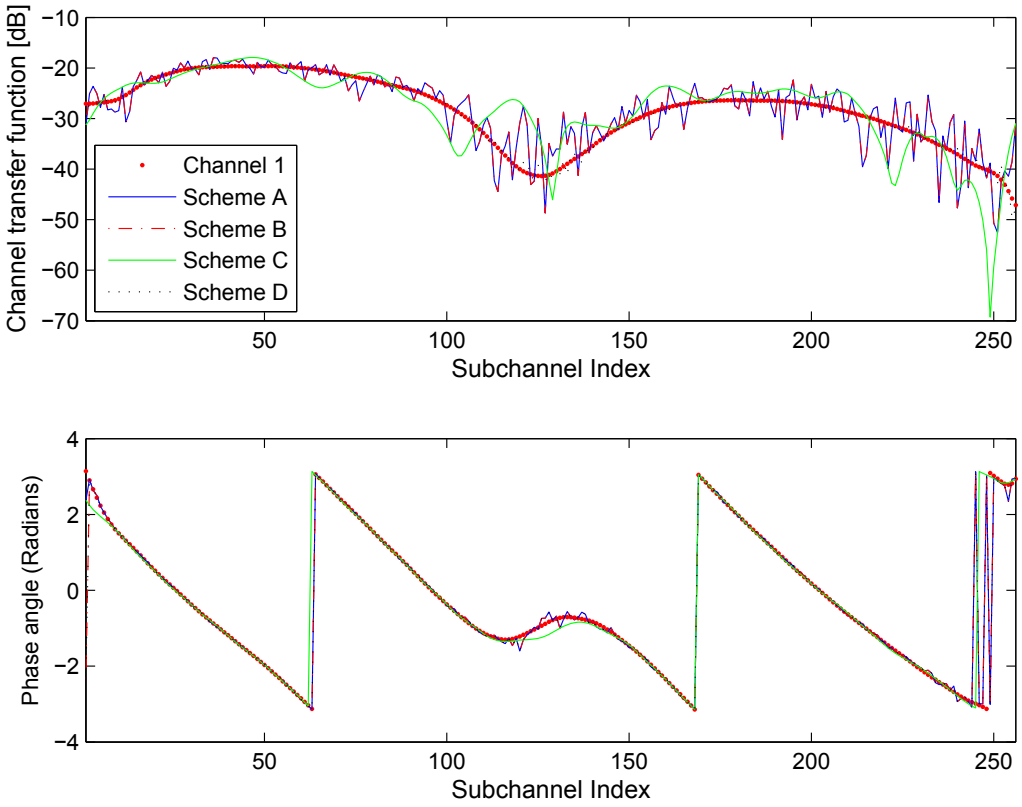

Figure 4.11. Case B channel estimates for the various schemes. The amplitude and phase of the channel transfer function are illustrated.

out of 256 subchannels, and Scheme D has a comparable average number of errors, 25.77 out of 229 compared to Scheme B. Additionally, Scheme D is aware of the presence of impulsive noise and the resultant high number of decoding errors via TD processing. Compared to Schemes C and E, Scheme D has a smaller decoding error average: 25.77 compared to 43.15. This is because Scheme D employs a better channel estimate than Schemes C and E to decode the noisy symbol. Therefore, the errors are only due to the increased noise level, but not due to the bad CE as for Schemes C and E. Hence, we propose to utilize Scheme D for Case B due to its better CE compared to all other schemes, low overhead compared to Scheme A, and relatively low decoding errors compared to Schemes C and E.

4.5.3 Case C

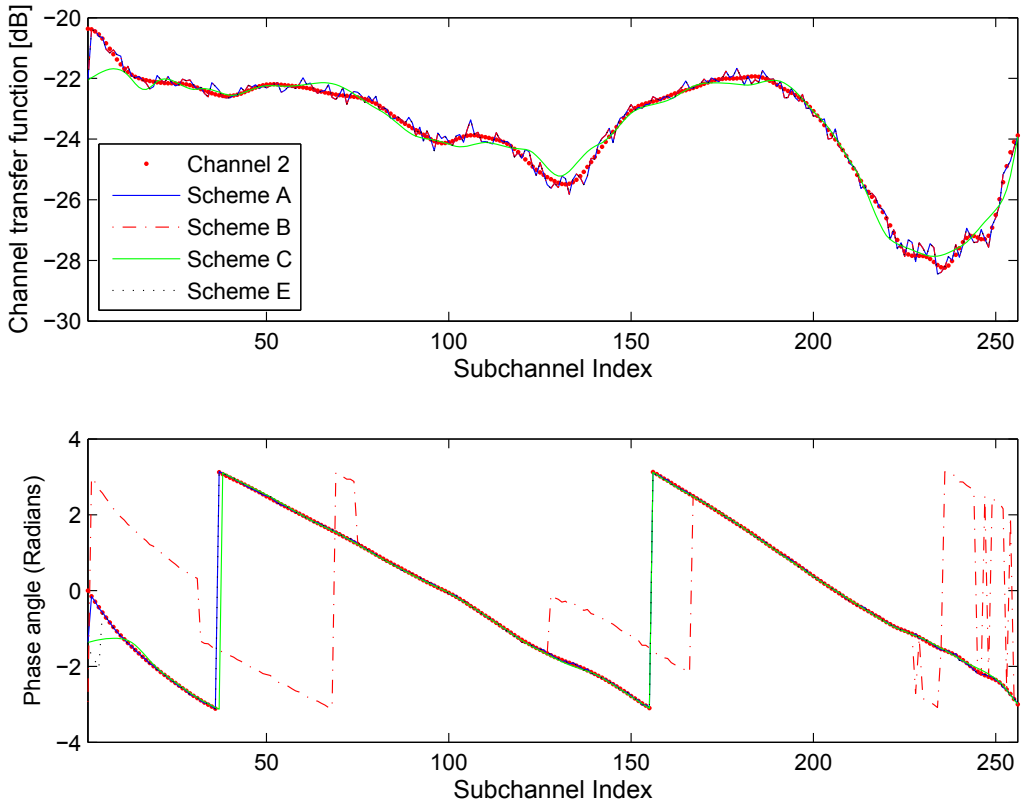

Figure 4.12. Case C channel estimates for the various schemes. The amplitude and phase of the channel transfer function are illustrated.

Case C is when the channel changes ($\mathbf{h_2} \neq \mathbf{h_1}$) and the noise is background AWGN. The amplitude and phase angle of the channel estimates for a single realization of the channel and noise are depicted in Fig. 4.12. In this case, Scheme A has the minimum NMMSE of -47.35 dB among all schemes. Since Scheme B uses the previous channel estimate to decode the symbols, and the channel has changed, this results in a large number of decoding errors and a bad estimate for the channel. The average number of decoding errors in this case is 192.92 out of 256 subchannels, and the NMMSE is -21.03 dB. Since QAM is used for modulation, the magnitude responses for Schemes A and B are the same, but the phase responses for Schemes A

and B are very different from one another. The reason for this is the large number of decoding errors for Scheme B. Scheme B in this case suffers the most among all schemes from the change in the channel transfer function. It has the worst channel estimate and the highest number of decoding errors among the data-carrying schemes B, C, D and E. For Schemes C and E, the average number of decoding errors is 1.54 out of 229 data-carrying subchannels, and the NMMSE is -42.02 and -42.74 dB, respectively. Both schemes utilize the current estimate—computed using the pilots placed widely apart and interpolation—to decode the symbols. This results in smaller number of decoding errors compared to Scheme B. This is the reason for 0.7 dB improvement in the channel estimate when these decisions are considered to replace the estimates obtained by interpolation for the non-pilot subcarriers. For this reason we propose to utilize Scheme E in this case, which has small number of decoding errors, a comparable channel estimate, and a much lower overhead for CE compared to Scheme A.

4.5.4 Case D

This is the case where the channel changes ($\mathbf{h_2} \neq \mathbf{h_1}$) and impulsive noise is present. The amplitude and phase angle of the channel estimates for a single realization of the channel and noise are depicted in Fig. 4.13. In this case, Schemes A, C and E have similar CE performance with NMMSE of -30.99, -30.10, and -29.89 dB, respectively. Scheme A results in noisy estimates due to the presence of impulsive noise similar to Case B. Scheme B utilizes the previous channel estimate, and provides a poor estimate and high decoding error, since the channel has changed and the impulsive noise is present. The NMMSE for Scheme B is -20.63, the worst among all schemes. The average number of decoding errors for Scheme B is 192.53 out of 256, which is much higher than Schemes C and E. The average number of decoding errors for Schemes C and E is 43.28, similar to Case B, but higher than Cases A and C due to the presence of impulsive noise. In this case, we propose to utilize Scheme C, because of its comparable CE and lower overhead compared to Scheme A, and slightly better CE than Scheme E. Scheme E does not improve the CE for Scheme C in this case, because of relatively high decoding errors compared

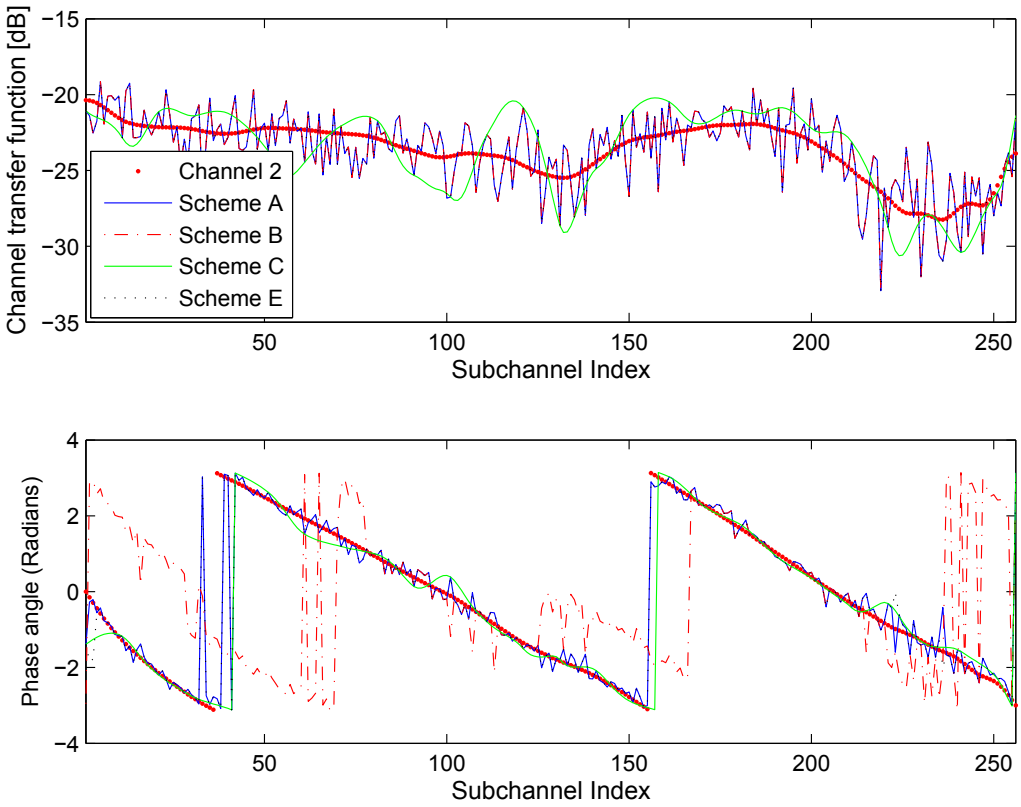

Figure 4.13. Case D channel estimates for the various schemes. The amplitude and phase of the channel transfer function are illustrated.

to Cases A and C.

4.5.5 Proposed Final Scheme

We illustrate the proposed final CE scheme based on the TD analysis in Fig. 4.14 to summarize our findings in this section. In the figure, the delay block D is a delay of one OFDM symbol time. When a new OFDM symbol is received, TD analysis is performed using the channel estimate from the previous symbol and an initial estimate of the current symbol based on comb-type arranged pilots and interpolation for the current symbol. HF and LF metrics are computed and the case type is determined based on whether the channel has changed or the impulsive noise is present. Then, depending on the case, the corresponding CE Scheme

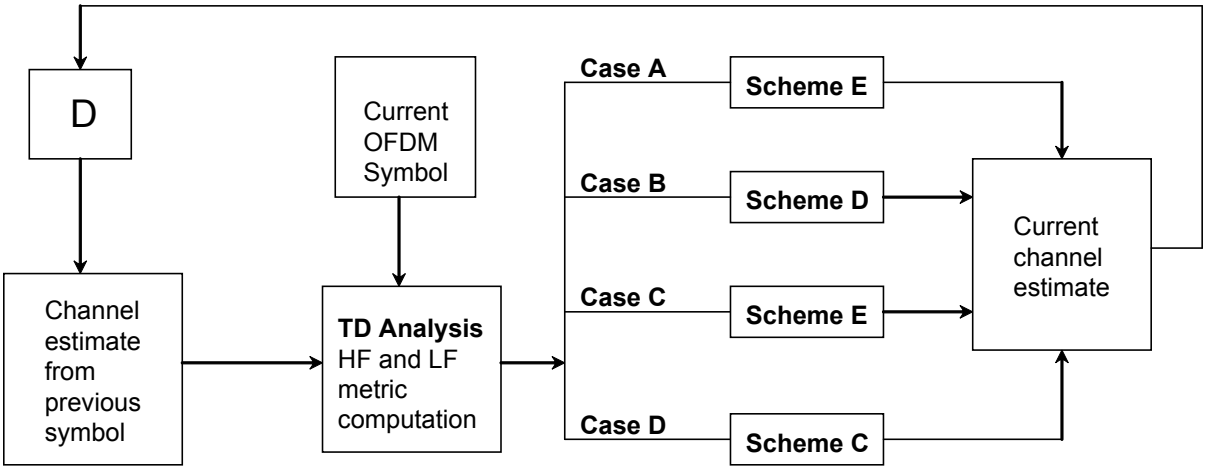

Figure 4.14. Proposed final channel estimation scheme based on TD analysis.

is utilized and the current channel estimate is computed. The advantage of performing TD analysis is the ability to utilize various type of CE schemes depending on the case, rather than using one conventional scheme for all cases. Based on how frequent the channel changes, and how frequent impulsive noise occurs in the power line, the amount of improvement in estimation accuracy compared to block-type pilot based and decision directed approaches will be different. The proposed final scheme is robust to changes in the channel and the noise compared to block-type pilot arrangement and decision directed approaches, and provides a low overhead solution for the BB PLC channel.

4.5.6 Optimal Schemes

Similar to the comb-type pilot arrangement, TD analysis can be combined with other CE schemes such as the block-type pilot arrangement and the decision directed scheme. If the design criteria is to minimize the NMMSE regardless of the estimation overhead, the optimal scheme would be the block-type pilot arrangement combined with TD analysis. Analyzing the performance results in Table 4.3, a final scheme that utilizes Scheme A for Cases A-C-D, and Scheme D for Case B would be optimal. On the other hand, if the design criteria is to minimize the estimation overhead regardless of NMMSE, the decision directed approach Scheme B would

be optimal. In this case, TD analysis can be performed on the decision directed estimates for two consecutive OFDM symbols in some cases to improve the performance of Scheme B. For instance for Cases A and B, considering the performance results in Table 4.3, NMMSE for Scheme B is about 5 dB less than Scheme C. Since TD analysis works well using the estimates of Scheme C, it also works well using the estimates of Scheme B for Cases A and B. Therefore, TD analysis for Case B results in dependable metrics and can be combined with Scheme B for Case B, provided that the previous channel estimate is one with a low NMMSE that has converged over time. Then, an improved version of Scheme B in terms of smaller NMMSE would utilize Scheme D instead of Scheme B for Case B.

4.6 Summary and Conclusions

In this chapter, we first examined LS and LMMSE estimators for pilot-based CE with different pilot geometry. We implemented incline-type pilot arrangement for BB PLC channels in order to help reduce interpolation error inherent in comb-type pilot arrangement. When incline-type pilot arrangement is utilized, the estimates for each subchannel is a combination of pilot based and channel based estimates, unlike the comb-type, where the estimates for non-pilot subchannels is only based on interpolation.

We then analyzed a new method for CE for the BB PLC channel based on TD analysis and pilots spaced widely apart. TD analysis is employed in identifying abrupt changes in the power line channel and the noise by examining the change in the channel estimate for two consecutive OFDM symbols. We defined four cases depending on the changes in the channel and the noise. For each case, five CE schemes are studied, and the proposed final scheme utilizes the scheme with the low or the lowest estimation error and low overhead. The block type pilot based CE Scheme A has the highest overhead, and the decision directed Scheme B suffers when the channel changes and impulsive noise is present with poor CE and high decoding errors. Scheme E utilizes decisions for non-pilot subcarriers unlike Scheme C, which performs interpolation for these subcarriers. For cases where the decoding error is small and the decisions are reliable,

Scheme E outperforms Scheme C, since there is no interpolation error introduced and decisions are mostly accurate. If the channel does not change and impulsive noise is present, it is better to discard the estimate and keep the previous estimate, which is Scheme D. This can be achieved by performing TD analysis. Hence, the proposed final scheme is aware of the changes in the channel and the noise via TD analysis, and switches between various schemes based on their performance with low estimation error and overhead, which makes it a good candidate for the BB PLC channel.

Additionally, the idea of TD analysis can also be combined with block-type pilot arrangement and decision directed CE schemes. The optimal scheme that minimizes NMMSE can be achieved by employing TD analysis with block-type pilot arrangement, and the optimal decision directed CE scheme that minimizes CE overhead can be improved by employing TD analysis in terms of estimation accuracy for certain cases.

Chapter 5

Conclusion

The objective of this work is to develop bit loading and CE schemes specifically designed for BB PLC channels. PLC has been a topic of interest for the past decades due to its economic advantage that it does not require additional investment for infrastructure, and is one of communication technologies envisaged for SG. However, since the power lines are not designed for data communication, challenges are involved in designing a communication system for power lines. In particular for BB PLC, LPTV channel and the impulsive noise are two characteristics of power lines that have to be taken into consideration. The main contributions of our work are: (i) LPTV-aware bit loading (ii) CE based on TD analysis, for an OFDM system. These contributions are listed below in more detail.

5.1 Contributions

1. Simplistic adaptation schemes in the literature lack the ability to view the entire AC mains cycle when allocating bits and power in each microslot. Therefore, they are not optimal for LPTV channels. Optimal LPTV-aware bit loading scheme based on a greedy-type algorithm is developed.

2. By utilizing representative values from microslots, the complexity of the optimal algorithm is greatly reduced without sacrificing performance. Power clipping is utilized to avoid peak

power levels for the reduced complexity algorithm.

3. The idea of LPTV-aware bit loading, complexity reduction, and power clipping is implemented for even-like power distribution algorithms and similar gains in bit rates are achieved.

4. LS, LMMSE algorithms with linear and cubic interpolation are implemented and compared from a practical perspective for BB PLC channels.

5. Incline-type pilots are examined to help reduce interpolation error inherent in comb-type pilot arrangement, and a comparison of block-type, comb-type, and incline-type pilot arrangements is made.

6. TD analysis for CE is developed. By examining the frequency content of the difference between two channel estimates, crucial information such as the cause for an abrupt change in the channel estimate can be extracted. TD analysis determines the changes due to a change in the transfer function and noise by computing high frequency and low frequency metrics in the TD.

7. A robust scheme that utilizes pilots placed widely apart and TD analysis is developed. The advantage of exploiting information from TD analysis is the ability to switch between various CE schemes based on the knowledge of a change in the transfer function or the noise. Unlike conventional CE schemes based on a single approach, CE scheme based on TD analysis is aware of the abrupt changes in the channel whether due to the LPTV channel or the impulsive noise.

5.2 Areas of Further Study

The bit loading and CE problems are treated separately in this work and solutions are provided for each problem. The interdependency of these two problems—for instance the effect of CE in error on the performance of bit loading—can be evaluated by investigating a system that utilizes both LPTV-aware bit loading and CE.

New TD analysis metrics can be developed for different power line noise models in the literature, and their performance can be evaluated. In this work, we developed TD analysis based on pilot symbols; however, the application of TD analysis to various decision directed schemes and their performances is an interesting topic to investigate in the future.

Page left intentionally blank.

Appendix A

Matroid Structures

A matroid $\mathfrak{M} \doteq (S, \mathfrak{I})$ is an algebraic structure composed of the following [19]:

- $S \doteq \{s_1, s_2, s_3, \ldots\}$, a finite set of elements, and
- $\mathfrak{I} \doteq \{\mathfrak{S}_0, \mathfrak{S}_1, \mathfrak{S}_2, \ldots\}$, a collection of subsets of S,

where $\mathfrak{I}$ satisfies the following conditions:

(C.1) The empty set $\emptyset$ is a member of $\mathfrak{I}$.

(C.2) If $A \subseteq \mathfrak{S}_i$ and $\mathfrak{S}_i \in \mathfrak{I}$, then $A \in \mathfrak{I}$; a subset of a subset in $\mathfrak{I}$ is also included in $\mathfrak{I}$.

(C.3) If $\mathfrak{S}_i \in \mathfrak{I}$ and $\mathfrak{S}_j \in \mathfrak{I}$, and $|\mathfrak{S}_i| < |\mathfrak{S}_j|$, then there exists an element $s \in \mathfrak{S}_j - \mathfrak{S}_i$ such that $\mathfrak{S}_i \cup \{s\} \in \mathfrak{I}$, where $|\mathfrak{S}|$ is the cardinality of set $\mathfrak{S}$.

S is the *ground set* of a matroid, and the members of $\mathfrak{I}$ are *independent sets* of a matroid. The *rank* is the cardinality of the largest member of $\mathfrak{I}$, and $\mathfrak{S}^* \in \mathfrak{I}$ is *maximal* when it is not a subset of any other member of $\mathfrak{I}$.

A simple example is the *uniform matroid* of rank c over the ground set $S = \{0, 1, 2, \ldots L-1\}$ with L elements and the collection of subsets of S, $\mathfrak{I}_c = \{\mathfrak{S} \subseteq S \ : \ |\mathfrak{S}| \leq c\}$, for which the cardinality does not exceed c. Since $(S, \mathfrak{I}_c)$ satisfies all three conditions listed above, it is a matroid with rank c.

Algorithm 2 Greedy algorithm to solve the optimization problem A.2

1: **while** an element $s \in S - \mathfrak{S}$ exists such that $\mathfrak{S} \cup \{s\} \in \mathfrak{I}$ **do**
2: Select an element $\bar{s}$ in $S - \mathfrak{S}$ such that: (i) $\mathfrak{S} \cup \{\bar{s}\} \in \mathfrak{I}$, and (ii) $w(\bar{s})$ is minimum over $S - \mathfrak{S}$
3: Update $\mathfrak{S} = \mathfrak{S} \cup \{\bar{s}\}$;
4: **end while**
5: exit.

A.1 Matroids and Greedy Algorithms

Matroids can be used for solving resource allocation problems related to greedy algorithms. Greedy algorithms are iterative searching algorithms that always move in the direction of largest increment (decrement) to the function to be maximized (minimized), and they only proceed in the forward direction and do not trace back.

In order to introduce greedy algorithms, the following are defined. Let the *independence system* over a finite set S be $(S, \mathfrak{I})$, where $\mathfrak{I} \doteq \{\mathfrak{S}_0, \mathfrak{S}_1, \ldots\}$ is a collection of subsets of S, which only satisfies conditions C.1 and C.2. Let us assume that each element in S has a weight that can be described by a weight function $w : S \to \mathbb{R}$, and the weight $W(\mathfrak{S})$ of a subset $\mathfrak{S}$ of S is the sum of the weight of its elements

$$W(\mathfrak{S}) \doteq \sum_{s \in \mathfrak{S}} w(s), \qquad \text{and } W(\emptyset) = 0. \tag{A.1}$$

The optimization problem to solve for the independence system matroid is to find a maximal member $\mathfrak{S}$ of $\mathfrak{I}$ with *minumum weight* $W(\mathfrak{S})$:

$$\text{find a maximal } \mathfrak{S} \in \mathfrak{I} \text{ with minumum } W(\mathfrak{S}). \tag{A.2}$$

The pseudocode for the greedy algorithm for this optimization problem is given in Algorithm 2. The algorithm starts with an empty set for $\mathfrak{S}$, and builds $\mathfrak{S}$ iteratively at each step by adding the minimum weight element $\bar{s}$ of $S - \mathfrak{S}$, such that the updated $\mathfrak{S}$ is also included in $\mathfrak{I}$. The algorithm stops when last condition can no longer be met, and final set $\mathfrak{S}$ is guaranteed to be

maximal. This is based on the following property:

Property 1: (Edmonds [29]) For any assigned weight function $w : S \to \mathbb{R}$, the greedy algorithm solves the problem A.2 if and only if $(S, \mathfrak{I})$ is a matroid.

A.2 Integer Bit Loading as a Matroid Structure

Consider an OFDM system with N subchannels. Let us assume that the total number of bits allocated to N subchannels is fixed to $B_{\text{tot}} = c$. The pair (k, i) represents the k-th bit transmitted in the i-th subchannel. For each subchannel, assume that there exists a maximum number of bits that can be transmitted at that subchannel (i.e. for i-th sunchannel $b_i^{\max}$). Then, the collection of all of these pairs forms the *finite set*:

$$S \doteq \{(k, i) : 0 \leq k \leq b_i^{\max},\ 0 \leq i \leq N-1\}. \tag{A.3}$$

For the ground set S and assumed cardinality $c = B_{\text{tot}}$, the collection of all possible subsets of S with cardinality not exceeding c is given by

$$\mathfrak{I}_c \doteq \{\mathfrak{S} \subseteq S \ : \ |\mathfrak{S}| \leq c\}. \tag{A.4}$$

In (A.4), $\mathfrak{I}_c$ includes all possible bit loading patterns, for which $B_{\text{tot}} = c$, and (S,$\mathfrak{I}_c$) in (A.3) and (A.4) is a uniform matroid of rank $c = B_{\text{tot}}$. This proves the matroid structure of the following integer bit loading maximization for any value of c:

$$\max_{\{b_i, i=0,\ldots,N-1\}} B_{\text{tot}} = \sum_{i=0}^{N-1} b_i, \tag{A.5}$$

subject to three constraints:

$$\sum_{i=0}^{N-1} \epsilon_i \leq \epsilon_{\text{tot}}, \tag{A.6a}$$

$$b_i \in \{0, 1, 2, \ldots, b_i^{\max}\}, i = 0, 1, 2, \ldots, N. \tag{A.6b}$$

Hence, the application of greedy Algorithm 2 with the weight function being the excess energy required to transmit k-th bit in the i-th subchannel pair in S:

$$w(k,i) = \Delta\epsilon_i(k),\ 0 \le k \le b_i^{\max},\ i = 0,1,2,\ldots,N-1, \tag{A.7}$$

results in finding the maximal member $\mathfrak{S}^*$ of $\mathfrak{I}_c$ with cardinality $c = B_{\text{tot}} = |\mathfrak{S}^*|$ and minimum weight

$$W(\mathfrak{S}^*) = \sum_{(k,i)\in\mathfrak{S}^*} \Delta\epsilon_i(k). \tag{A.8}$$

The rate function for subchannel i can be written as

$$\mathfrak{R}(\sigma_i) = \log_2\left(1+\frac{\sigma_i}{\Gamma}\right) = \log_2\left(1+\epsilon_i\frac{|H_i|^2}{N_0(i)\Gamma}\right) \quad \text{(bits/symbol)},$$

where σ_i is the overall SNR at subchannel i, Γ is the SNR-gap which accounts for non-ideal issues in implementation, H_i is channel frequency response at subchannel i, and $N_0(i)$ is the noise power spectral density. The rate function for the ideal case of no SNR-gap as a function of $\sigma_i = \epsilon_i(|H(i)|^2/N_0(i))$ is illustrated in Fig. A.1. When this relation applies, the energy required to transmit k bits at subchannel i is

$$\epsilon_i(k) = \frac{\Gamma N_0}{|H_i|^2}(2^k - 1), \tag{A.9}$$

where the expression outside the paranthesis is the same for different k for subchannel i. Therefore,

$$\Delta\epsilon_i(k) = 2\Delta\epsilon_i(k-1). \tag{A.10}$$

This implies that the greedy algorithm picks pairs corresponding to a subchannel starting from the first bit in an increasing fashion, since it requires more energy to transmit the next bit in a subcahnnel compared to the previous bits transmitted, which results in a bit loading pattern that practically makes sense. Due to the strictly increasing concave nature of the rate function

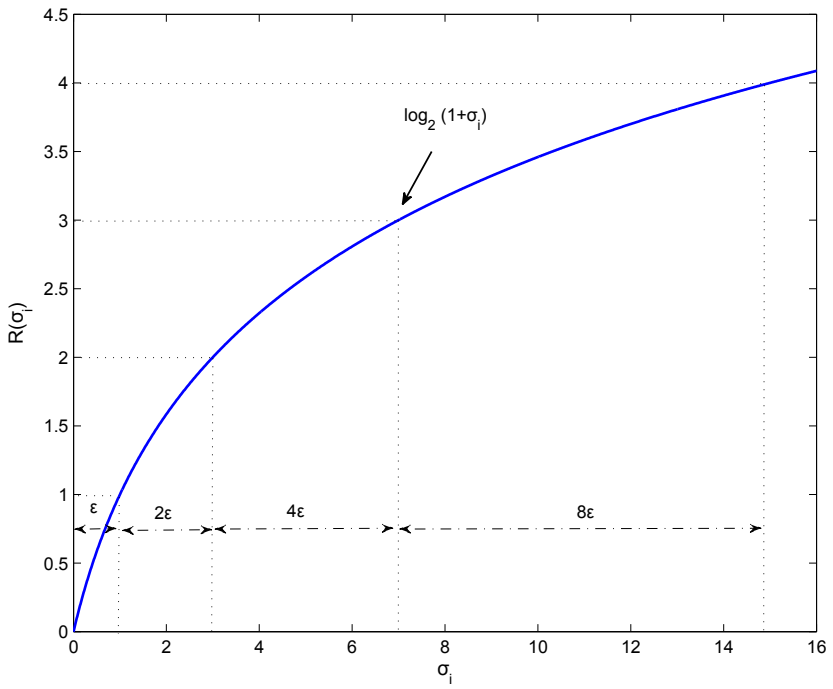

Figure A.1. Strictly increasing concave rate function illustrated as a function of overall SNR with ideal case of no SNR-gap.

for a communication channel, the greedy algorithm solution converges to the globally optimal bit allocation for the maximization problem. From an implementation point of view, B_{tot} is unknown at the beginning of the bit loading process. However, the greedy algorithm can be applied in an iterative fashion starting at an initial $B_{\text{tot}} = 0$, then increasing B_{tot} by one at each step.

Page left intentionally blank.

Appendix B

Channel Interpolation

If the number of subchannels carrying pilot symbols is N_p and the total number of subchannels is N, the set of N_p complex values is interpolated to obtain the channel frequency response. The interpolation is a linear filtering process that can be performed in frequency or time domain. When one out of L subchannels are placed pilot symbols, for the comb-type geometry, the frequency index of pilot subcarriers is $k = nL$, where L is the pilot spacing, and $0 \leq n \leq N_p - 1$. The CE algorithms (i.e. LS, LMMSE etc.) estimate the channel at pilot locations, then interpolate to estimate the remaining locations. The received symbol at the pilot locations can be expressed as

$$Y_p = X_p H_p + n_p, \tag{B.1}$$

where X_p is the complex pilot QAM symbol transmitted at the pilot location, H_p is the corresponding channel response, n_p is the complex additive noise, and $p = nL$. The LS channel estimate is then

$$\hat{H}_p = Y_p / X_p = H_p + \mathrm{e}_p, \tag{B.2}$$

where e_p is the estimation error given by

$$\mathrm{e}_p = n_p / X_p. \tag{B.3}$$

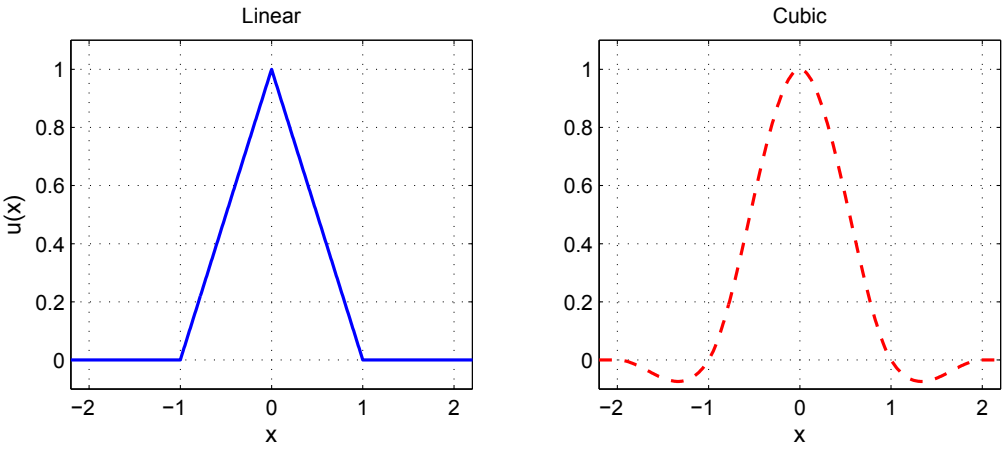

Figure B.1. Linear and cubic interpolation kernels.

For the i-th subchannel, where $0 \leq i \leq N-1$, the channel estimate via interpolation is defined by the following relation

$$\hat{H}_i = \sum_n \hat{H}_{nL}.u\left(\frac{i-nL}{L}\right), \tag{B.4}$$

where $u(x)$ is the interpolation kernel [22] (i.e. linear, cubic, nearest neighbor, B-spline, DFT zero padding, second order Gaussian etc.). For instance, $u(x)$ for linear interpolation is given by

$$u(x) = \begin{cases} 1-|x| & 0 \leq |x| \leq 1 \\ 0 & \text{elsewhere,} \end{cases} \tag{B.5}$$

and for cubic interpolation

$$u(x) = \begin{cases} \frac{3}{2}|x|^3 - \frac{5}{2}|x|^2 + 1 & 0 \leq |x| \leq 1 \\ -\frac{1}{2}|x|^3 + \frac{5}{2}|x|^2 - 4|x| + 2 & 1 \leq |x| \leq 2 \\ 0 & \text{elsewhere.} \end{cases} \tag{B.6}$$

The linear and cubic interpolation kernels are illustrated in Fig. B.1.

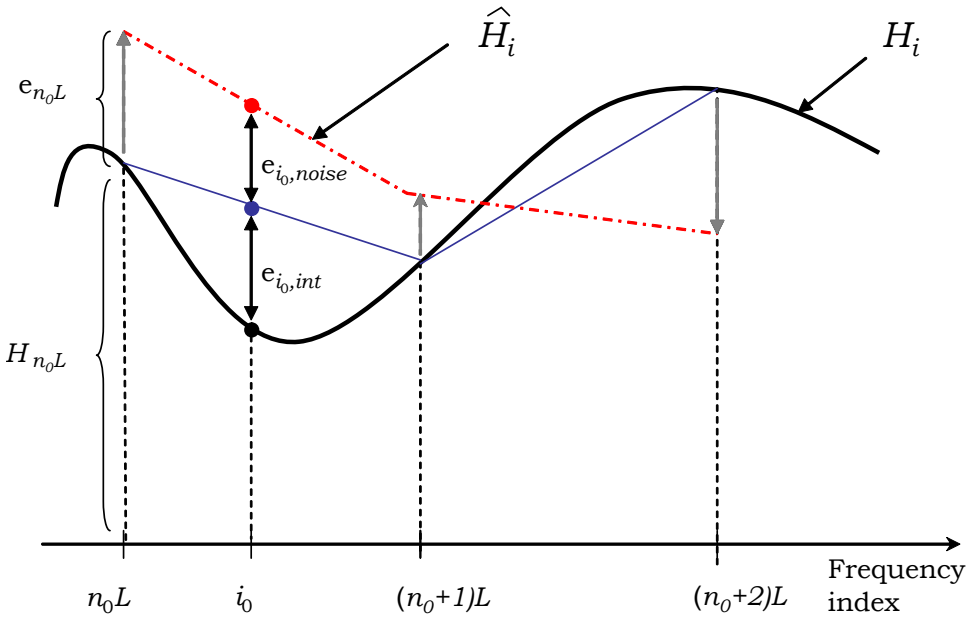

Figure B.2. Estimation error decomposition [22, Fig. 3]

.

B.1 Estimation Error

The estimation error e_i for the i-th subchannel is the difference between the true channel response at that subchannel and the estimated value:

$$\begin{aligned} e_i &= H_i - \hat{H}_i \\ &= \left(H_i - \sum_n H_{nL}.u\left(\frac{i-nL}{L}\right)\right) - \left(\sum_n e_{nL}.u\left(\frac{i-nL}{L}\right)\right). \end{aligned} \tag{B.7}$$

Equation B.7 is composed of two error sources: (i) *interpolation error*, and (ii) *noise error*:

$$e_i = e_{i,\text{int}} + e_{i,\text{noise}}, \tag{B.8}$$

where

$$e_{i,\text{int}} = H_i - \sum_n H_{nL}.u\left(\frac{i-nL}{L}\right), \tag{B.9}$$

$$\mathrm{e}_{i,\mathrm{noise}} = \sum_{n} \mathrm{e}_{nL}.u\left(\frac{i-nL}{L}\right). \tag{B.10}$$

If we assume that there is no noise in the communication channel, this results in perfect channel estimates with no error at the pilot locations. However, the non-pilot subchannels' estimates will be obtained by interpolation, and the estimation error for the non-pilot subchannels will only be caused by interpolation in this case. This error is the interpolation error portion of the actual estimation error. The interpolation error depends on the interpolation kernel, channel characteristics, and pilot spacing L. The noise error is the second component of estimation error and is a function of noise at pilot subcarriers and the interpolation kernel. The decomposition of estimation error in terms of interpolation and noise errors is illustrated in Fig. B.2 for real H_i and linear interpolation.

References

[1] H. C. Ferreira, L. Lampe, J. Newbury, and T. G. S. (Editors), *Power Line Communications: Theory and Applications for Narrowband and Broadband Communications over Power Lines*. John Wiley & Sons, June 2010.

[2] S. Galli, A. Scaglione, and Z. Wang, "For the grid and through the grid: The role of power line communications in the smart grid," in *Proceedings of the IEEE*, vol. 99, pp. 998 –1027, June 2011.

[3] V. Oksman and J. Egan, "Applications of ITU-T G.9960, ITU-T G.9961 transceivers for smart grid applications: Advanced metering infrastructure, energy management in the home and electric vehicles," in *ITU-T Technical Paper*, Jun 2010.

[4] HomePlug Powerline Alliance, "Homeplug Green PHY specification," June 2010. Release Version 1.00.

[5] "IEEE standard for broadband over power line networks: Medium access control and physical layer specifications," *IEEE Std 1901*, pp. 1 –1586, 2010.

[6] F. Cañete Corripio, J. Cortés Arrabal, L. Díez Del Río, and J. Entrambasaguas Muñoz, "Analysis of the cyclic short-term variation of indoor power line channels," *IEEE Journal on Selected Areas in Communications*, vol. 24, pp. 1327–1338, July 2006.

[7] S. Katar, B. Mashbum, K. Afkhamie, H. Latchman, and R. Newman, "Channel adaptation based on cyclo-stationary noise characteristics in PLC systems," in *IEEE Intl. Symp. on Power Line Commun. and Its Appl.(ISPLC)*, pp. 16–21, 2006.

[8] S. Honda, D. Umehara, T. Hayasaki, S. Denno, and M. Morikura, "A fast bit loading algorithm synchronized with commercial power supply for in-home PLC systems," in *IEEE Intl. Symp. on Power Line Commun. and Its Appl. (ISPLC)*, pp. 336–341, April 2008.

[9] K.-H. Kim, H.-B. Lee, Y.-H. Kim, and S.-C. Kim, "Channel adaptation for time-varying powerline channel and noise synchronized with AC cycle," in *IEEE Intl. Symp. on Power Line Commun. and Its Appl. (ISPLC)*, pp. 250–254, April 2009.

[10] T.-E. Sung, A. Scaglione, and S. Galli, "Time-varying power line block transmission models over doubly selective channels," in *IEEE Intl. Symp. on Power Line Commun. and Its Appl.(ISPLC)*, pp. 193 –198, Apr 2008.

[11] F. Cañete Corripio, J. Cortés Arrabal, L. Díez Del Río, and J. Entrambasaguas Muñoz, "A channel model proposal for indoor power line communications," *IEEE Communications Magazine*, vol. 49, pp. 166–174, Dec 2011.

[12] J. G. Proakis and M. Salehi, *Digital Communications*. New York: McGraw-Hill, 2008.

[13] A. Picorone, L. Amado, and M. Ribeiro, "Linear and periodically time-varying PLC channels estimation in the presence of impulsive noise," in *IEEE Intl. Symp. on Power Line Commun. and Its Appl.(ISPLC)*, pp. 255–260, Mar. 2010.

[14] K. Watanabe, D. Umehara, S. Denno, and M. Morikura, "An initial acquisition method for channel synchronization on in-home power line communications," in *IEEE Intl. Symp. on Power Line Commun. and Its Appl. (ISPLC)*, pp. 137–142, April 2009.

[15] D. Umehara, T. Hayasaki, S. Denno, and M. Morikura, "The influence of time-varying channels synchronized with commercial power supply on PLC equipments," in *IEEE Intl. Symp. on Power Line Commun. and Its Appl. (ISPLC)*, pp. 30–35, April 2008.

[16] A. Tonello, J. Cortes, and S. D'Alessandro, "Optimal time slot design in an OFDM-TDMA system over power-line time-variant channels," in *IEEE Intl. Symp. on Power Line Commun. and Its Appl.(ISPLC)*, pp. 41 –46, Apr 2009.

[17] M. A. Tunç, E. Perrins, and L. Lampe, "The effect of LPTV channel adaptation on the performance of broadband PLC for smart grid," in *IEEE International Conference on Smart Grid Communications (SmartGridComm)*, Oct 2011.

[18] J. Campello, "Optimal discrete bit loading for multicarrier modulation systems," in *IEEE International Symposium on Information Theory*, Aug 1998.

[19] E. Baccarelli and M. Biagi, "Optimal integer bit-loading for multicarrier ADSL systems subject to spectral-compatibility limits," *Elsevier Signal Processing*, pp. 729–741, 2004.

[20] A. Cully and O. Logvinov, "Optimizing power consumption in networked devices," in *IEEE Intl. Symp. on Power Line Commun. and Its Appl.(ISPLC)*, Mar 2012.

[21] M. A. Tunç, E. Perrins, and L. Lampe, "Reduced complexity LPTV-aware bit loading for channel adaptation in broadband PLC," in *IEEE Intl. Symp. on Power Line Commun. and Its Appl. (ISPLC)*, Mar 2012.

[22] D. Bueche, P. Corlay, M. Gazalet, and F.-X. Coudoux, "A method for analyzing the performance of comb-type pilot-aided channel estimation in power line communications," *IEEE Transactions on Consumer Electronics*, vol. 54, pp. 1074–1081, Aug. 2008.

[23] A. Nayagam, S. Katar, D. Rende, K. Afkhamie, and L. Yonge, "Tradeoff between channel estimation accuracy and application throughput for in-home MIMO power line communication," in *IEEE International Symposium on Power Line Communications and Its Applications (ISPLC)*, pp. 411–417, Apr. 2011.

[24] J. Cortes, A. Tonello, and L. Diez, "Comparative analysis of pilot-based channel estimators for DMT systems over indoor power-line channels," in *IEEE International Symposium on Power Line Communications and Its Applications (ISPLC)*, pp. 372–377, Mar. 2007.

[25] M. Noh, Y. Lee, and H. Park, "Low complexity LMMSE channel estimation for OFDM," *Communications, IEE Proceedings-*, vol. 153, no. 5, pp. 645–650, 2006.

[26] L. Liu, X. Yang, J. Li, M. Bi, H. He, and W. Hu, "Experimental evaluation of pilot arrangement for channel estimation in OFDM systems," in *Communications and Photonics Conference and Exhibition, ACP. Asia*, pp. 1–6, 2011.

[27] Y. Zhao and A. Huang, "A novel channel estimation method for OFDM mobile communication systems based on pilot signals and transform-domain processing," in *IEEE Vehicular Technology Conference*, vol. 3, pp. 2089–2093, 1997.

[28] M. A. Tunç and E. Perrins, "Pilot based channel estimation and transform domain analysis in broadband PLC for smart grid," in *IEEE International Conference on Smart Grid Communications (SmartGridComm)*, Oct 2013.

[29] J. Edmonds, *Matroids and greedy algorithms, Math Programming 1.* 1971.